ULSAN NATIONAL INSTITUTE OF
SCIENCE AND TECHNOLOGY

Doctoral Thesis

Molecular Exchange Bias at Ferromagnet/Organic Interfaces

Junhyeon Jo

Department of Materials Science and Engineering

Graduate School of UNIST

2019

Molecular Exchange Bias
at Ferromagnet/Organic Interfaces

Junhyeon Jo

Department of Materials Science and Engineering

Graduate School of UNIST

Molecular Exchange Bias at Ferromagnet/Organic Interfaces

A thesis/dissertation
submitted to the Graduate School of UNIST
in partial fulfillment of the
requirements for the degree of
Doctor of Philosophy

Junhyeon Jo

December/24/2018 of submission
Approved by

Advisor
Jung-Woo Yoo

Molecular Exchange Bias
at Ferromagnet/Organic Interfaces

Junhyeon Jo

This certifies that the thesis/dissertation of Junhyeon Jo is approved.

December/24/2018 of submission

Advisor: Jung-Woo Yoo

Thesis Committee Member #1: Hyung-Joon Shin

Thesis Committee Member #2: Ki-Suk Lee

Thesis Committee Member #3: Hosub Jin

Thesis Committee Member #4: Jaekwang Lee

Abstract

An organic molecule, the carbon-based complex of several atoms, is an innovative and essential element to create nano-structural platforms, as a building block. Because of its variety and functionality via widely studied synthetic methods, molecules have played an important role in electronics as not only a transport channel by bulk-forms but also a tuning layer at the interface of heterostructures. The potential of molecular layers has also stood out in spintronics, owing to its mass-low composition producing long spin life time. Beyond this advantage, the on-surface configuration of molecules to a metal film displays unique phenomena as it can control the molecular spins and interfacial coupling between them, resulting in the emergence of molecular spinterface. With a great effort to unveil fundamental mechanism of the hybrid interface via various spectroscopies and theoretical simulations, future-oriented research of molecular spintronics to practical device application has received enormous attentions. Among them, exchange bias is an attractive phenomenon, because it is closely related to the fundamental concept of spinterface and is a critical factor in practical magnetic devices. Thus, introducing molecular spinterface to exchange bias will take advantage of its functionality for device applications and enrich the research of molecular spintronics.

This thesis will show the comprehensive study of molecular exchange bias induced by newly developed molecular spinterfaces between paramagnetic metalloporphyrins and ferromagnetic layers. Magnetometry showed that various kinds of metalloporphyrins resulted in different degree of interfacial couplings and a wide range of exchange bias on the ferromagnetic layers. Varying the underlying ferromagnetic layers allowed to control the interfacial exchange interaction such as ferromagnetic and antiferromagnetic coupling, and the latter can even tune the degree of exchange bias depending on cooling magnetic field. Magnetotransport measurement provided an alternative assessment of the exchange bias through anisotropic and angle-dependent magnetoresistance which are essential ingredients to expand spintronics applications of the hybrid magnetic layers. The emergence of magnetic moment and interfacial coupling were calculated by theoretical approaches with demonstrations of incommensurately antiferromagnetic interlayers of the molecules and indirect exchange coupling between the molecule and metal layer. These fundamental studies of the hybrid interfacial coupling and its impact on the magnetic and magnetotransport characteristics open a new channel for controlling hybrid magnetic layers. The demonstrated tuning of magnetic exchange bias via the molecular approach will certainly extend versatile functionalities of organic spinterfaces.

Contents

I. Molecular Spinterface

II. Exchange Bias

III. Experimental Methods

IV. Exchange Bias in Co/MOEP Systems with Ferromagnetic Coupling

V. Exchange Bias in a Fe/CoOEP System with Antiferromagnetic Coupling

List of Figures

List of Tables

List of Abbreviations

AFM	Antiferromagnetic
Alq_3	Tris(8-hydroxyquinolinato)aluminium
AMR	Anisotropic Magnetoresistance
CAICISS	Collision Ion Scattering Spectroscopy
DFT	Density Functional Theory
DOS	Density of States
EB	Exchange Bias
FC	Field-Cooled
FM	Ferromagnetic
GGA	Generalized Gradient Approximation
GMR	Giant Magnetoresistance
HDD	Hard Disk Drive
HFC	Applied Magnetic Field in Field-Cooled Procedure
HOMO	Highest Occupied Molecular Orbital
LED	Light Emitting Diode
LSMO	Lanthanum Strontium Manganite
LUMO	Lowest Unoccupied Molecular Orbital
MFM	Magnetic Force Microscopy
MOKE	Magneto Optic Kerr Effect
MPMS	Magnetic Property Measurement System
MR	Magnetoresistance
MTJ	Magnetic Tunnel Junction
NEB	Negative Exchange Bias
NM	Non-Magnetic
OEP	Octaethyl Porphyrin
OLED	Organic Light Emitting Diode
PBE	Perdew–Burke–Ernzerhof
Pc	Phthalocyanine
PEB	Positive Exchange Bias
PHR	Planar Hall Resistance
PM	Paramagnetic
PPMS	Physical Property Measurement System
RT	Room Temperature

SG	Spin Glass
SHE	Spin Hall Effect
SHIPS	Spin-Hybridization-Induced Polarized States
SOT	Spin Orbit Torque
SPMDS	Spin Polarized Metastable Deexcitation Spectroscopy
SP-STM	Spin Polarized Scanning Tunneling Microscopy
SP-UPS	Spin Polarized Ultraviolet Photoelectron Spectroscopy
SQUID-VSM	Superconducting Quantum Interference Device-Vibrating Sample Magnetometer
SSE	Spin Seebeck Effect
STT	Spin Transfer Torque
T6	Sexithiophene
TB	Tunneling Barrier
TMR	Tunneling Magnetoresistance
TPP	Tetraphenyl Porphyrin
UPS	Ultraviolet Photoelectron Spectroscopy
VL	Vacuum Level
VSM	Vibrating Sample Magnetometer
XAS	X-ray Absorption Spectroscopy
XMCD	X-ray Magnetic Circular Dichroism
XPS	X-ray Photoelectron Spectroscopy
XRD	X-ray Diffraction

I. Molecular Spinterface

Molecules on a metal film have played important roles not only in electronics using electron charge but also in spintronics dealing with both electron charge and spin. The interface between metal and organic molecular layers can change magnetic moment and coupling of the layers and further develop the ordering of the molecular layers. These interesting phenomena have triggered researcher's fancy to low dimensional structures and enriched the field of organic spintronics. This chapter will show the brief introduction for molecular spinterface. The background of spintronics, the emergence of molecular spinterface, and its recent research will be presented for helping to understand the results of this thesis.

1.1. Spintronics

Spintronics is a multidisciplinary research area focusing on manipulation of the electron's spin degree of freedom in condensed matters. Although the conventional use of electrons has been limited to electron charge as electronics, spintronics as its name says encompasses a wide range of electronics with spin properties of electrons. A basic concept for spin is described as the spin state of $m_s = +\frac{1}{2}$ and $m_s = -\frac{1}{2}$ called spin up and spin down respectively, which originates from the component of spin quantized as $S_z = m_s\hbar$ (where m_s is the quantum number and $\hbar$ is the Planck constant divided by 2π). The first approach to spintronics was the discovery of anisotropic magnetoresistance (AMR) by W. Thomson[1]. He demonstrated different electrical conductivity in a ferromagnet according to the direction of applied magnetic field, but its small amplitude of anisotropy less than a few percent was not attractive. The emergence of giant magnetoresistance (GMR) in metal superlattices by A. Fert[2] and P. Grünberg[3] made the difference of the electrical signal surprisingly up to 50% at low temperature. This important discovery encouraged to investigate on spin-dependent phenomena and accelerated development for magnetic device applications. Following spin-dependent transport in magnetic tunnel junction (MTJ) achieved up to a few hundred percent of magnetoresistance (MR), called tunneling magnetoresistance (TMR)[4-7]. Based on these early and critical studies, there has been a lot of state-of-the-art research manipulating electron spins such as spin transfer torque (STT), spin orbit torque (SOT)[8], spin Hall effect (SHE)[9], spin Seebeck effect (SSE)[10], spin transistor[11], spin LED[12], and so on. Generation of the spin-dependent signal could be controlled not only by using magnetic field and electric field but also other energy forms like photonic field and mechanical deformation, which enrich fundamental understanding of the spin and variety of device applications in various circumstances.

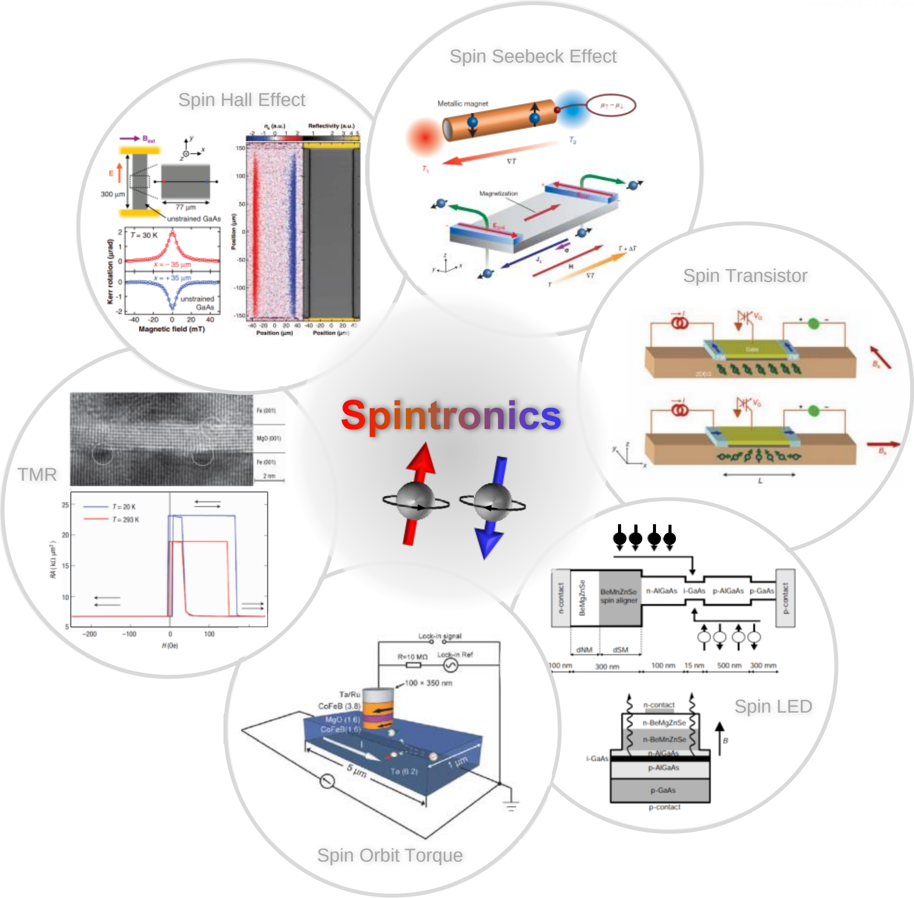

Figure 1.1. Representative research fields in spintronics [reproduced from Referenece$^{7-12}$].

GMR and TMR are the representative spin-dependent phenomena which have utilized in the recent commercial magnetic sensors and related devices owing to their simple device structures and fast response in switching states. The basic structure of GMR, called spin valve, consists of two ferromagnetic (FM) metal films and a non-magnetic (NM) metal film where the NM film is sandwiched between the two FM films. When a constant current is applied and flows through a FM/NM/FM structure, the overall resistance is determined by the magnetization of the two FM films. There are two states of resistance in the structure that one is a high resistance state and the other is a low resistance state (Figure 1.2(a)). When the magnetic field is high enough to align parallel configuration of the FM 1 and FM 2 layer that is the low resistance state, the majority spin in a spin-polarized current can flow well, but the minor spin undergoes spin-scattering because of different direction of magnetization. On the contrary, when an intermediate magnetic field is applied causing antiparallel configuration of the two FM layers that is a high resistance state, the major spin passes through easily into the FM 1 layer but not in the FM 2 layer. The opposite situation occurs for the minor spin that undergoes more spin-scattering into the FM 1 layer, but easily passes through the FM 2 layer. Thus, parallel configuration of the two FM layers makes a low resistance state and antiparallel alignment of the FM layers induces a high resistance state. Based on these two resistance states, a switching device by varying applied magnetic field can operate widely used in the commercial magnetic devices. Figure 1.2(b) represents schematic illustrations of magnetic field dependent magnetoresistance, defined as,

$$\mathrm{MR} = \frac{\Delta R}{R_P} = \frac{R_{AP} - R_P}{R_P}$$

where R_{P} (R_{AP}) is the resistance at the parallel (antiparallel) state between two FM layers. There have been two important aspects to apply to practical devices. One is to achieve sufficiently separated two resistance states. In Figure 1.2(b), to obtain a stable high resistance state, large difference between $H_{\mathrm{C,FM1}}$ and $H_{\mathrm{C,FM2}}$ is essential. However, it will lead to large applied magnetic field that is a severe disadvantage for energy efficiency and device durability. The method to solve is to insert an antiferromagnetic (AFM) metal layer in the basic spin valve, which induces exchange bias resulting in large unidirectional anisotropy to applied magnetic field direction (see details in Section Π). The other aspect for device applications is a switching ratio to get clear and accurate difference for better device performance. Unfortunately, MR devices did not exceed the difference of 100 % that is much less than a required value in practical applications.

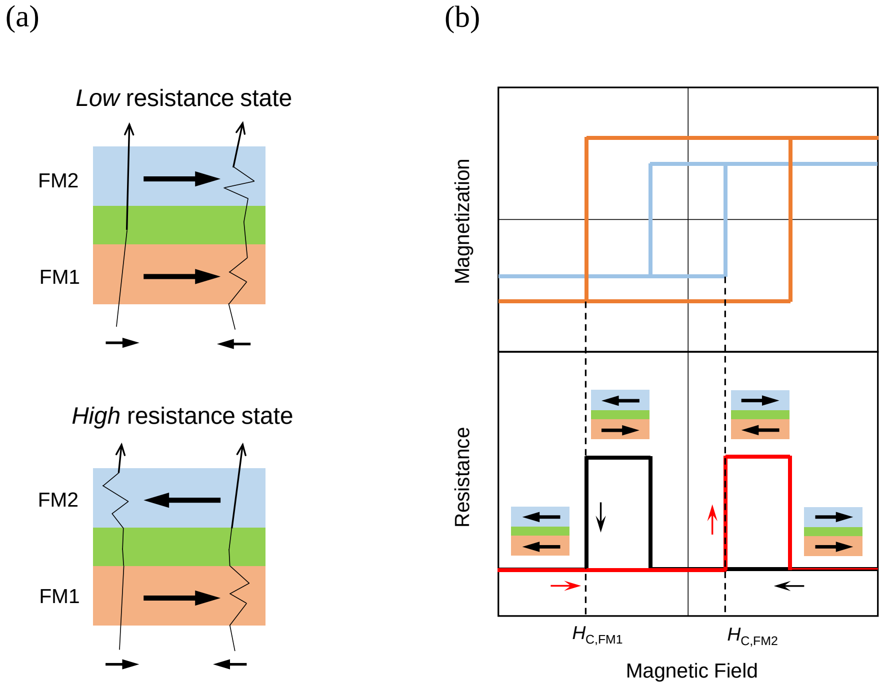

Figure 1.2. Resistance states for spin-dependent transport. (a) Low and high resistance states by controlling the direction of magnetization. (b) Magnetization and magnetoresistance curves with different spin configuration. These spin-dependent schematic illustrations can describe the behavior of not only a spin valve for GMR but also a MTJ for TMR.

The MTJ as a next generation of a magnetic device has been received enormous attention for a much simpler structure and high improved device performance up to 600% MR at room temperature[13]. Compared to a GMR structure, the structure of a MTJ involves an insulating layer between two different FM layers (Figure 1.3). The insulating layer acts as a tunneling barrier which can reduce spin-scattering event (compared to the NM thick-medium in a GMR device) and further improve spin-dependent tunneling by specific tunnel barriers having a spin-filtering function. Figure 1.3 represents spin-dependent transport in a MTJ. The electrons near the Fermi level play a critical role for the transport, having the interaction between *s* electrons for conduction and *d* electrons for magnetism.

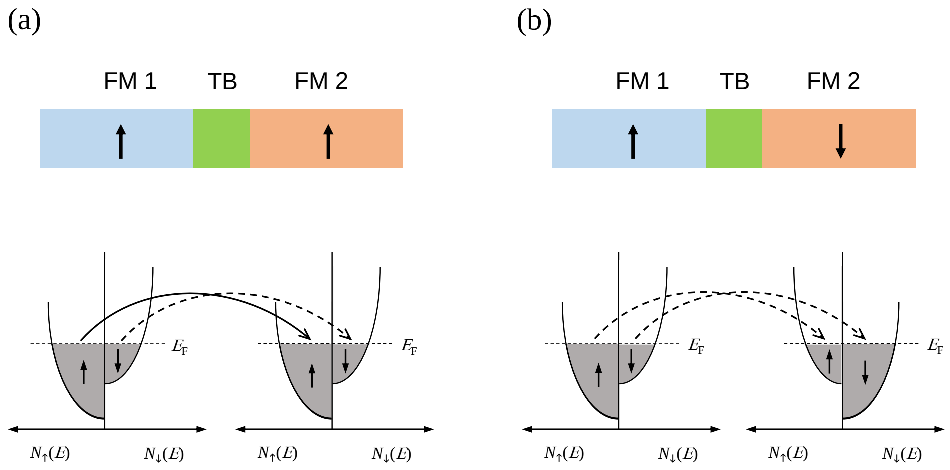

Figure 1.3. Concept of spin transport in TMR with spin-polarized density of states. (a) Parallel and (b) antiparallel configuration for two FM layers separated by a tunneling barrier. When the separating layer changes from the tunneling barrier to a NM metal, it will be GMR having similar spin-dependent transport. Dot-arrow lines from the left density of states to the right represent limited electron tunneling than the solid-arrow line.

1.2. Spinterface

Organic materials have been a promising candidate in the research of spintronics in which inorganic matters such as metals and oxides played a main role. As new and less explored matters having versatile aspects like various kinds and functionality, researchers got interested in organic materials that would enrich the spintronics research. Above all the advantages, the most attractive point of organic matters to spintronics is long spin relaxion time of spin-polarized electrons owing to rare spin-flip scattering events than inorganic ones, because a carbon atom as the main component of organic materials has a low atomic number (Z) leading to weak spin-orbit interaction, which is proportional to Z^4. The first approach for using organic materials to spintronics was employing them as a channel medium in which a spin-polarized current flows between two FM electrodes. An experiment with T_6 molecule spacer layers between ferromagnetic LSMO electrodes showed feasibility of organic spin transport layer, exhibiting 30% of different resistance when applying magnetic fields (Figure 1.4)[14]. The next experiment further extended the research by applying an organic matter to a spin valve device, resulting in different resistance depending on spin-states of a flowing current by applying magnetic fields. The well fabricated organic spin valve of a LSMO/Alq$_3$/Co structure showed a clear and giant MR signal[15], large enough to compare inorganic spin valves (Figure 1.4). These leading investigations for organic spintronics have encouraged people to extend the research of organic spintronics with various molecules. A small molecule Alq$_3$ based structure showed 40% of GMR at 11 K[15], and carbon nanotube based spin valve also recorded up to 60% at 5 K[16], but both exhibited ignorable MR results at room temperature. However, fullerence (C_{60}), the representative small molecule with high affinity, recorded 5% of MR at 300 K[17,18]. Long spin diffusion length also achieved about 40 nm for Alq$_3$[15], 130 nm for carbon nanotube[19], and 200 nm for T_6 polymer[14]. Other various molecules like rubrene[20], P3HT[21], PPV[22], and NPD[23] also well functioned as the medium of spin vale devices[24].

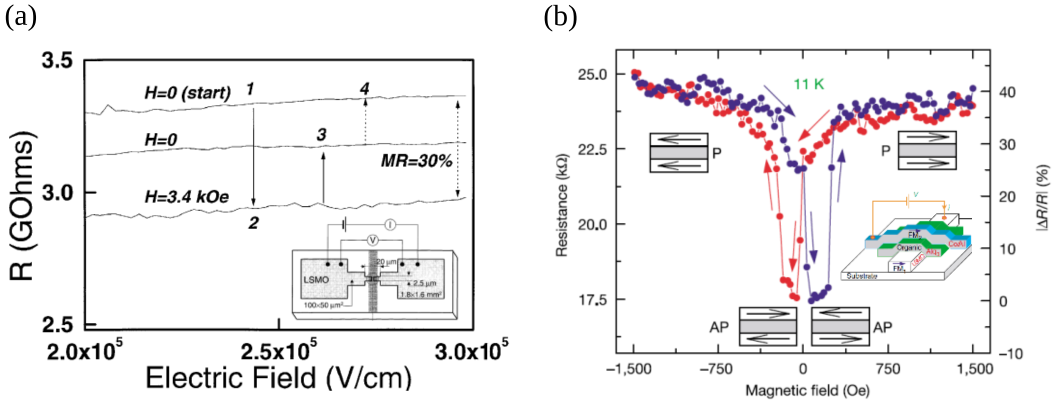

Figure 1.4. MR results with organic spacer. (a) An initial discovery of organic MR difference in a LSMO/T_6/LSMO structure [reproduced from Reference[14]]. (b) GMR in a spin valve device of a LSMO/Alq$_3$/Co structure [reproduced from Reference[15]].

Although organic materials revealed their advantages in spintronics and upgraded their performances, the mechanism of a spin-dependent current flowing in the sandwiched structure of a FM/organic/FM was not unveiled. One of the puzzled aspects concerned about the mechanism was the unexpected sign of MR that was difficult to explain by using conventional analysis for inorganic spin valves[15,25,26]. Although adjusting different voltages can tun the sign of MR through the modulation of energy levels of the two ferromagnetic electrodes in a spin valve[27], it was not able to satisfactorily solve the peculiar MR problem in organic spin valves. Barraud and colleagues suggested a conceptual solution for a spin transport model considering spin-hybridization induced polarized states (SHIPS) at the interface of a FM/organic that were both $P_{\mathrm{Co/Alq3}}$ and $P_{\mathrm{LSMO/Alq3}}$, explaining the phenomenon of the changing MR sign[28]. They also demonstrated effective organic spin valve by eliminating a large junction area problem which could contain pin holes and inhomogeneous structures resulting in different interface states being able to cancel out the effective performance. The result showed 300% of MR in a LSMO/Alq$_3$/Co structure the highest value in organic spin valves owing to nanometer scaled contact area. From this point of time, the term "Molecular Spinterface" have started to mention practically[29] and extended its research widely.

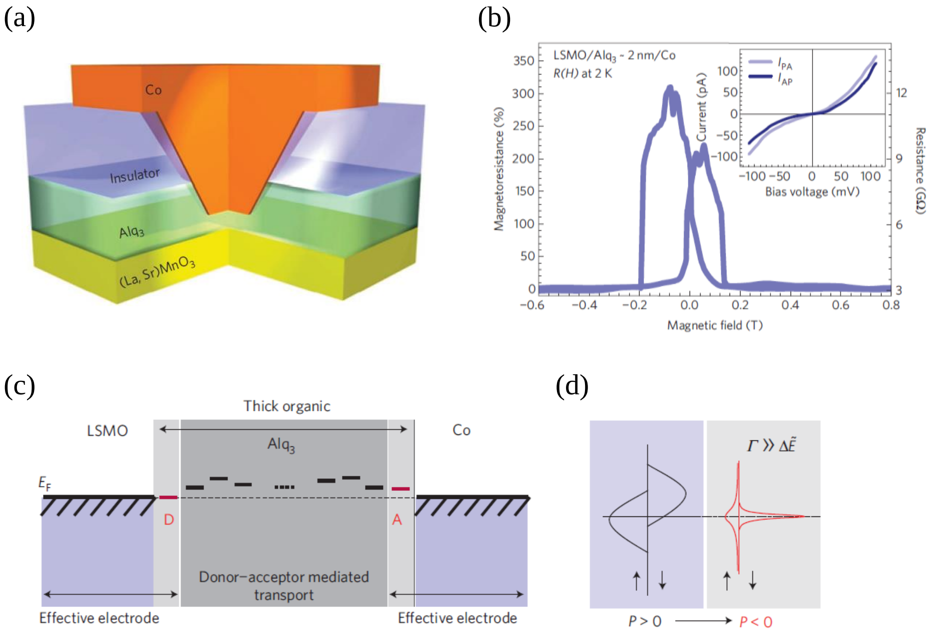

Figure 1.5. Organic MTJ of a LSMO/Alq$_3$/Co structure. (a) A structure of the organic MTJ. (b) MR result for a 2 nm Alq$_3$ device. The MR curve was obtained at 2 K with -5 mV. An inset indicates I-V curves recorded at 2 K in the parallel (I_{PA}) and antiparallel (I_{AP}) spin configurations. (c) A model for donor–acceptor-mediated transport. The coupled states of donor (D) with the left LSMO and acceptor (A) states with the right Co, shown in red color. (d) Illustration of the SHIPS obtained for strong coupling to a ferromagnetic electrode in the limited condition [reproduced from Reference[28]].

Fundamental studies for the metal-organic interface have constantly proceeded through spectroscopy and theoretical study (detailed in the Section 1.3), and further modulating molecular interface achieved notable results in spintronics. One of them was to realize an organic spin valve device by using one ferromagnetic film and one molecular film. Raman and colleagues fabricated a Co/ZMP/Cu structure having a newly induced interfacial ferromagnetic layer at the interface of the Co/ZMP, which exhibited 25% of MR at 4.2 K[30]. Theoretical calculation explained that the first interfacial ZMP layer adjacent to the Co film acted as a ferromagnetic film making the device having two coercivities necessary to a spin valve device. Another fascinating phenomenon of molecular spinterface was inducing magnetic ordering in molecular layers on the underlying FM film. Gruber and colleagues stacked MnPc molecules layer by layer, and they found that the first interfacial layer was ferromagnetically ordered and the consecutive layers were antiferromagnetically ordered on the Co film[31]. This delicate experiment by XMCD reconfirmed the antiferromagnetic molecule layers on the ferromagnet via temperature dependent the exchange bias effect. Besides, creating Rashba-split quantum-well interface states and controlling the Dirac point by topmost interfacial molecules on a topological insulator[32] and modulating the property of top molecules on a ferroelectric poling[33] implied that the hybrid interfacial features are not limited to metal-combinations but further can extend to various systems of functional and interfacial specialized materials.

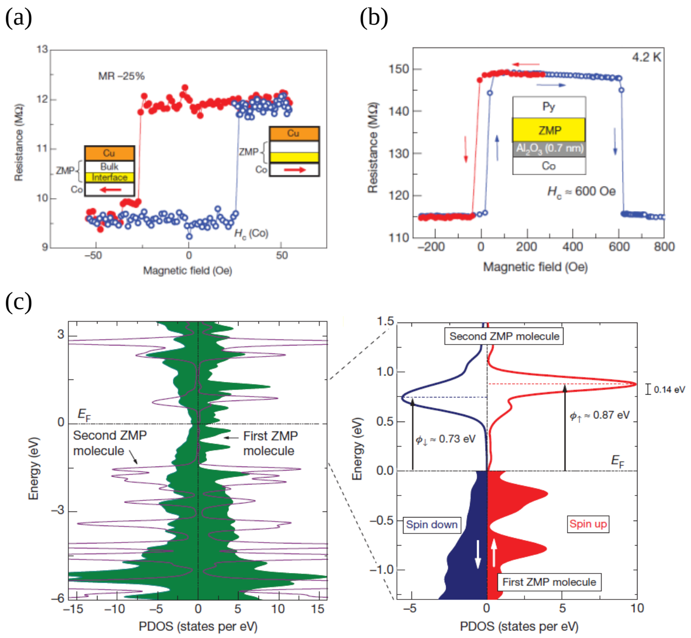

Figure 1.6. Interfacial MR effect. (a) MR of 25% in a Co/ZMP/Cu structure at 4.2 K. (b) Comparable MR data for a Co/ZMP/Py structure at 4.2 K. (c) Spin-resolved DOS of the *p*-states for the first and second ZMP molecule layer of the relaxed interface system. Interfacial $p_{z\text{–}d}$ hybridization creates spin unbalanced electronic structure in the two molecules [reproduced from Reference[30]].

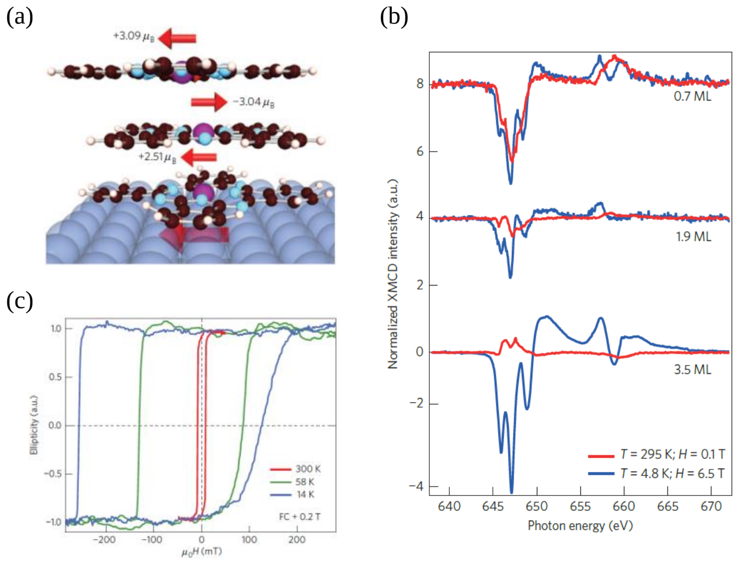

Figure 1.7. Magnetic ordering of the MnPc molecules on a Co film. (a) Schematic configuration and theoretical calculated spin moments. (b) Mn XMCD spectra for 0.7, 1.9, and 3.5 ML MnPc molecule on the Co film. The red line indicates the condition at 295 K with a field of 0.1 T to test the robustness of the effect, and the blue at 4.8 K with 6.5 T is to align the uncoupled paramagnetic molecules. (c) Exchange bias for a Co(20 ML)/MnPc(25 ML) [reproduced from Reference [31]].

1.3. Planar Molecule

A molecule is a complex of more than two atoms through chemical bonds, acting as a single entity which can even gather to the form of aggregation. Compared to a polymer by a solution process, thermally deposited molecules can have high purity and form a low dimensional structure that are great advantages for surface science. Small molecules such as Alq_3, pentacene, C_{60}, rubrene, T_6, etc. have played a key role as a building block especially in electronics, optics, and spintronics. Among them porphyrin and phthalocyanine are broadly utilized molecules owing to their planar geometry and various kinds. In early days, these two materials were used as components of dyes and pigments extracted from plants. The single molecular form of porphyrin and phthalocyanine was first discovered as a by-product when people started to synthesize these materials, in the early 18th century. Their applications to industry have extended from the conventional dye, coating, and pigment to biomedicine and optics in bulk forms and even electronics as a film. A porphyrin consists of four pyrrole type subunits interconnected each other through methine bridges. A phthalocyanine also possesses the similar geometric structure, but four isoindole units constitute the structure by nitrogen bridges. Both molecules have eighteen π-electrons constituting a planar and cyclic ring structure maintaining a stable structure called an aromatic structure. Various and functional characteristics of the two molecules come from the variety of a central metal ion. The two H atoms from pyrrole or isoindole subunits in normal porphyrins and phthalocyanines can be replaced with central metal ions having various oxidation states and geometries. This results in wide ranges of material properties such as electrical conductivity, band edge energy, ionization energy, photoconductivity, absorption wavelength, etc[34]. These engineered features play a key role not only in biochemistry and biomedicine but also electronics research like organic light-emitting diode, organic field-effect transistor, organic photovoltaics, and so on.

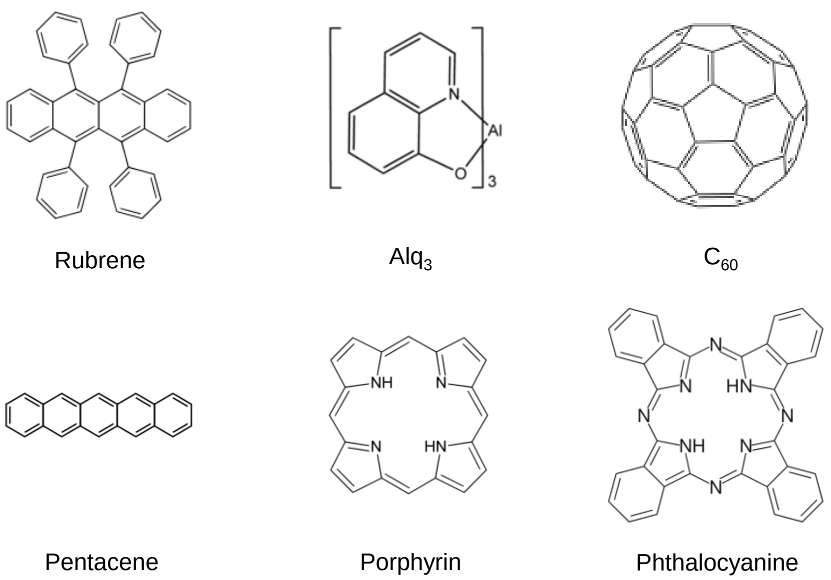

Figure 1.8. Representative small molecules. They are rubrene, Alq3, C_{60}, pentacene, porphyrin, and phthalocyanine.

Material	Absorption Wavelenth				Band edge		Conductivity (S/cm)
	Q (nm)	B (nm)	N (nm)	L (nm)	VB (eV)	CB (eV)	
PcCo	657	312.5	-	240	-5.0	-3.3	10^{-10}
PcNi	651	327.5	-	235	-5.3	-3.6	10^{-9} to 10^{-15}
PcCu	657.5	325	276	240.5	-5.1	-3.6	10^{-7} to 10^{-14}
PcZn	661	326.5	276	240	-5.0	-3.3	10^{-8} to 10^{-12}
PcPb	698	332.5	280	245	-5.1	-3.8	-
PcVO	671	333	280	243.5	-5.5	-3.9	10^{-7}
PcTiO	676	337	266	250	-5.5	-3.7	10^{-10}

Table 1.1. Absorption wavelength[35], band edge energy[36], and electrical conductivity for phthalocyanine series. The absorption data was from the vapor phase. The conductivities were measured at 300 K and the range came from different material phase of α and β [reproduced from Reference[34]].

1.4. Interface at Organic/Inorganic Heterostructures

Recently, functional organic materials have been widely studied in electronic and optic research and further applied to practical applications. This functionality comes from not only various bulk properties but also the interface between two different materials such as inorganic/organic or organic/organic[37,38]. The study for organic interface has been conventionally interested in the region of organic light-emitting diode (OLED) and organic solar cell. One of the main issues is energy level alignment at a metal/organic interface. It is a critical factor for OLED structures to perform efficient carrier injection, involving energy level formation from the surface dipole layer in the tailing electron cloud at the surface and the interfacial dipole layer because of charge transfer and other charge distribution related phenomena (Figure 1.9(a,b)). Another issue is energy band bending at a metal/organic interface that is essential point to improve efficiency of charge separation especially in organic solar cell. Non-equilibrium electrical states at the interface between different materials make the charge redistribution, and this leads to align their Fermi level. If the organic film is thick enough, the energy level of the film adjacent to the interface bends between the bulk organic and interfacial organic film, making built-in potential V_{bi} playing an important role in operating devices (Figure 1.9(c)). Other important factors such as inserted tunneling layer and the influence of applied bias also affect the behaviors of heterostructure interface. These fundamental studies for energy level at the metal/organic interface have enormously impacted on device applications such as organic transistor, OLED, and organic solar cell, and indirectly improved the method and skills for analysis such as XPS and UPS.

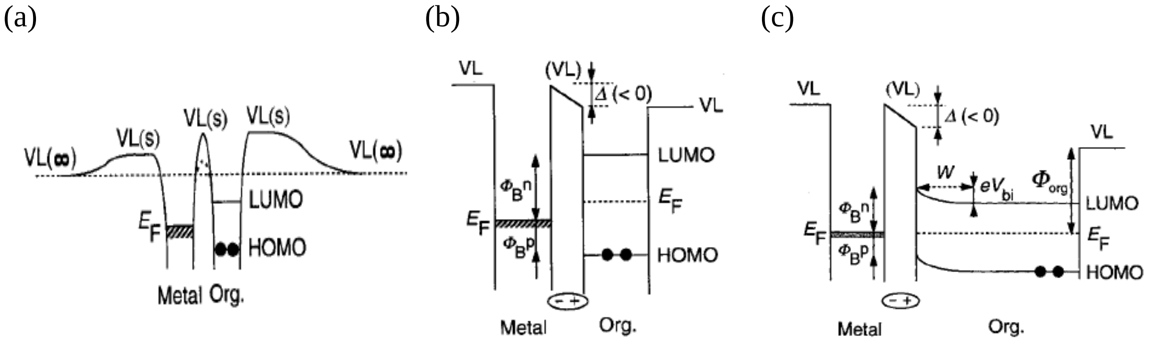

Figure 1.9. Energy level of a metal/organic junction. (a) Vacuum level aligned interface including the surface dipole effect. VL(s) and VL(∞) are the vacuum level of a surface and infinite location. (b) Metal/organic energy alignment with the interfacial dipole layer. Here, VL indicates VL(s) in (a), and Δ is the energy related to the dipole layer. (c) Energy band bending of a thick organic film at the interface. The bending makes the built-in potential V_{bi} near the interface [reproduced from Reference[37]].

With the emergence of spintronics in 1980s, the concept of electron spin has been familiar to researchers in the field of the heterostructure interface. They have tried to extend the research of interface to spin-dependent interfacial phenomena. However, the lack of experimental equipment which can detect and analyze spin-dependent properties of thin films (from a monolayer to a nanometer scale) made the research stagnated. Eventually, the study for spin-polarized molecules begun and extended explosively in 2000s with the initial report for spin-polarized molecules on a metal film consisting of copper-phthalocyanine molecules on the underlying Fe(100) substrate[39]. They showed planarly stacked molecule on the interface by coaxial impact collision ion scattering spectroscopy (CAICISS) and revealed that its spin-polarization followed the underlying Fe film by using spin-polarized metastable deexcitation spectroscopy (SPMDS). Similar studies through SPMDS have been performed to various molecules such as pentacene, benzene, and so on[40,41]. X-ray magnetic circular dichroism (XMCD) is a very powerful technique because of its ability to detect the spin-polarized element and orbital selectivity. The first experiment of XMCD was performed to magnetized iron in 1987[42], and various kinds of inorganic materials have been analyzed and revealed their magnetic properties via XMCD, thanks to its extremely high sensitivity and resolution. This technique was first applied to a metal/molecule film composed of paramagnetic Mn(III)–tetraphenyl-porphyrin chloride and the underlying ferromagnetic Co film, showing the ferromagnetically ordered Mn element in respect to the Co[43]. This study demonstrated the magnetic proximity effect at the interface between a molecule and ferromagnet film by direct element analysis, and it led to further work for Fe(III)-octaethyl-porphyrin chloride molecules on a Co and Ni film showing spin orientation ordering and following theoretical calculation to elucidate the interfacial coupling and the route to transfer the polarized spin from the ferromagnet to the molecules (Figure 1.10)[44].

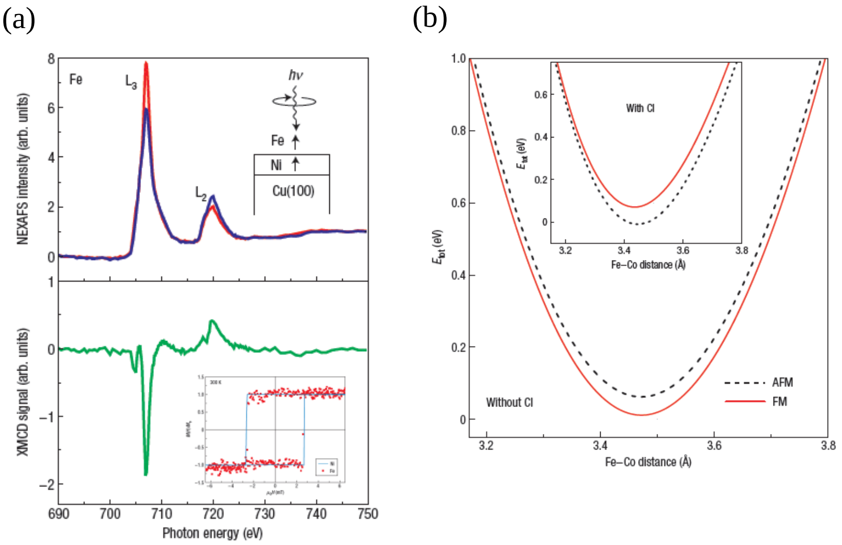

Figure 1.10. Magnetic ordering of Fe(III)-octaethyl-porphyrin chloride on a ferromagnetic film. (a) XMCD result of the iron element in the molecule. Inset indicates a schematic image of the stacking structure (up) and corresponding hysteresis loops for Ni and Fe (down). (b) Theoretical calculations for ferromagnetic and antiferromagnetic ordering between the Fe element in the molecule and the underlying Co film [reproduced from Reference[44]]

In this way, introducing XMCD analysis has enriched the research of metal/molecule spinterface with a variety of combinations for a heterostructure. Ferromagnetic Fe, Co, and Ni and antiferromagnetic Mn and FeMn metal layers have been adopted as a trigger to emerge molecular spinterface. Planar molecules such as metallo series of tetraphenyl-porphyrin (MTPP), octaethyl-porphyrin (MOEP), and phthalocyanine (MPc) with a central metal ion (M = Fe, Co, Ni, Cu, Zn, Cr, and Mn) have been enormously investigated on their structural and spin orientations, thanks to a well-stacked layer by layer structure[31,45-62]. Further, controlling interfacial exchange coupling has been succeeded by inserting interlayer such as Cu[60], graphene[55,62], and oxygen species[45,48,49] which converted the coupling among ferromagnetic, antiferromagnetic, or non-spin-polarized (Figure 1.11). The coupling has influenced not only to the interfacial layer but also further stacking molecular layers. This stacked molecules could form antiferromagnetic interlayers[63] which can induce unidirectional anisotropy to the underlying ferromagnet[31,59].

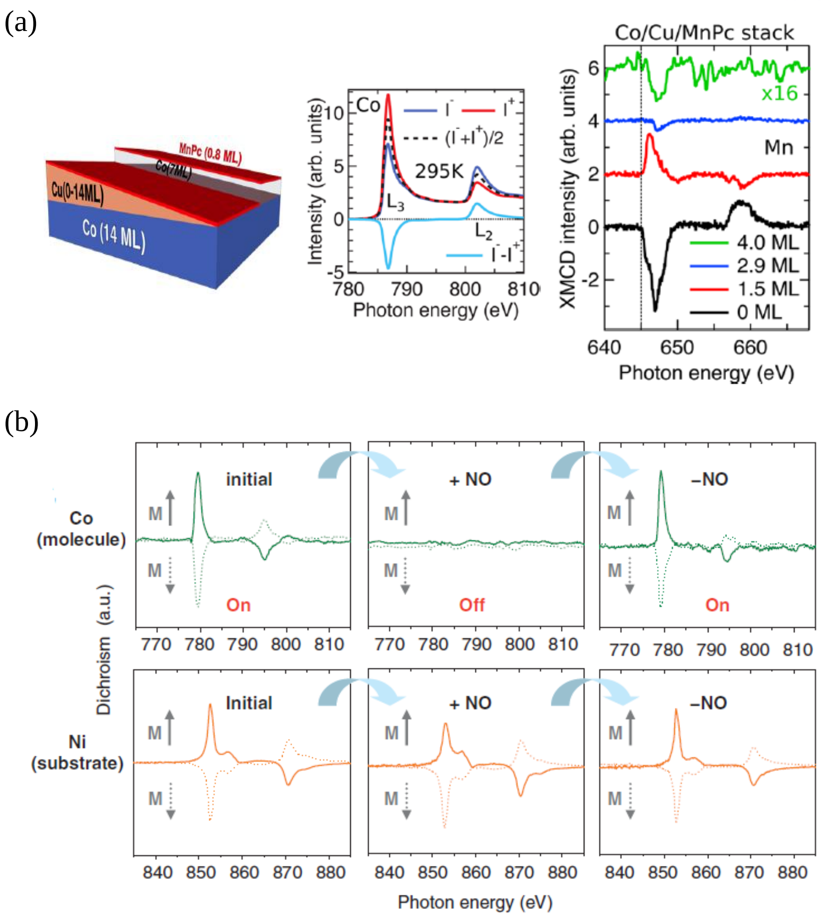

Figure 1.11. Change of interfacial exchange coupling by an inserting layer. (a) Variation in the XMCD sign of a Mn element in a Co/Cu/MnPc structure by controlling the thickness of the Cu (0, 1.5, 2.9, and 4.0 ML) layers [reproduced from Reference[60]]. (b) Switching of XMCD signals of the Co element in a Ni/CoTPP structure by adjusting nitric oxide (NO) [reproduced from Reference[46]].

Another notable technique for investigating the hybrid spinterface is spin-polarized ultraviolet photoelectron spectroscopy (SP-UPS) which gives the applicative information of different spin-dependent interface states at the Fermi level of a ferromagnet/molecule bilayer. For example, although they were similar kinds of Pc species, CuPc molecules on the underlying Co film showed notable spin-polarization near the Fermi level, but other CoPc and ZnPc molecular systems exhibited less distinctive polarization states, because of the different degree of interaction with the *d*-orbital in the central metal ions[64]. Further advanced results realized almost 100% polarized spin states near the Fermi level at room temperature in a Co/MnPc bilayer[65], and revealed the role of inserting normal metal layers for preventing degradation at the ferromagnet/molecules[66]. A spin-polarized single molecule by using spin-polarized scanning tunneling microscopy (SP-STM) exhibited spin-polarized molecules on a ferromagnet having a spin up and down state[67] and spin-split molecular LUMO (Figure 1.12)[68].

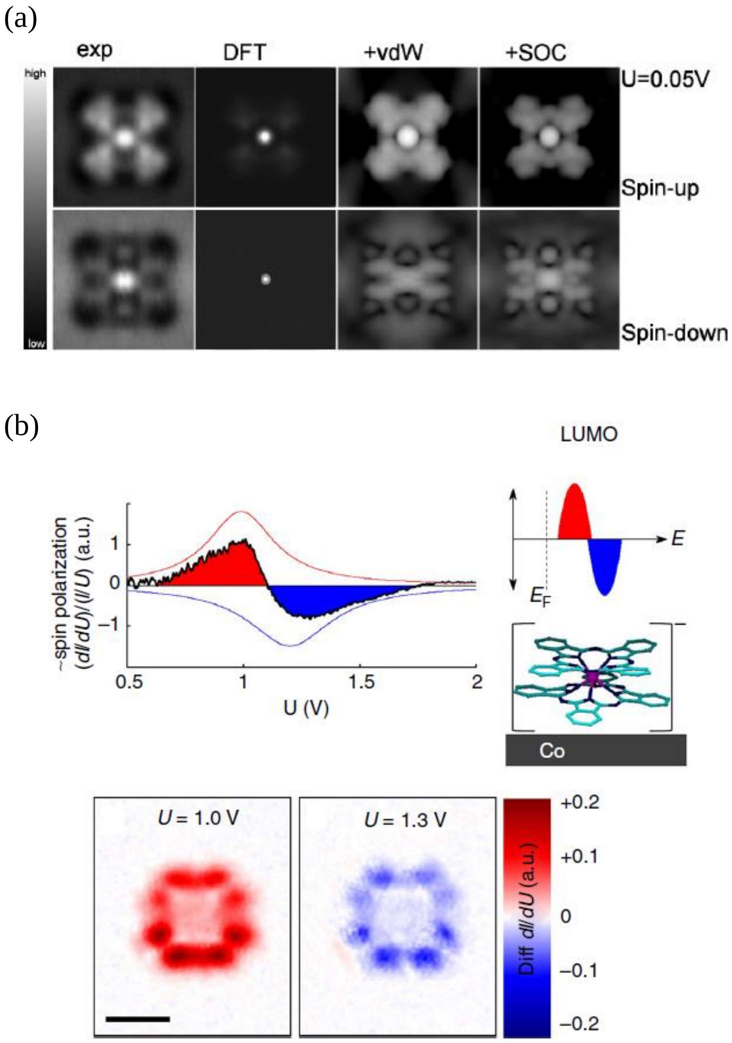

Figure 1.12. SP-STM images for a single molecule on a ferromagnet. (a) SP-STM images for a FePc molecule on a Co film. The experimental and simulated images for various states are presented for each spin directions [reproduced from Reference[67]]. (b) Spin-resolved data for a TbPc$_2$ molecule on a Co film. Difference of the spectroscopic curves and tunneling conductance provides the information about the spin-polarization [reproduced from Reference[68]].

II. Exchange Bias

In a FM/AFM heterostructure, the AFM layers induce interfacial magnetic anisotropy to the FM layers, which is called exchange bias. Conceptually simple mechanism and notable ability to control magnetic properties have made exchange bias as an indispensable component for practical magnetic devices. From the invention of exchange bias in a metal/metal oxide system, occurrence of exchange bias has extended to various systems such as ferrimagnet, spin glass, oxide, and further organic systems. This chapter will introduce a broad background of exchange bias from the mechanism to device applications.

2.1. Mechanism of Exchange Bias

When a FM film meets an AFM film and then develops interface, this FM/AFM structure can have unidirectional anisotropy of its magnetic hysteresis loop via cooling through the Neel temperature (T_N) of the AFM with a static magnetic field. The AFM spins aligned in a preferred direction via the interfacial coupling of the FM/AFM structure impact on spins of the FM film resisting or assisting to flip in a magnetic field sweep. This interaction between the FM and AFM film results in unidirectional anisotropy called (magnetic) exchange bias. The first exchange bias effect was discovered by Meiklejohn and Bean when they studied Co particles surrounded by a native oxide of the Co[69]. After the researches with the particle systems, the heterostructure of thin films started to be widely used to figure out the mechanism of exchange bias owing to well defined interface and controllable structures with the improved technique of thin film fabrication. Exchange bias has not been limited in the initial FM/AFM system but occurred also in the systems of FM/ferrimagnet[70], AFM/ferrimagnet[71], SG[72], FM/PM[31], and so on.

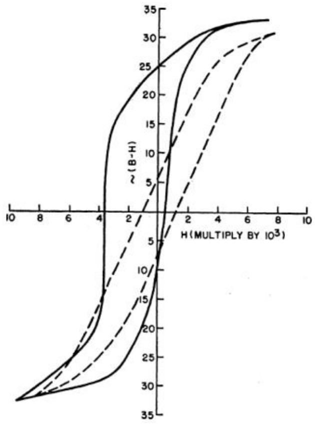

Figure 2.1. The first exchange bias feature, in Co/CoO particles. Anisotropic hysteresis loops (solid line) at 77 K was shown for a field cooling procedure in $H = 10000$ Oe, but there was no asymmetry when cooled in zero field [reproduced from Reference[69]].

The phenomenon of exchange bias in a stacking structure can be intuitively understood with spin configuration of layers at the FM/AFM structure, depicted in Figure 2.2. At the temperature below the Curie temperature (T_C) and above T_N, the FM spins are aligned to the direction of an applied magnetic field (H), but the spins of the AFM layers are in a randomly distributed paramagnetic state (0). As temperature decreases with a static H and passes by the T_N (to $T < T_N$), the AFM layers become an antiferromagnetic state with parallel interfacial spins to the FM under an uncompensated spin configuration (1). When the field is applied to the negative direction, the spins of the FM layers flip to the H direction, but the underlying AFM layers exert a torque to the FM layers (for ferromagnetic coupling between the FM and AFM layers). Then, the FM layers need more energy to fully flip its spins overcoming the torque. This turns into the shift of a left coercivity to the opposite direction to the H during cooling (2). In the opposite H region (3), when the field is applied to the positive direction, the spins of the FM layers flip earlier (4). Thus, the overall hysteresis loop has unidirectional anisotropy that is the shift to the opposite direction to the H (negative exchange bias).

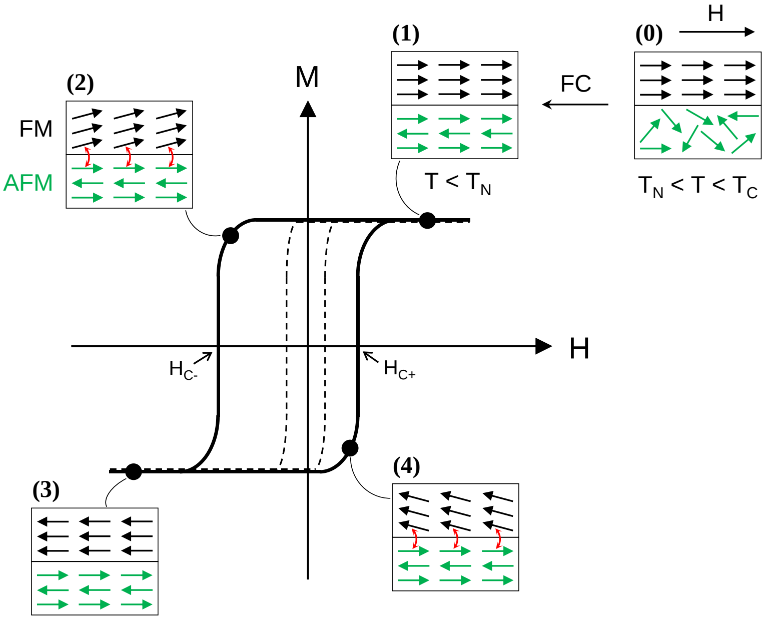

Figure 2.2. Schematic illustration for (negative) exchange bias. Dot lines indicate the hysteresis loop of the FM layers without AFM layers, showing small loop width and a symmetrical hysteresis loop. Bold lines represent exchange-biased FM layers with AFM layers via a FC procedure. H_{C-} and H_{C+} indicate coercivities in the exchange-biased system.

The origin of exchange bias was proposed by several researchers with theoretical and analytical models. The first model called the Meiklejohn and Bean model introduced a comprehensive relation of rotational anisotropies and simplified amplitude of exchange bias. In the initial version of the model, ideal conditions were considered such as a single domain of the FM and AFM layer, atomically smooth interface, fully uncompensated interface, rigid AFM layers, uniaxial anisotropy (in-plain), etc. Based on the Stoner–Wohlfarth model which described a magnetization of a single domain about varying H, the Meiklejohn and Bean model has a realistic form of the energy per unit area[73,74],

$$E_A = -\mu_0 H M_{\mathrm{FM}} t_{\mathrm{FM}} \cos(\theta - \beta) + K_{\mathrm{FM}} t_{\mathrm{FM}} sin^2(\beta)$$

$$+K_{\mathrm{AFM}} t_{\mathrm{AFM}} sin^2(\alpha) - J_{\mathrm{EB}} \cos(\beta - \alpha)$$

where μ_0 is the vacuum permeability, M is the saturated magnetization, t is the thickness, K is the volume anisotropy constant, J_{EB} is the interfacial exchange energy per unit area, and $\theta, \alpha,$ and β are the angles described in Figure 2.3. The first term is for the Zeeman energy and the second is for the magnetic crystalline anisotropy for the FM layers. The third term makes this model realistic by inserting the new concept of the AFM layers slightly rotating during the magnetization reversal, but it remains the rigid state for the average AFM layers. When the energy is stable as $\partial E_A/\partial\theta = 0$ and minimized in respect to the α and β, the amplitude of exchange bias can be expressed as below[74]. This simple equation well represents the relation among the factors.

$$H_{\mathrm{EB}} = -\frac{J_{\mathrm{EB}}}{\mu_0 M_{\mathrm{FM}} t_{\mathrm{FM}}}$$

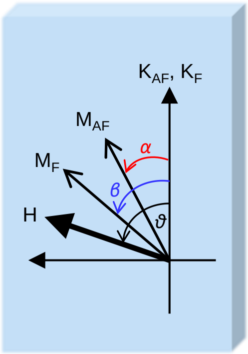

Figure 2.3. Diagram for vectors and energy terms related to the rotational hysteresis in the Meiklejohn and Bean model.

The models considered realistic interfaces has also been proposed with a microscopic perspective. Malozemoff postulated a randomness of the exchange interaction arising from the interfacial roughness[75]. The interaction acts as a random field to AFM layers, which makes the AFM layers breaking into domains. Then, if the AFM layers has different interfacial energy denoted σ_1 and σ_2 in Figure 2.4(a) for two FM domains, the exchange field is determined by balancing between the applied field and the effective energy difference of the interface (σ), expressed by,

$$H_{\mathrm{EB}} = \frac{\Delta\sigma}{2M_{\mathrm{FM}}t_{\mathrm{FM}}}$$

In this case, if the AFM layers are compensated, neighbor AFM sublattices have different spins which result in the net exchange interaction zero. On the contrary, when the AFM layers are uncompensated, the exchange bias value will be the ideally highest. However, observed experimental values were two orders lower than the theoretical results which made the concept of the model assumed most regions for the compensated and a very little of the uncompensated region, depicted in Figure 2.4(b-d).

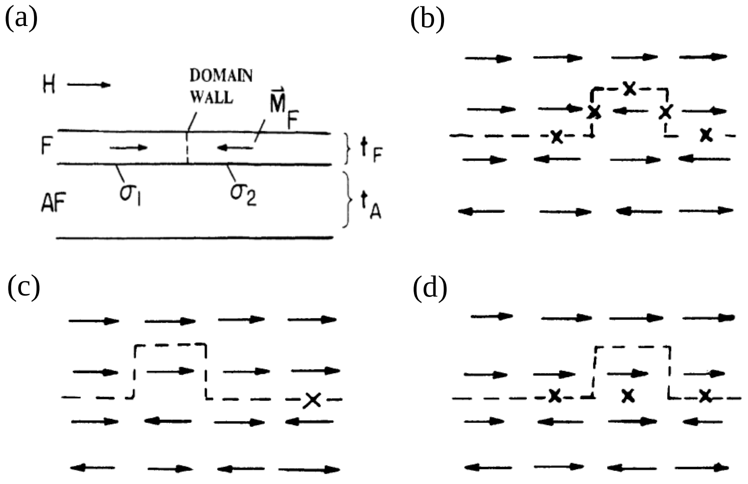

Figure 2.4. Schematic figures of the Malozemoff model. (a) A side view of a FM-AFM sandwich film with a ferromagnetic domain wall driven by H. σ_1 and σ_2 indicate different interfacial energies because of the FM domains. (b-d) Possible spin configurations. (d) Lower energy state of (b). (c) The shifted bump is energetically equivalent to flip the spin of the (b) [reproduced from Reference[75]].

Mauri also tried to find the reason for the different exchange bias values from the experiment and theoretic calculation[76]. One of the possible reasons suggested was poor interface coupling on account of imperfect interfaces, but a fundamental model was also proposed in respect to the formation of the AFM domains parallel to the interface, described in Figure 2.5. The energy relation was also modified with the partial domain wall energy in the fourth term, as below.

$$E_A = -\mu_0 H M_{\mathrm{FM}} t_{\mathrm{FM}} \cos(\theta - \beta) + K_{\mathrm{FM}} t_{\mathrm{FM}} sin^2(\beta)$$

$$-J_{\mathrm{EB}} \cos(\beta - \alpha) - 2\sqrt{A_{AFM} K_{AFM}}(1 - \cos(\alpha))$$

The new relation considered in the total magnetic energy generates the interface energy $\lambda = J_{\mathrm{EB}}/(2\sqrt{A_{\mathrm{AFM}} K_{\mathrm{AFM}}})$, where A is the exchange stiffness constant. This model concluded two limiting cases for the λ. If $\lambda < 1$ which means the strong interfacial coupling, this model is similar with the conventional Meiklejohn and Bean model. However, in the weak coupling condition as $\lambda > 1$, the exchange bias value decreases, depending on the domain wall motion and related parameters. Other models has also made an effort to interpret the phenomenon of exchange bias such as the thermal fluctuation aftereffect model by Fulcomer and Charap[77], the random field model by Imry[78], the domain state model by Nowak[79], the partial domain wall model by Kim and Stamps[80], the spin glass model[72], and so on[81,82].

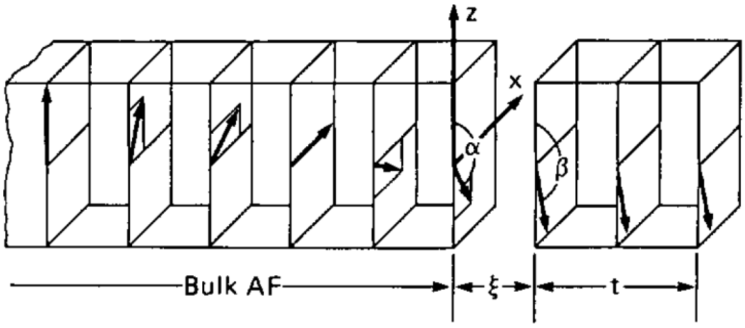

Figure 2.5. Schematics of the Mauri model [reproduced from Reference[76]].

A training effect is one of the symbolic feature of exchange bias. The hysteresis loops with consecutive field sweeps show decrease of the exchange bias effect. Earlier research reported that the decrease via the training effect followed power law dependence, but the analysis considered detail factors resulted in the following relation below[83],

$$H_{\mathrm{EB}}^{n} = H_{\mathrm{EB}}^{\infty} + A_{\mathrm{f}} \exp(-n/P_{\mathrm{f}}) + A_{\mathrm{i}} \exp(-n/P_{\mathrm{i}})$$

where the n is exchange bias of the n^{th} repetition, the f and i mean the frozen spins and evolved interfacial disorder, A and P are parameters related to the spins. The term interfacial disorder contributes sharp decrement with low anisotropy for the initial state, and the frozen spins in the AFM domains contribute a saturated long tail. As exchange bias is defined as the half of the sum of coercivities, both the left and right coercivity are directly related to reduction of the exchange bias. The left coercivity under the FC procedure with a positive magnetic field decreases exponentially with the repetition. On the other hands, the right coercivity in the loop shows various tendencies depending on the exchange-biased system which even results in an opposite sign of exchange bias. The reason for the training effect has been considered as interfacial disorder and the motion of domains through the repetition of magnetic field sweeps. By using magnetometry and magnetoresistance, clear difference among consecutive loops has been reported, explained that the first sharp loop was dominated by domain wall nucleation and domain wall propagation, and the consecutive loops resulted from the rotation of the magnetizations in Figure 2.6. Magnetoresistance results further exhibited the portion of less rotated spins in the exchange-biased system in Figure 2.6(b). Direct evidence for the domain motions also proved through MFM analysis under exchange-biased conditions displaying different field states and domain structures[84], shown in Figure 2.7.

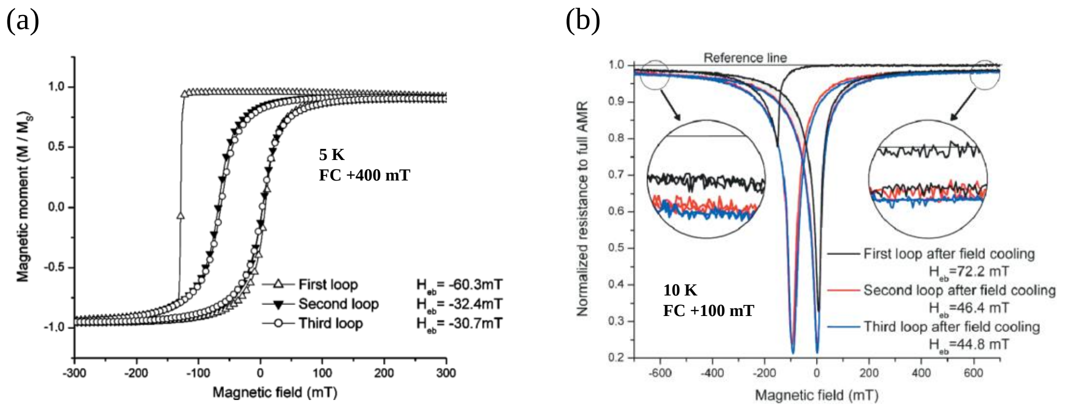

Figure 2.6. Exchange bias and its training effect of a CoO/Co bilayer. (a) Hysteresis loops measured at 5 K with VSM magnetometry after cooling in a field of +400 mT. The first loop at negative field is dominated by domain wall nucleation and domain wall propagation and is abrupt. All consecutive loops

are dominated by rotation of the magnetization and are more rounded. (b) Magnetoresistance at 10 K after cooling in a field of +100 mT applied along the length of the stripe. A smaller resistance change (less rotation) is observed during the first loop when compared to the consecutive reversals. The insets compare the resistance at saturated magnetization to the maximum (reference line), which ideally corresponds to the case of all spins oriented along the cooling field direction [reproduced from Reference[85]].

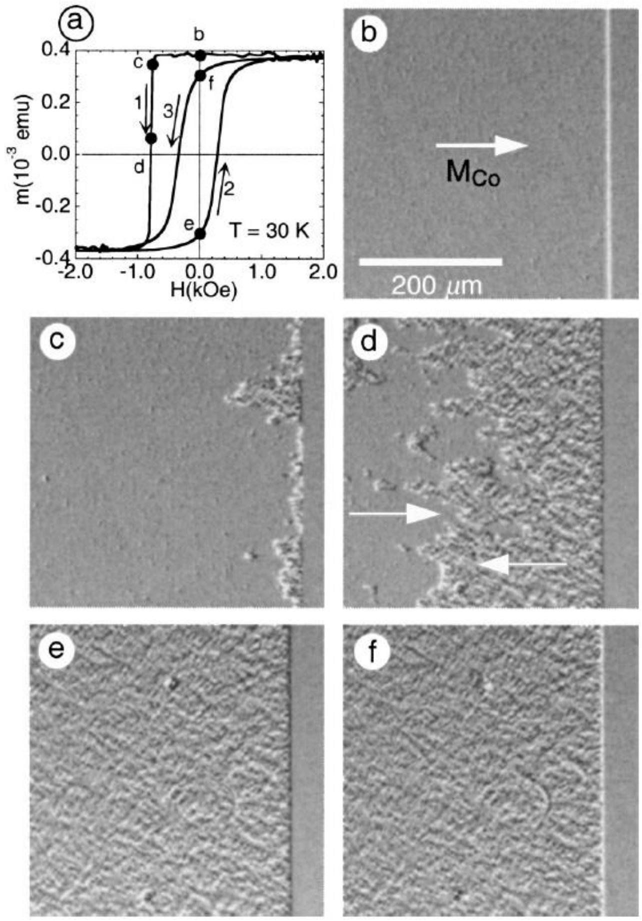

Figure 2.7. Exchange bias and domain structures of a Co/CoO at 30 K along the easy axis after cooling in 10 kOe. (a) Magnetization loop with a denoted sequence from 1 to 3. (b-f) Domain structures corresponding to the states during the magnetic field sweeps in (a) [reproduced from Reference[84]].

2.2. Positive/Negative Exchange Bias

In some interfacial systems between a FM and AFM film, the magnitude and sign of exchange bias can be controlled[86]. When interfacial coupling at a FM/AFM structure is ferromagnetic, the direction of unidirectional anisotropy is to a negative field side via a cooling in a positive applied magnetic field in a FC procedure (H_{FC}). The degree of the anisotropy is not affected by the magnitude of H_{FC}, because the interfacial spins of the AFM layer are parallel to the spins of FM layers. On the other hands, when a FM/AFM structure has antiferromagnetic interfacial coupling, the sign and magnitude of the anisotropy are going to change by varying H_{FC} (Figure 2.8). In the case of low H_{FC} meaning that interfacial exchange coupling between a FM and AFM film is more dominant than the interaction between H_{FC} and AFM layers (Zeemann energy), the interface has antiferromagnetic spin alignment. This stable state in the system results in conventional negative exchange bias which represents that the direction of anisotropy is opposite to the H_{FC} direction. In the case of high H_{FC}, Zeemann energy in the AFM layers overcomes the interfacial exchange coupling, making parallel spin configuration with the FM film (and H_{FC}) at the interface. As the parallel interfacial spins are unstable in this antiferromagnetic interfacial system, a hysteresis loop exhibits positive exchange bias having a same direction to the H_{FC}.

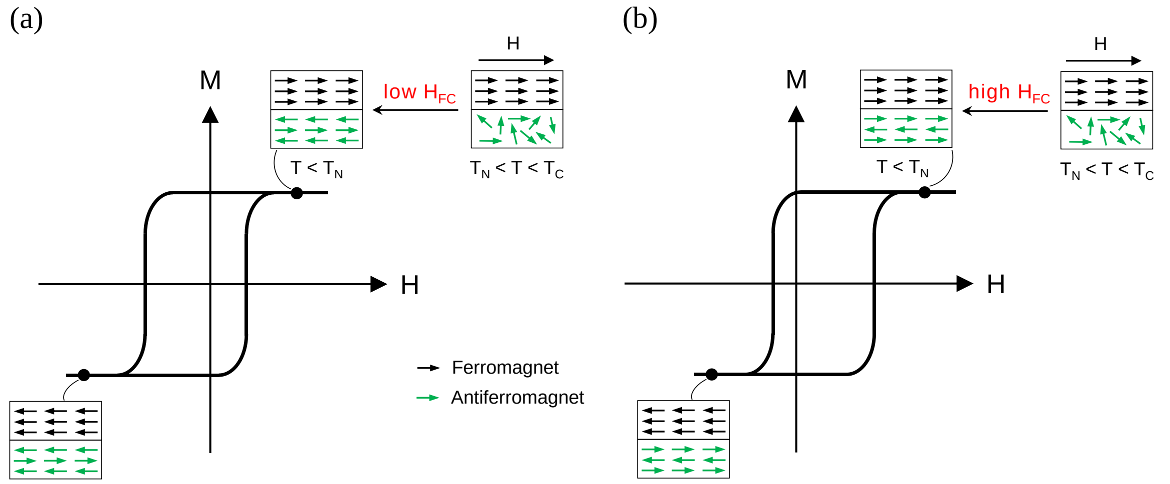

Figure 2.8. Schematic illustrations for exchange bias in an antiferromagnetic interfacial coupling system. Spin configurations for (a) low H_{FC} and (b) high H_{FC} conditions.

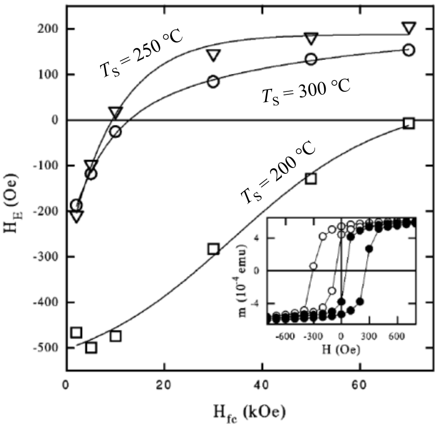

Figure 2.9. Exchange bias of FeF_2/Fe bilayers as a function of H_{FC} at $T = 10$ K for samples with varying FeF_2 grown temperatures (T_S). An inset shows magnetization loops of a T_S = 300 °C sample for H_{FC} = 2 kOe (open circles) and H_{FC} = 70 kOe (closed circles) [reproduced from Reference[86]].

A competition between interfacial exchange coupling and the interaction of H_{FC}-AFM layers was represented by Nogues etc., the first discoverer of positive exchange bias, under several deposition conditions of samples (Figure 2.9)[86]. Comprehensive studies with two interfacial antiferromagnetic systems of FeF_2 and MnF_2 with a ferromagnetic Fe film, clarified the competition theoretically based on experimental results (Figure 2.10). With similar J_{AF} (-1.2 meV and -1.3 meV) for the both cases, the Fe/Fe_2 system having strong $J_{F/AF}$ (-1.2 meV) showed only the changing magnitude of exchange bias but not the inversion of the sign, but the Fe/MnF_2 with comparably weak $J_{F/AF}$ (-0.35 meV) represented both change of the sign and magnitude[87-89]. An XMCD study for an exchange bias system experimentally revealed spin configurations of each element and layer depending on magnetic states of the exchange-biased hysteresis loop (Figure 2.11)[90].

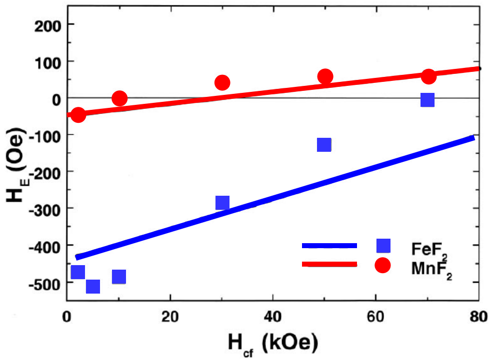

Figure 2.10. H_{FC} dependent H_{EB} for Fe/FeF_2 and Fe/MnF_2. The lines are theoretical results, and the circles and squares correspond to the experimental results [reproduced from Reference[87,89]].

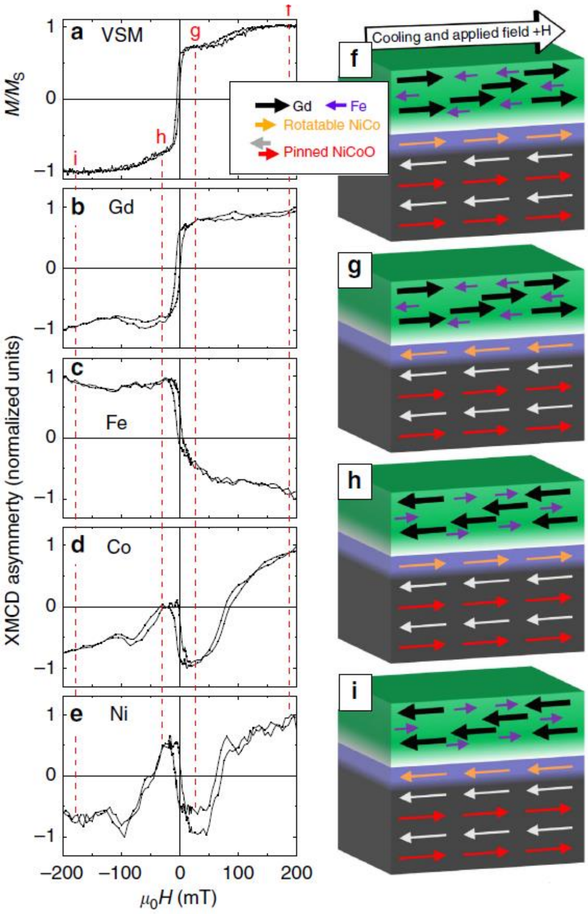

Figure 2.11. Element-specific magnetic hysteresis loops and spin configurations. Hysteresis loops of a Gd$_{0.42}$Fe$_{0.58}$/NiCoO sample measured by (a) VSM and XMCD for (b) Gd, (c) Fe, (d) Co, and (e) Ni at room temperature. (f-i) Schematic illustrations of the spin configuration at various states of the magnetic reversal. Arrows indicate the magnetization direction of each layer [reproduced from Reference[90]].

2.3. Exchange Bias with Molecules

Exchange bias has been one of attractive features that the research of molecular spinterface got interested in, because it can simply and effectively figure out the structure and phenomenon of a FM film, AFM film, and further their interfaces. Initial approach to the exchange bias with molecular interface was started with antiferromagnetic metal Mn and paramagnetic molecule $TbPc_2$ layers[91]. The interfacial elements of Tb and Mn showed ferromagnetic signals in XMCD measurement, meaning that the induced ferromagnetic-like interfacial layer between the paramagnetic $TbPc_2$ and antiferromagnetic Mn layer was pinned by the antiferromagnetic Mn film, realizing exchange bias (Figure 2.12). There was a surprising report displaying clear exchange bias at the structure with paramagnetic molecular MnPc and ferromagnetic Co layers[31]. The peculiar interfacial features were unveiled by XMCD measurement and a theoretical calculation, showing the antiferromagnetic ordered MnPc interlayers on the Co film. These newly developed MnPc layers acted as an AFM film which pinned the underlying Co film presenting exchange bias via a FC procedure (Figure 1.4). One fundamental question has arisen to figure out which layers played an effective role to make exchange bias by acting AFM layers, between an underlying FM and molecule layers. By using different kinds of MPc molecules having various spins from $S = 0$ to $S = 3/2$[92], molecular AFM spin chains from molecular layers[63] and magnetic hardening from underlying FM layers[30] both contributed to induce exchange bias at the hybrid interface. In these points, the hybrid interface between molecules and metals showed its possibility to develop unexpected and interesting functionalities compared to the rigid interface between inorganic matters.

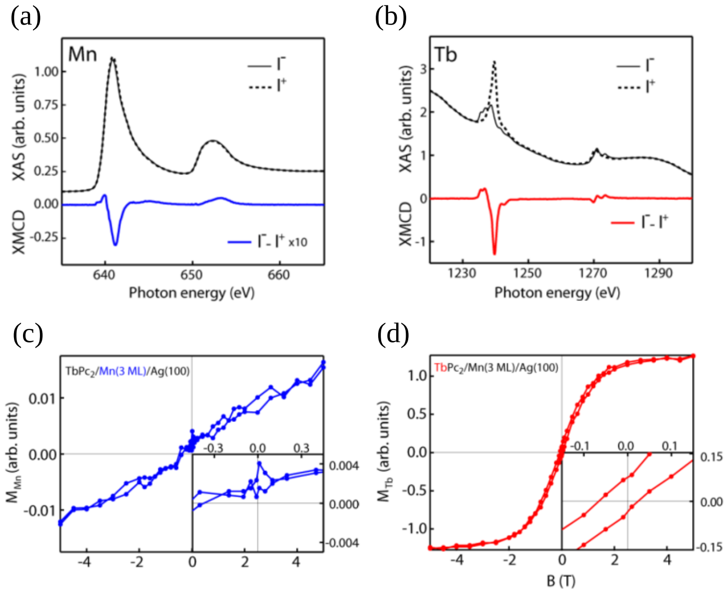

Figure 2.12. Magnetic properties of $TbPc_2$/Mn(3 ML)/Ag at 8 K after a FC procedure with 5 T. XAS and XMCD spectra for (a) $L_{2,3}$ Mn and (b) $M_{4,5}$ Tb edges. Magnetization loops of (a) Mn and (b) Tb. Inset indicates detail of the low field region [reproduced from Reference[91]].

2.4. Applications

An initial use of magnetic materials begun with material itself or simply modified form like a magnetic compass and electromagnet. With fundamental understanding of the magnet, well-engineered magnetic sensors were developed which controlled and detected spin states. AMR, well-known phenomenon in a FM film, was the initial method for reading and writing in a magnetic sensor with its sensitivity and potential in low volume. GMR and TMR have been the next generation technique for a magnetic recording head, having lower volume, suitable geometry, and two orders of magnitude larger than in signal to noise than that of previous AMR head, which could allow the high density of magnetic storage[93], shown in Figure 2.13. In these MR devices consisting of a multilayer structure with two FM films, exchange bias has played an indispensable role for operating as a commercial device. An inserted AFM film made a reference FM film shifted from the center because of exchange bias[94]. In that case, a free FM film only responds to the applied magnetic field that is much smaller than the exchange bias field of the reference FM film, making the device precise and effective as low magnetic field is sufficient for device operations (Figure 2.14).

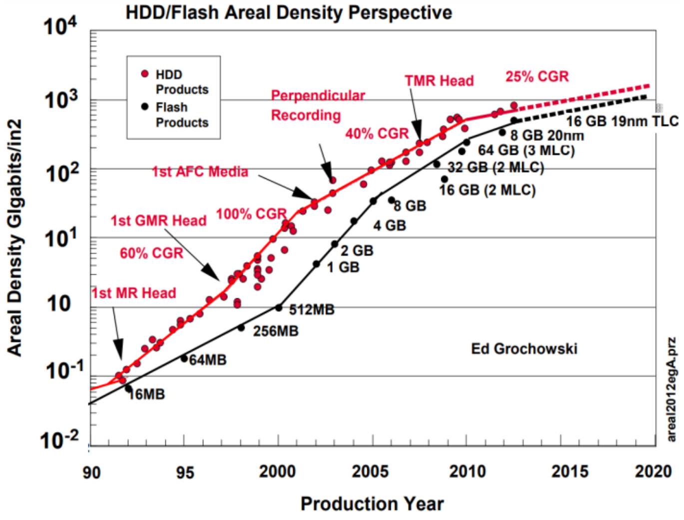

Figure 2.13. Area density for HDD and Flash products [reproduced from Reference[93]].

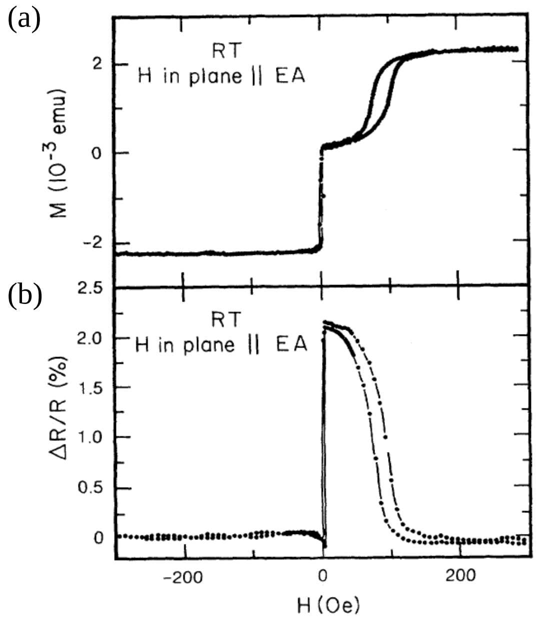

Figure 2.14. Exchange-biased system of a Si/NiFe(150 Å)/Cu(26 Å/NiFe(150 Å)/FeMn(100 Å)/Ag structure. (a) Magnetization curve and (b) relative change in resistance. The magnetic field is applied parallel to the exchange bias field created by the FeMn film [reproduced from Reference[94]].

A recent state-of-the-art application of a magnetic device requires high density and fast switching with reliability. A spin transfer torque (STT) switching method with a MTJ was a promising candidate for a logic device, but low endurance by high current density causing the degradation of an ultra-thin tunnel barrier and questioned reliability owing to use of the same path for reading and writing. Development of spin orbit torque (SOT) device has been expected to overcome the previous problems of the STT by separating a reading and writing path and inducing current in plain direction. Also, the SOT switching even exhibited faster switching than the STT (Figure 2.15). In these switching devices, exchange bias using an antiferromagnetic film also demonstrated an indispensable role. Notably recent studies exhibited magnetic field-free switching of SOT devices[95-97], which can advance the commercialization to device industry (Figure 2.16).

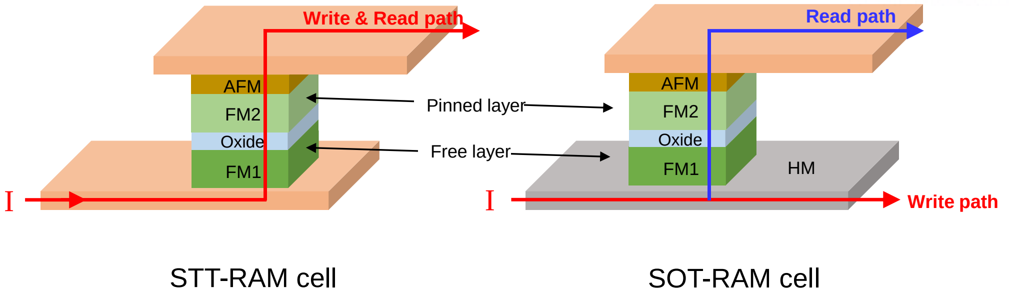

Figure 2.15. Schematic illustrations for magnetic switching devices. A STT device has the same path for write and read, but a SOT device has separated paths.

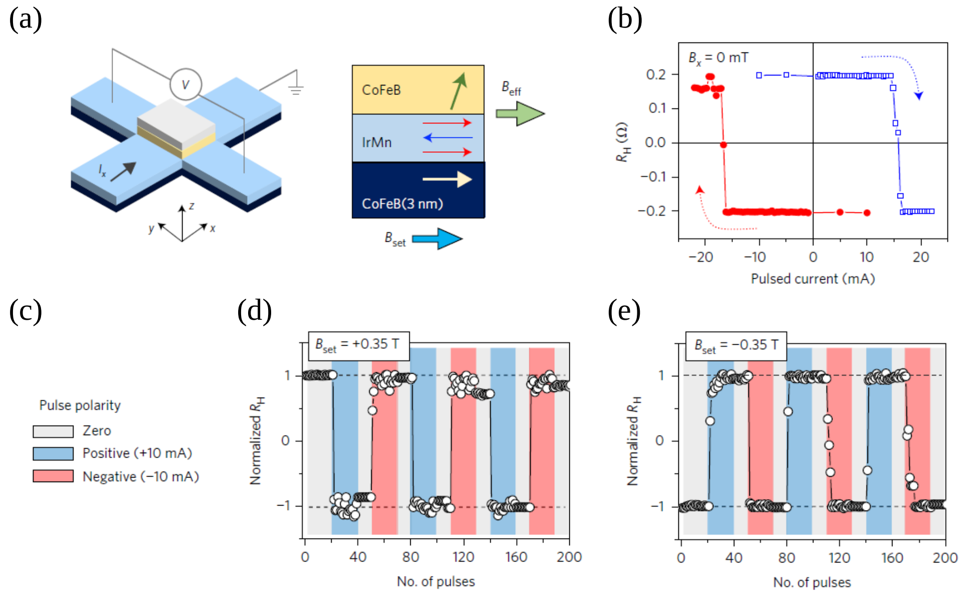

Figure 2.16. Field-free SOT torque switching in a Ta(5 nm)/CoFeB(3 nm)/IrMn(3 nm)/CoFeB /MgO device. (a) A conceptual schematic structure of the SOT device. (b) Field-free SOT switching in the fabricated device (the initial B_{set} = +0.35 T). (d,e) The control of magnetization direction by repeated current pulses of +10 mA, 0 mA, or −10 for B_{set}=+0.35 T and B_{set} = −0.35 T, respectively [reproduce from Reference[96]].

III. Experimental Methods

Characterization of the organic/inorganic interface between the sandwiched bulk films needs interface-sensitive measurements. Differing from the spectroscopic analyses mostly using in-situ deposition and characterization, the sample for magnetoelectrical measurement needs more considerations including a device patterning, capping layer for preventing oxidation, and optimal thickness of films. In this chapter, the process for a sample preparation is introduced step by step. The prepared samples were analyzed by magnetometry and magnetoelectrical transport measurement.

3.1. Sample preparation

Samples were fabricated on a *p*-Si/SiO_2 (300 nm) substrate prepared with a cleaning process with acetone, ethanol, deionized water, and an Ar plasma treatment prior to thin film depositions. A Ta (6 nm) film was used as a buffer layer on the *p*-Si/SiO_2 substrate to enhance the crystallinity of ferromagnetic films. Then, Co (2-8 nm) layers were deposited by using an electron beam evaporation at a typical rate of 0.2 Å/s (Figure 3.1.). A series of the MOEPs (NiOEP, CuOEP, ZnOEP, CoOEP, and FeOEP-Cl) was purchased from Sigma Aldrich. The MOEP powder was sublimed at 220°C and the rate of deposition was critically controlled to be less than 0.2 Å/s to develop a highly uniform hybrid interface. To prevent oxidation of the film, an AlO_x (20 nm) film on top of the MOEP film was deposited. All samples were fabricated at room temperature, unless indicated otherwise. A deposition procedure of all the samples were performed in a high vacuum under a base pressure of 10^{-7} Torr, without breaking a vacuum. The thickness of each layer was controlled with a quartz crystal monitor.

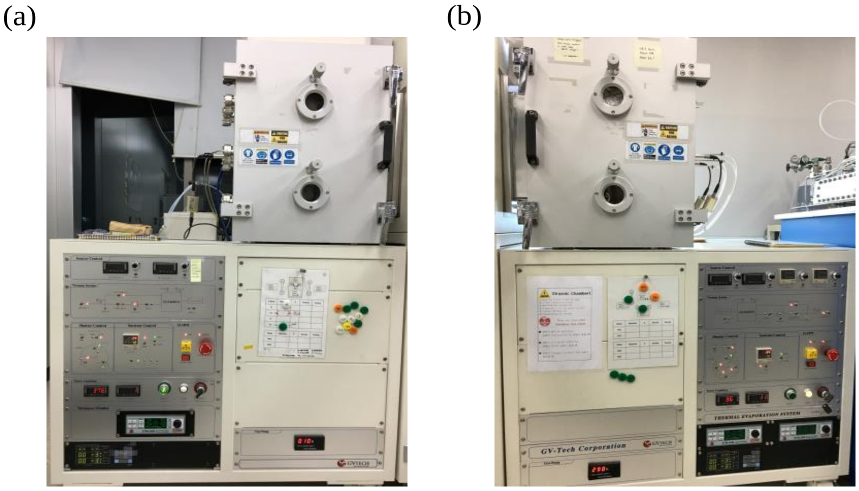

Figure 3.1. Deposition chambers for thin film fabrication. (a) E-beam and thermal deposition chamber. (b) Thermal deposition chamber.

To measure magnetoelectrical properties, a Hall bar pattern was introduced in the deposition process. Because of the importance of the interface, a shadow-mask technique was used to form the films. The Hall geometry for a channel consisted of the width (500~700 μm) and the length (2~3 mm) in the x direction. The width of the y sensing lines was less than 200 μm which satisfied the conventional ratio for the Hall pattern (Figure 3.6(b)). Each contact was comprised of Ti(2 nm)/Au(10 nm) pads.

Deposited FM films on a Ta buffer layer showed smooth roughness, but they did not show atomically smooth surface. The surface of a Co and Fe film displayed R_q = 1.43 Å and R_q = 1.23 Å, respectively (Figure 3.2). X-ray diffraction analysis confirmed the polycrystalline FM films with broaden peaks. The Co film had a FCC (111) structure, and the Fe film had a BCC (110) structure (Figure 3.3). Compared to the metal films, molecule OEP layers had a little bit rough surface with R_q = 2.86 Å, regardless of the series of MOEPs. Thus, deposition of the molecule layer should be under careful conditions, especially about powder pre-heating, deposition rate, and substrate temperature.

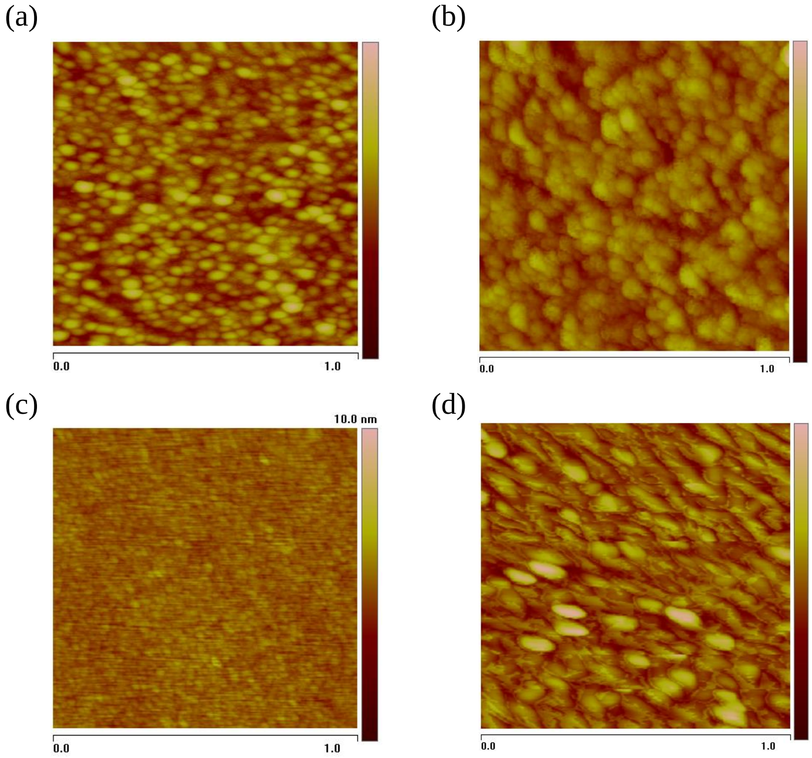

Figure 3.2. AFM images for each film. Surface morphology of a (a) Co film with R_q = 1.43 Å, (b) Fe film with R_q = 1.23 Å, (c) Ta film with R_q = 0.38 Å, and (d) OEP film with R_q = 2.86 Å.

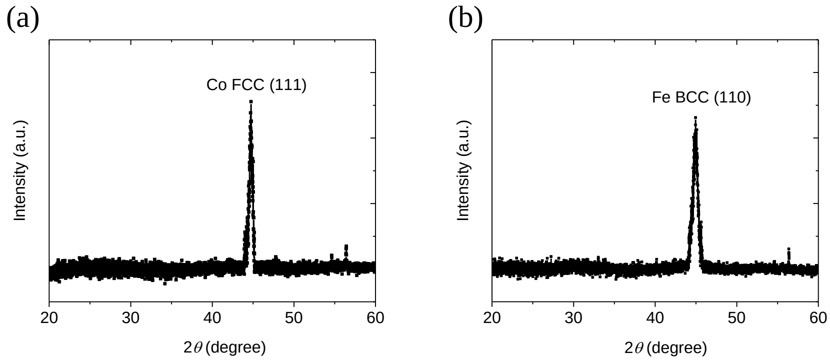

Figure 3.3. XRD data for a Co and Fe film. (a) Diffraction peaks for the Co film. Predominant peaks near 44° indicates the Co film has a polycrystalline FCC (111) structure. (b) XRD peaks for the Fe film. The Fe had a BCC (110) structure. Sharp peaks between 55° ~ 60° came from the substrate both cases in the Co and Fe.

3.2. Measurement

Magnetoelectrical measurement was performed in the chamber of a Physical Property Measurement System (PPMS, Quantum Design). A Hall bar patterned device was attached to a rotator puck and then electrically connected with the contact pads in the device and the puck by copper wires and indium bonding wires (Figure 3.5). The device on the puck was installed to a horizonal rotator which can rotate -5° to 365° in the PPMS chamber. All measurements were in vacuum conditions, but there was not difference between a high and low vacuum condition. As an electrical instrument, Keithley 2636A was adopted for source and measure in local measurement, and Keithley 2182 nano-voltmeter was used for measure in non-local measurement. Considering several conditions like heating effect and the clarity of data for the measurement, applied current was typically less than 500 μA.

FC measurement was started with setting a magnetic field from 0.2 T to 6 T at 300 K and then cooled down to low temperatures. After approaching set temperature, less than an hour was gave to stable the temperature of the sample because the heating/cooling line was a little far from the sample position. All FC procedures were same for all series of FM/MOEP systems to eliminate unwanted side effect. The device was very stable in the period of the measurement. Measurement in the first day and the final fourth day showed identical data.

Figure 3.4. PPMS and Keithley instruments for magnetoelectrical measurement. The PPMS provides a chamber to control a temperature from 1.8 K to 400 K, a magnetic field from 0 T to 9 T, and a high vacuum.

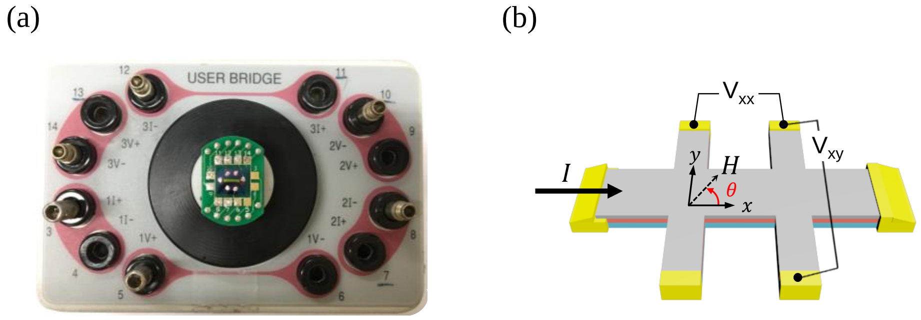

Figure 3.5. A prepared device for magnetoelectrical measurement in the PPMS. (a) Electrically contacted device to the PPMS puck. (b) A Hall bar geometry for the device.

Magnetometry with a Superconducting Quantum Interference Device-Vibrating Sample Magnetometer (SQUID-VSM) in a Magnetic Property Measurement System (MPMS, Quantum Design) was executed with the same kinds of the samples in the magnetoelectrical measurement. A prepared sample covered with thin films in all areas was cut by 4.5 mm x 8 mm and mounted on a plastic capsule. Then, the capsule with the sample was tightly fixed in a plastic straw (Figure 3.7). The plastic capsule and straw were proper substitutes because of low mass compared to the thin film. Also, a *p*-Si/SiO_2 (300 nm) substrate displayed only a diamagnetic signal which was negligibly smaller than the ferromagnetic signal of the thin film itself. Similar with the magnetoelectrical measurement, an investigation via a FC procedure was under careful considerations including stable time, the sweeping rate of a magnetic field, and remanent magnetization. A typical sweeping rate of a magnetic field was less than 20 Oe/s, and the data was recorded less than each 40 Oe step. In the case of a low field scan, much less rate of 2 Oe/s was adopted and recording step was also less than 5 Oe step. All the measurements were performed directly after the deposition of the films to avoid oxidation and unexpected effects, but there was no distinct difference between the fresh sample and the sample after storage in a vacuum for 3 months.

Figure 3.6. MPMS for magnetometry. The MPMS allows to control a temperature from 1.8 K to 400 K and a magnetic field from 0 T to 7 T.

Figure 3.7. A prepared sample in a gelatin capsule for magnetometry in the MPMS.

IV. Exchange Bias in Co/MOEP Systems with Interfacial Ferromagnetic Coupling

Molecular spins as individual are promising quantum states for emerging computation technologies. The “on surface” configuration of molecules in proximity to a magnetic film allows control over the orientations of molecular spins and coupling between them. The stacking of planar molecular spins could favor antiferromagnetic interlayer couplings and lead to pinning of the magnetic underlayer via exchange bias, which is extensively utilized in ultrafast and high-density spintronics. However, a fundamental understanding of the molecular exchange bias and its operating features on a device has not been unveiled. Here, this study showed a tunable molecular exchange bias and its asymmetrical magnetotransport characteristics on a device by using the hybrid interface of metalloporphyrin/ ferromagnetic Co films. A series of the distinctive molecular layers showcased a wide range of interfacial exchange coupling and bias. The transport behavior of the hybrid bilayer films revealed the molecular exchange bias effect on a fabricated device, representing asymmetric behaviors on anisotropic and angle-dependent magnetoresistances. Theoretical simulations demonstrated close correlations among the interfacial distance, magnetic interaction, and exchange bias. This study of the hybrid interfacial coupling and its impact on magnetic and magnetotransport behaviors will extend functionalities of molecular spinterfaces for emerging information technologies.

4.1. Motivation

Molecular spins have been considered as intriguing platforms for exploring spin-dependent phenomena at the nanoscale with promising potential for data storage and computation technologies[98-100]. Applications of molecular spins for information technology have traditionally approached based on switchable magnetic ground states via classical thermodynamics[101], photo-induced excitations[102,103], and quantum spin tunneling[104,105]. With the emergence of spintronics, the long-lived spin states and their transport in molecular species have been extensively explored by injecting spin currents from ferromagnetic electrodes[15,106-108]. Later, molecular magnetic films were further successfully employed for polarizing itinerant electron spins[109,110]. The metal-organic interfaces in hybrid magnetic devices often form strong interfacial interactions, which can even break the spin degeneracy of molecular orbitals at the interface[28,30,111-114]. This so called “organic spinterface” leads to a spin selective tunnel barrier improving on-off ratios of the spin valve devices[28,30]. Besides, charge transfer at the metal-organic hybrid interfaces could even transform non-magnetic metallic films to be ferromagnets by modifying the Stoner’s criterion[115].

Molecular species carrying unpaired electron spins offer further tuning of interfacial magnetic coupling. The "on-surface" configuration of molecules with ferromagnetic thin films provides an archetype platform for studying couplings between molecular spins and their environment, which have been extensively studied with planar organometallic complexes, such as metalloporphyrins[43-45,51,55,116] and metallophthalocyanies[33,68,117-120]. Individual unpaired spins in these complexes have shown to exhibit exchange coupling to magnetic substrates[48,50], and they could couple themselves not only over the entire surface also across further stacking layers. Some of these organometallic stacks may form antiferromagnetic interlayer couplings[120] that can even induce exchange bias to the underlying ferromagnetic films[31]. Subsequent study reported the contribution of molecular magnetic hardening effect on the exchange bias at the hybrid interface[92].

Exchange bias in an antiferromagnet/ferromagnet film is a key element in spintronics. Exchange coupling at the interface between an antiferromagnet and ferromagnet, facilitated by a magnetic field-cooling procedure, strongly pins the magnetization of an entire ferromagnet. Thus, the ferromagnet should cost extra energy to reverse its spin, resulting in the shift of a magnetic hysteresis loop as well as broadening of the loop[31,72,121-123]. These features render the exchange bias indispensable to commercial magnetic read heads and nonvolatile magnetic memory technologies[124-126]. Moreover, the exchange bias expands the scope of its functionality to state-of-the-art spin-orbit torque devices, enabling field-free ultrafast switching of magnetization[96,97,127]. Thus, fundamental studies of the exchange bias in metal-organic hybrid interfaces are essential for extending the functionality of molecular spins in spintronic applications.

In this work, the emergence of molecular magnetic exchange bias and its tunability at the hybrid interface between metalloporphyrin and ferromagnetic cobalt films has been demonstrated. In particular, the molecular magnetic exchange bias was shown to be as high as 170 mT at 10 K. Magnetotransport studies in the hybrid devices provided an alternative assessment of the exchange bias by measuring anisotropic and angle-dependent magnetoresistances, which are essential ingredients to expand spintronics applications of the hybrid magnetic layers. The emergent magnetic interaction and ordering predicted by theoretical simulations at the studied hybrid interfaces are amenable to display such a large magnetic exchange bias. The interfacial interactions between a metal substrate and metalloporphyrin molecule and the interaction between subsequent molecular layers were found to rely on the indirect coupling. The magnetic moments of the planar stacked metalloporphyrins were highly affected by the surface effect, producing incommensurate antiferromagnetic layers. These fundamental understanding of the molecular interfacial coupling and transport behaviors at the hybrid layers will certainly extend the use of molecular spinterfaces for a variety of functional spin-electronic applications.

4.2. Experimental Methods

Devices were fabricated on a *p*-Si/SiO$_2$(300 nm) substrate prepared with an Ar plasma treatment prior to thin film depositions. A Ta(6 nm) film was used as a buffer layer[128] on the *p*-Si/SiO$_2$ substrate. Then, Co(2-8 nm) layers were deposited by using an electron beam evaporator at a typical rate of 0.2 Å/s. A series of the MOEPs (NiOEP, CuOEP, and ZnOEP) was purchased from Sigma Aldrich. The MOEP films were sublimed at 220°C and the rate of deposition was critically controlled to be less than 0.2 Å/s to develop a highly uniform hybrid interface. To prevent oxidation of the film, an AlO$_x$ (20 nm) film was deposited on top of the MOEP film. All samples included a Ta buffer layer and AlO$_x$ capping layer, unless indicated otherwise. The sample fabrication procedure was performed in a high-vacuum under a base pressure of 10^{-7} Torr without breaking the vacuum. The thickness of each layer was controlled by using a quartz crystal monitor.

Magnetic properties were measured using a SQUID-VSM (Quantum Design) magnetometer. The sample (4 mm × 6 mm) was placed in a gelatin capsule and fixed in a plastic straw to minimize unnecessary background signals. Measurements were performed in a static field mode with an 1 mT step for a small field range and an 20 mT step for a high field range. Three to four samples were used to determine the reproducibility of the thickness-dependent data. All measurements were collected immediately after sample fabrication to minimize unexpected changes, although consistent results were obtained, even after storage under a low vacuum over a few months. Measurements for exchange bias were performed after cooling the sample under an applied in-plane field from 300 K to a low temperature at which the experiments were performed.

The electrical measurement was carried out in a PPMS (Quantum Design) with a horizontal rotator. A Keithley 2636 and Keithley 2182A nanovoltmeter were used for a current source and voltage measurement. The Hall bar pattern was fabricated using two shadow mask geometries; one was used for the Ta/Co/OEP/AlO$_x$ channel with dimensions of 500 μm width and 2 mm length, and the other was used for the leads to detect Hall voltage with dimensions of 200 μm width and 1 mm length. The current applied at the Hall bar channel was 500 μA, which displayed the highest precision for measurements without heating effects. The magnetic field sweep rate remained fixed for the magnetotransport measurements to reduce confounding factors relating to the magnetic properties. Angle-dependent magnetoresistance were collected with a rotational rate of 0.24°/s in the sweep mode, and there was no delay between the measurements for a positive (0° to 360°) and negative (360° to 0°) angle scan.

All calculations were carried out using DFT with the plane wave-based Vienna Ab initio Simulation Package[129]. The projector augmented wave method of Blöchl[130] in the implementation of Kresse and Joubert[131] was used. The Perdew–Burke–Ernzerhof (PBE) generalized gradient approximation (GGA) was employed for the exchange-correlation functional. The Hubbard U_{eff} = 3.0 eV (U = 4, J = 1) was used to consider the on-site Coulomb repulsion in the metal octaethylporphyrins. An energy cut-off of 450 eV for the plane wave and a gamma point k-point mesh were used for geometry optimization. The 2 × 2 × 1 k-point meshes were used for the density of states and magnetization calculations. The calculations were converged in energy to 5×10^{-4} eV/cell, and the geometries were allowed to relax until the forces did not exceed 5×10^{-2} eV/Å. Three unit cells of the Co layer consisting of 192 atoms, oriented as (111), were considered to be the substrate. A large cell size of 30 Å along the stacking direction was used to avoid the spurious interactions within the Co/OEP systems.

4.3. Magnetometry Analysis

This study focused on realizing an exchange-biased system in a bilayer composed of a ferromagnetic cobalt (Co) film and an organic film of paramagnetic octaethyl-porphyrin (MOEP, M = Ni, Cu, and Zn) molecules, which accommodated ionized metal atoms as M^{2+} at the center. A schematic diagram in Figure 4.1(a) illustrates the bilayer system comprising planarly stacked MOEP layers on a Co substrate. Figure 4.1(b-d) displays magnetic hysteresis loops of Ta(6 nm)/Co(4 nm)/MOEP(8 nm)/AlO_x structures (denoted as Co/MOEP systems) measured at 10 K after cooling the samples under applied magnetic fields of +2 T (black) or -2 T (red). The observed hysteresis loops showed significant broadening in all the Co/MOEP systems. The widths of the hysteresis loops for the Co/MOEP bilayers were typically about 100 mT, which is two orders of magnitude wider than that of our Co film without MOEP (Figure 4.2). In particular, the recorded magnetization for the FC sample with +2 T displayed a shifted hysteresis loop to the opposite direction of the applied field. The same trend was observed for the negative FC sample with −2 T, and the degree of the shift was nearly identical to that obtained from the positive FC sample. These features suggested the presence of the magnetic exchange bias arising from the interfacial interactions between the Co and MOEP layers. Note that the observed exchange bias did not originate from a Co/CoO structure owing to the surface oxidation of the Co layer. A reference sample of a Ta(6 nm)/Co(4 nm)/AlO_x structure was tested to confirm the absence of exchange bias without MOEP layers (Figure 4.2). Another Co/FeOEP-Cl bilayer was also tested magnetization, where a chlorine (Cl) atom attached on the planar FeOEP would prohibit a planar stacking of molecules as well as the antiferromagnetic interlayer coupling (Figure 4.2). The observed hysteresis loop was nearly identical to a Co bare layer, indicating the important role of molecular spin textures in inducing both magnetic hardening and magnetic pinning effect. In addition to the Co/MOEP, a series of FM films (Fe, Ni, and Py ($Ni_{80}Fe_{20}$)) was tested for the exchange bias induced by AFM molecular stacking. All the series of the FM films showed exchange bias with significant variation (Figure 4.3). The Co was chosen as the underlying FM film for the further study of molecular tunability of the exchange bias with various MOEP layers because this structure displayed largest magnitude of the molecular exchange bias. The magnitude of exchange bias is generally defined as $H_{\mathrm{EB}} = (H_{\mathrm{c}}^{+} + H_{\mathrm{c}}^{-})/2$, where H_{c}^{+} and H_{c}^{-} are the coercivities in positive and negative fields. At 10 K, the values of H_{EB} for NiOEP, CuOEP, and ZnOEP were estimated to be -170 mT, -162 mT, and -95 mT, respectively. Note that the degree of the exchange bias far exceeded that observed in the Co/MnPc[31]. The magnitudes of exchange bias were significantly dependent on the central metal ion in MOEP. These results assured of the existence of ferromagnetic exchange coupling at the interface between the Co and the first monolayer of MOEP as well as antiferromagnetic coupling between subsequent MOEP layers, which will be confirmed by first-principles calculations.

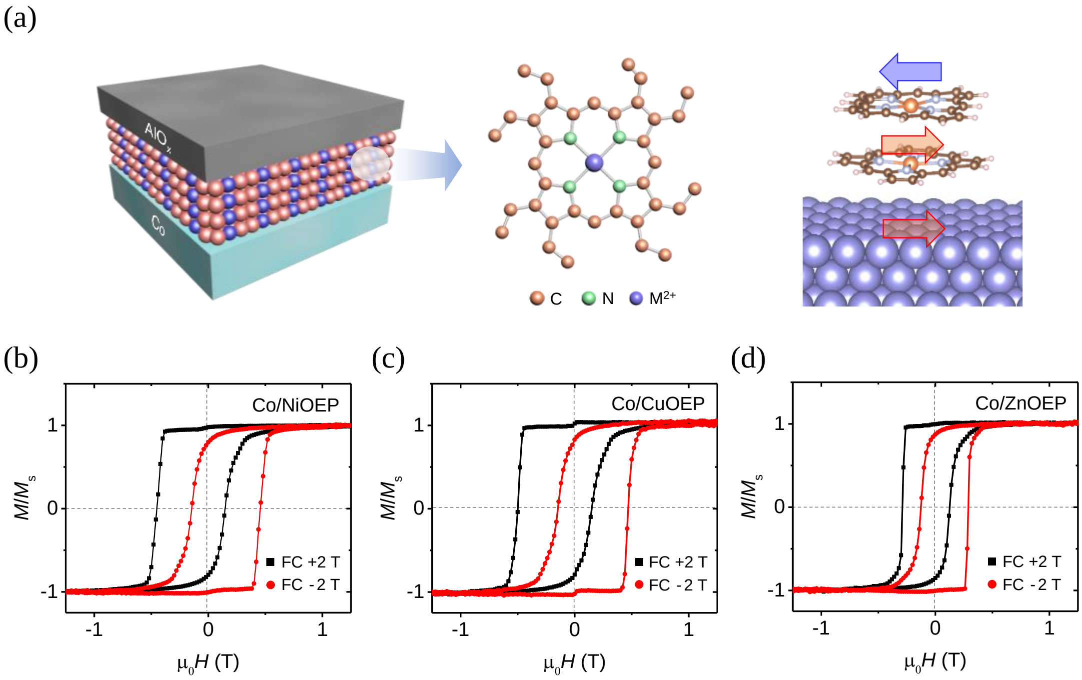

Figure 4.1. Exchange bias at the hybrid interfaces of Co/MOEP systems (M = Ni, Cu, or Zn). (a) Schematic illustration of the Co/MOEP bilayer and magnetic coupling therein. The planar MOEP molecules were stacked on the Co(111) substrate. A conceived magnetic ordering to induce the exchange bias at the hybrid interface is represented on the right side. (b-d) Normalized magnetic hysteresis loops of the Co(4 nm)/NiOEP(8 nm), Co(4 nm)/CuOEP(8 nm), and Co(4 nm)/ZnOEP(8 nm) samples, respectively. Measurements were performed at 10 K after cooling the samples under the applied fields of +2 T (■) and -2 T (●). Each system displayed exchange bias characterized by a unidirectional shift in the hysteresis loop from the center. The magnitudes of exchange biases H_{EB} for the NiOEP, CuOEP, and ZnOEP systems were estimated to be -170 mT, -162 mT, and -95 mT, respectively.

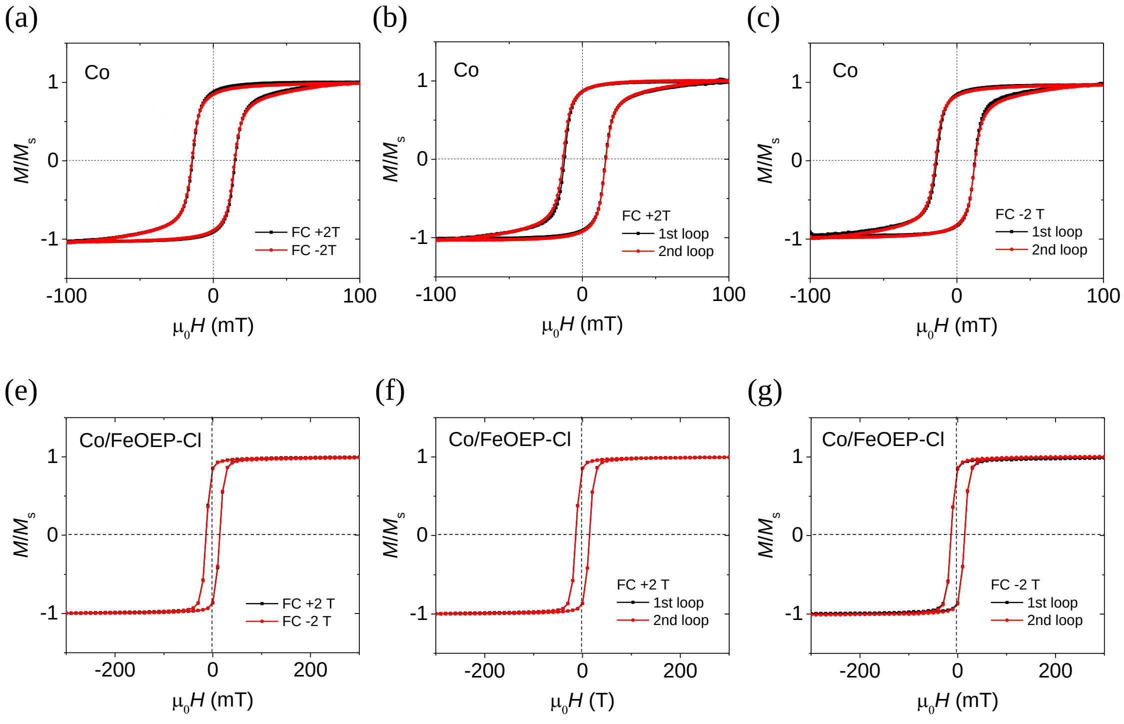

Figure 4.2. Absence of unidirectional anisotropy in hysteresis loops of a Co/AlO_x and Co/FeOEP-Cl/AlO_x structure at 10 K with a FC procedure. (a) Magnetization measured for a control sample of a Co(4 nm)/AlO_x film with FC +2 T (black) and -2 T (red). (b,c) Consecutive hysteresis loops measured for the FC sample with FC +2 T and -2 T, respectively. (e) Magnetic hysteresis loop for a Co(6 nm)/FeOEP-Cl(8 nm)/AlO_x. (f,g) Consecutive hysteresis loops measured for the FC sample with +2 T and -2 T, respectively. A cholrin (Cl) atom attached on the planar FeOEP would prohibit planar stacking of molecules as well as the antiferromagnetic interlayer coupling, leading to absence of exchange bias.

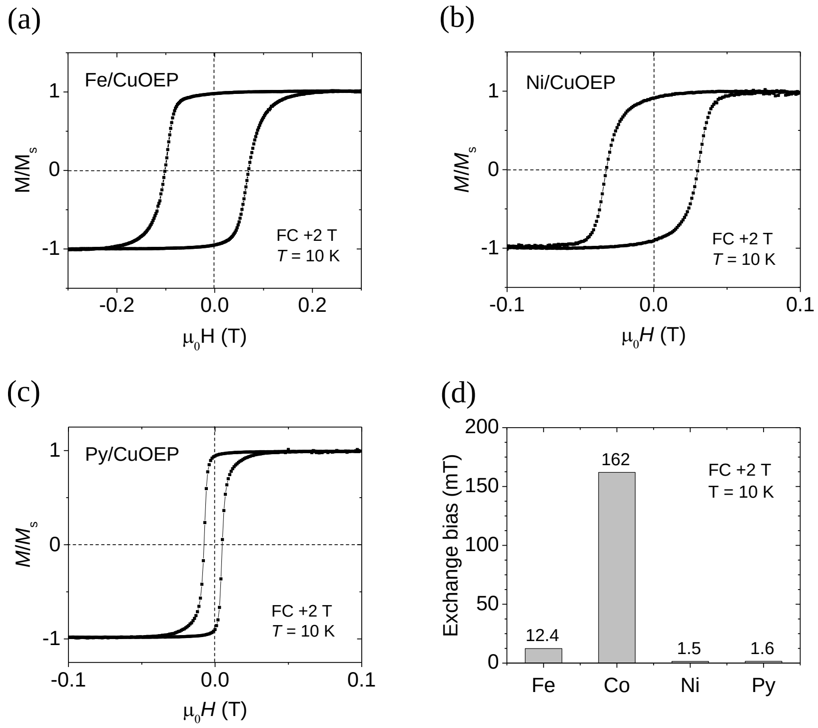

Figure 4.3. Magnetization for various FM(4 nm)/CuOEP(8 nm)/AlO$_x$ films at 10 K. All measurements were performed after field cooling with +2 T from 300 K to 10 K. All samples showed exchange bias as (a) 12.4 mT for the Fe/CuOEP, (b) 1.5 mT for the Ni/CuOEP, and (c) 1.6 mT for the Py/CuOEP. (d) A plot for ferromagnet-dependent exchange bias values.

Further experiments were performed to establish the exchange bias of the Co/MOEP systems in detail. Figure 4.4 displays the recorded hysteresis loops for a Co/NiOEP bilayer at various temperatures. The exchange bias and hysteresis width were reduced at higher temperatures. Then, the exchange bias disappeared as the temperature approached the blocking temperature (T_B) (Figure 4.4(a,b)). The temperature dependence of exchange bias depends on the characteristics of spin systems. It is known that the exchange bias in conventional spin systems is usually inversely proportional to temperature[132]. By contrast, the Co/MOEP systems follow an exponential dependence, which typically occurs in frustrated spin systems, ferro/antiferro-superlattices, and so on[133,134]. Such temperature dependence can be described with the phenomenological formulas, as follows,

$$H_{\mathrm{EB}}(T) = H_{\mathrm{EB}}^{0} \cdot \exp(-T/T_1) \qquad (1)$$

$$H_{\mathrm{C}}(T) = H_{\mathrm{C}}^{0} \cdot \exp(-T/T_2) \qquad (2)$$

where H^0_{EB} and H^0_{c} are the extrapolations to the absolute zero, and T_1 and T_2 are constants. According to Figure 4.4(b,c), the blocking temperatures of the Co/NiOEP and Co/CuOEP system exceed 150 K. However, it would be around 100 K for the Co/ZnOEP system. The overall temperature dependence of H_{EB} could be fit to the equation (1), as indicated by the solid line in Figure 4.4(b). The width of the hysteresis loop agreed well with the equation (2), with slight deviations at the intermediate temperatures (from 100 K to 200 K). Note that our vacuum-deposited molecular films could have partially irregular layered structure, but the temperature dependent behavior of exchange bias and loop width do not display a peculiar peak which has been observed in the exchange bias systems induced by strong frustration[72,135]. The observed hysteresis loops in our hybrid films do not completely shift to one polarity of magnetic field. This incomplete loop shift can be also attributed to the presence of frustration by some degree as our molecular film likely includes disordered regions. These deviations may indicate enhanced thermal excitation at higher temperatures[134]. Another notable feature of the observed hysteresis loops was the asymmetry of the magnetization reversal curve (Figure 4.4(a)). After cooling to a low temperature under a positive magnetic field, the first magnetization reversal observed during a positive to a negative field scan displayed a sharp turn. However, this reversal became more rounded during the following opposite sweep. Subsequent hysteresis loops displayed decreased coercivity with a rounded shape in both field sweep directions. Further decrements in the coercivity over repeated field scans were negligible (Figure 4.5). This feature is generally referred to as the training effect in exchange bias systems[74]. Differences in the hysteresis loops of the first and the subsequent field sweeps could be described by using the following mechanism. The first abrupt magnetization reversal is the consequence of domain wall nucleation and propagation, whereas the subsequent s-shaped reversals originate from magnetization reversal through domain rotation[136,137]. The different process of the magnetic reversal originates from the reconstruction of AFM domain during the first field sweep resulting in the formation of pinned domain that is perpendicular to the interface[138-140]. Consecutive field sweeps made the exchange bias to be saturated (Figure 4.5). The residual exchange bias after completing 50 cycles of field sweep was -55 mT and -45 mT for the Co/NiOEP and Co/CuOEP, and a comparably small value of -16 mT for the Co/ZnOEP. The thickness of a FM film is a critical factor for the magnitude of exchange bias. As the driving energy for exchange bias relies on the exchange coupling at the interface, increasing the thickness of a FM film generally reduces the magnitude of exchange bias. Figure 4.4(e) shows the obtained H_{EB} for various thicknesses of Co layers (2, 4, 6, and 8 nm) with a fixed OEP thickness (8 nm). The thickness dependence of the exchange bias in our Co/OEP systems followed a conventional $1/t_{\mathrm{FM}}$ dependence for 4, 6, and 8 nm thick Co layers. Deviations from $1/t_{\mathrm{FM}}$ were observed for systems with 2 nm Co layers, which can be attributed to the inhomogeneity of the thin Co layer. Such deviations from $1/t_{\mathrm{FM}}$ have also been observed in various conventional FM/AFM bilayers and depend on the microstructure of the ultrathin FM layer[74,141].

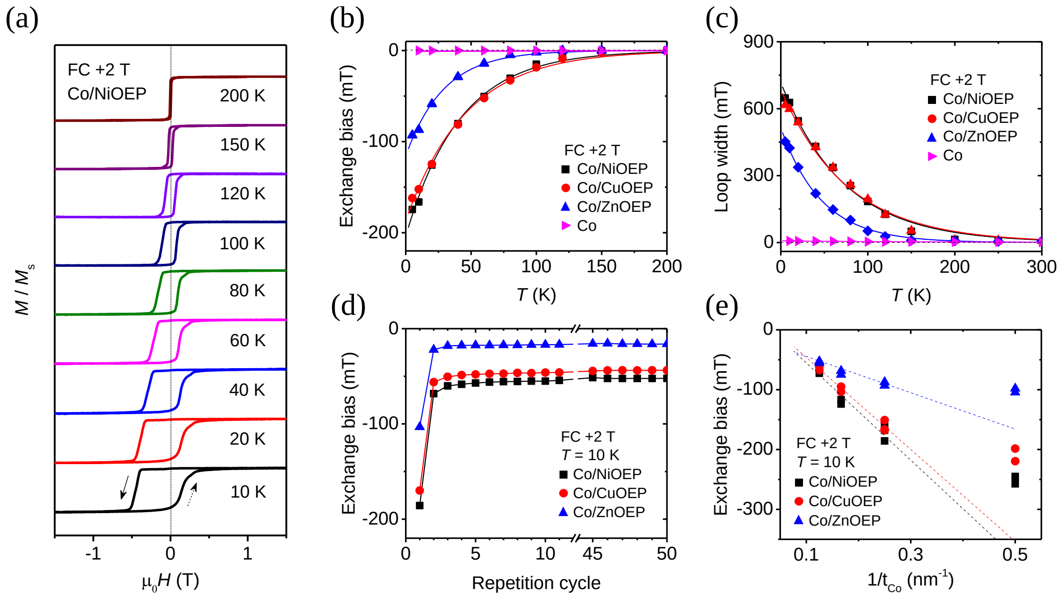

Figure 4.4. Magnetic characteristics in the series of Co/MOEP systems. (a) Magnetic hysteresis loops of a Co/NiOEP bilayer measured at different temperatures for a FC sample with +2 T. Hysteresis loops were shifted from the center and broadened, and the anisotropy was gradually decreased as the temperature increased. (b) The temperature dependence of exchange biases in the Co/MOEP systems. The measured exchange bias was decreased exponentially as the temperature increased. The results agreed well with the fitting curves (solid line) by the equation (1). (c) The temperature dependence of hysteresis loop widths of Co/MOEP systems. The results were in good agreement with the fitting curves (solid line) by the equation (2). A control sample prepared without MOEP (▶ in b, c) exhibited zero exchange bias and a much narrower loop. (d) Evolution of the exchange bias obtained by the consecutive field sweeps for Co/MOEP systems. Initially, the measured exchange bias displayed rapid drop for the repeated measurements, but it approached saturation after 5 cycles, and this bias was maintained over 50 cycles. (e) Exchange bias as a function of the Co layer thickness in Co/MOEP systems. Increasing the thickness of the Co layer reduced the exchange bias of our hybrid films. The solid lines are the guide to eye.

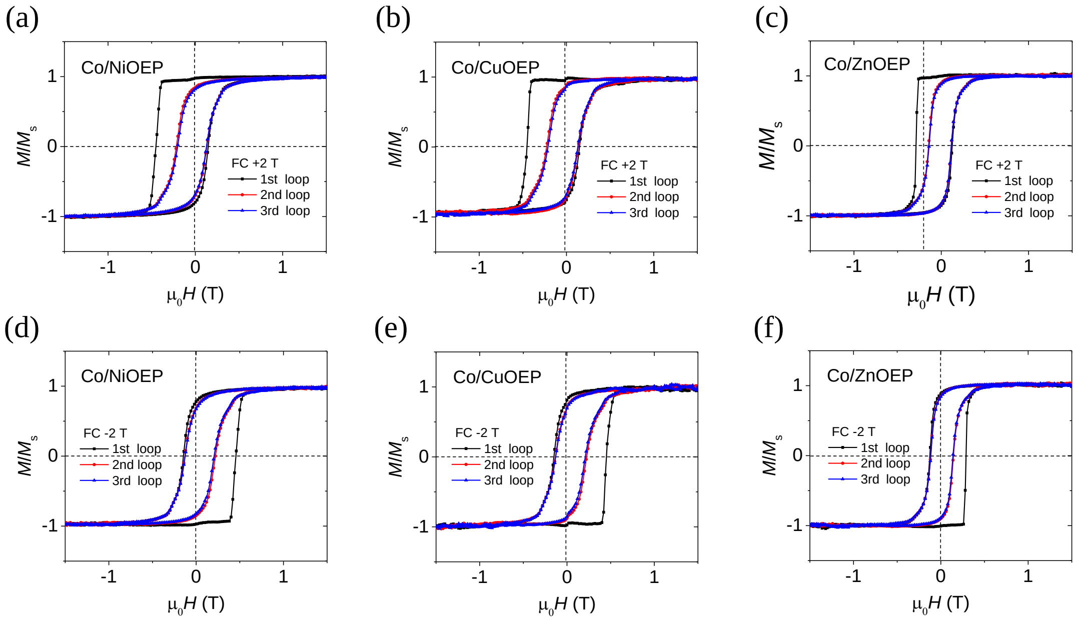

Figure 4.5. Magnetization curves of repeated measurements for FC samples with ±2 T at 10 K. (a-c) Normalized hysteresis loops of Co(4 nm)/MOEP(8 nm)/AlO$_x$ (M=Ni, Cu, and Zn) systems measured for FC samples with +2 T. (d-f) Normalized hysteresis loops measured for FC samples with -2 T. Results exhibit nearly saturation behavior of H_{EB} after the second cycle

4.4. Magnetotransport Analysis

Magnetotransport measurements are essential to characterize the Co/MOEP hybrid bilayers and further realize the device applications. A conventional Hall bar geometry was used to measure the anisotropic magnetoresistance (AMR) and the planar Hall resistance (PHR) in a representative Co/NiOEP bilayer. All measurements were carried out under a magnetic field applied in the sample plane, with an angle (θ) between the magnetic field and current (Figure 4.6). The AMR and PHR for a single-domain model are described as $R_{\mathrm{AMR}}(\theta) = R_{\perp} + (R_{\parallel} - R_{\perp})\cos^2\theta$ and $R_{\mathrm{PHR}}(\theta) = (R_{\parallel} - R_{\perp})\cos\theta\sin\theta$, where $R_{\parallel}$ and $R_{\perp}$ are the resistances in response to the applied magnetic fields parallel and perpendicular to a current direction, respectively. Figure 4.6(b) exhibits the angle-dependent AMR and PHR measured at 300 K under a magnetic field of +2 T. The AMR and PHR showed a sinusoidal variation of magnitude as a function of angle which are identical for both a positive (θ= 0° to 360°) and negative (θ= 360° to 0°) angle sweep. A difference between the positive and negative sweep were observed at low temperatures when the sample was FC under +2 T. The measured AMR and PHR curves were shifted to the opposite direction depending on the angle sweep direction (Figure 4.6(c,d)). In the case of the AMR at 10 K, the first highest peak for the positive sweep was located at θ= 8° instead of θ= 0°. The second peak appeared at θ= 188°, whereas the corresponding second peak of the negative sweep was located at θ= 172°. These shifts in the angle-dependent AMR and PHR is the characteristic behavior of exchange bias[142,143]. As the temperature increased, the shift gradually disappeared and became negligible at T > 150 K, which corresponded to the blocking temperature estimated from the magnetization results. Similar trends of the angle shifts were also observed in the PHR measurements (Figure 4.6(d)).

The training effect of the exchange bias in a Co/NiOEP bilayer can be also probed through magnetotransport measurements. Figure 4.7(a) shows the AMR measured at 10 K after a sample was FC with +2 T from 300 K. The measurements were performed with an applied magnetic field parallel to the current direction (θ= 0°) for all repeated field sweeps. The first AMR curves showed a strong asymmetry of coercivities and a significantly reduced AMR, reflecting the process of magnetic inversion is different from the subsequent field sweeps[144]. During the subsequent field sweeps, the asymmetry was significantly reduced, reflecting the training effect. Also, there was a distinct feature that the maximum resistance in the AMR under a negative field decreased by 4.7%, compared to the maximum resistance under a positive field, denoted as the dashed line (Figure 4.7(a)). This decreased resistance at the opposite magnetic field to the FC direction in AMR is associated with the unidirectional magnetic anisotropy induced by molecular exchange bias observed in Co/CoPc/Co[145]. Incompletely aligned Co spins to the applied magnetic field due to exchange bias can partially make the smaller scattering cross-section of orbitals, resulting in the lower resistance state. In the microscopic viewpoint, the exchange biased hybrid layers undergo partial domain pinning during domain wall nucleation and propagation in the first magnetic field sweep, which can cause the incompletely aligned Co layer in a negatively saturated magnetic field (opposite to the direction of FC)[137,144,146]. Consecutive PHR measurements also reproduced the training effect with a missing upturn peak at the first reversal and a steady feature in subsequent curves (Figure 4.7(b)). The temperature dependence of AMR shown displayed asymmetries including a coercivity and the magnitude of the AMR, which gradually disappeared as the temperature approached 150 K (Figure 4.7(c)). These magnetotransport behaviors were consistent with the magnetometry results. Also, other Co/MOEP systems was tested for magnetotransport behaviors, which exhibited consistent features of exchange bias (Figure 4.8). To summarize the observed features in this exchange bias system, three different analysis data of the Co/NiOEP bilayer was arrayed in a single plot (Figure 4.7(d)). This plot shows that the exchange bias fields in the studied hybrid films probed via various experimental methods are identical.

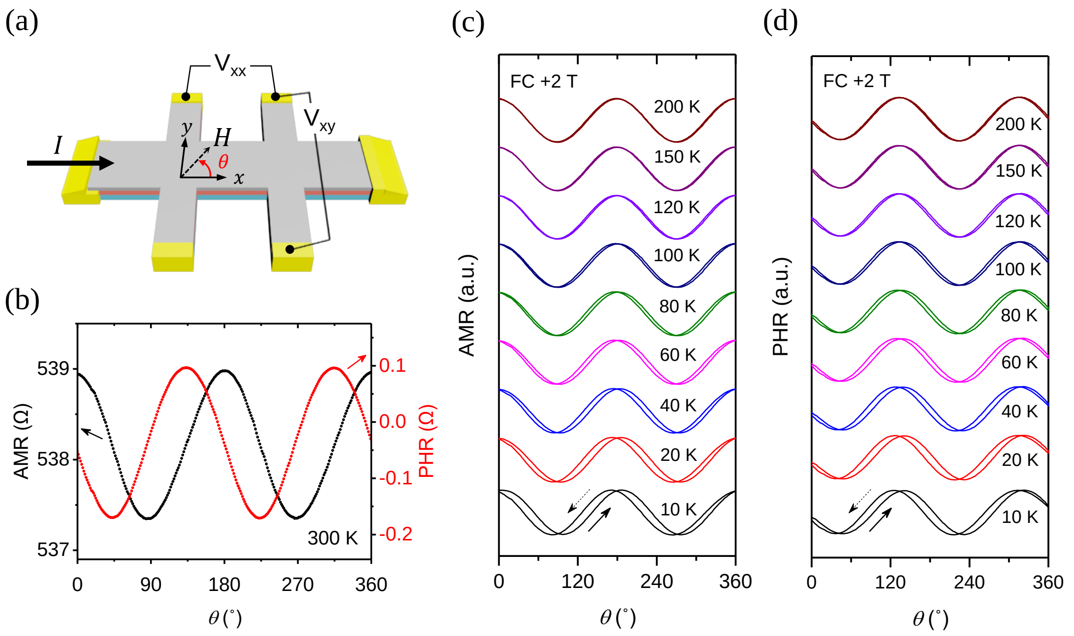

Figure 4.6. Angle-dependent magnetoresistance in a Co/NiOEP bilayer. (a) Schematic illustration of magnetotransport measurements. A magnetic field was applied in the sample plane, and the AMR(V_{xx}) and PHR (V_{xy}) were measured simultaneously. (b) The in-plane angle-dependent AMR and PHR recorded at 300 K. Conventional cosine and sine curves were observed for the AMR and PHR, respectively. (c,d) Angle-dependent AMR and PHR measured at different temperatures for a FC sample under +2 T. At low temperatures, both curves displayed opposite phase shifts for the positive and negative angle sweeps. Phase shifts of 8˚ occurred in both the positive and negative directions at 10 K, which gradually disappeared with increasing temperature.

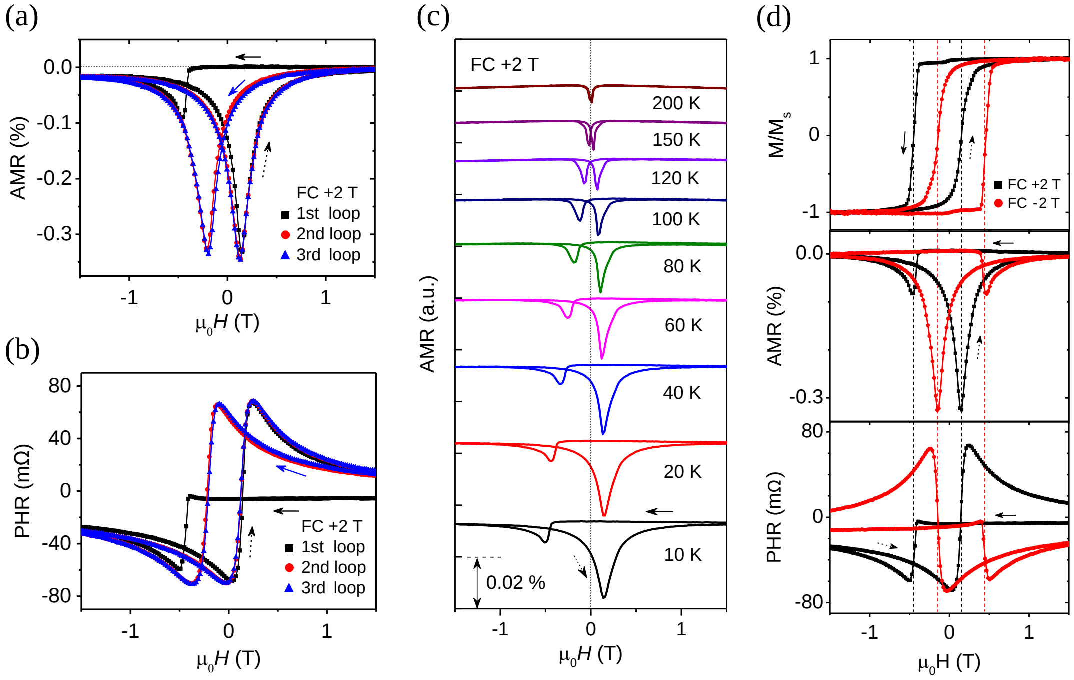

Figure 4.7. Magnetoresistance in a Co/NiOEP bilayer for the in-plane field sweep. (a,b) Consecutive measurements of the AMR and PHR measured at 10 K for a FC sample under +2 T. The observed AMR and PHR obtained during the first field sweep displayed a notable shift and anisotropy in the resistances at the point of magnetization reversal, but the subsequent sweeps displayed diminished shifts and saturation behaviors. (c) The measured AMR for the first field sweep at various temperatures for a FC sample with +2 T. The anisotropy gradually decreased with increasing temperature and finally disappeared for T > 150 K. (d) Comparison of the magnetization, AMR, and PHR measured at 10 K for a FC sample with ±2 T. The plots indicate common points of magnetization inversions (vertical dotted lines are the guide to eye). The arrows indicate the directions of the field sweep.

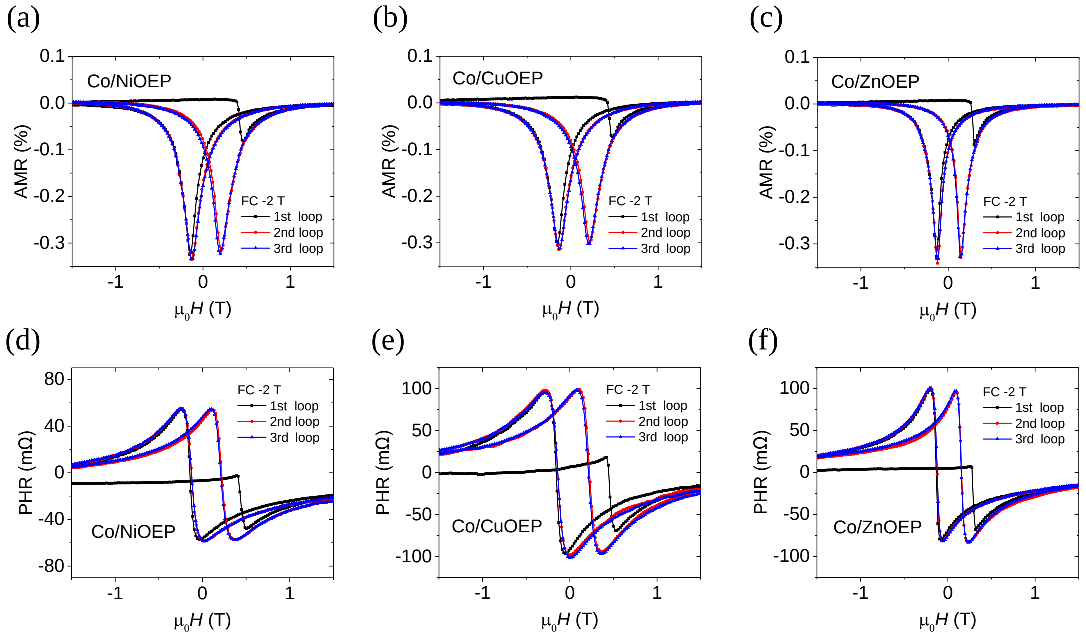

Figure 4.8. Magnetoresistance of Co(4 nm)/MOEP(8 nm)/AlO$_x$ (M=Ni, Cu, and Zn) systems at 10 K measured for FC samples with -2 T. (a-c) AMR of Co(4 nm)/MOEP(8 nm)/AlO$_x$ (M=Ni, Cu, and Zn) films. (d-f) PHR of Co(4 nm)/MOEP(8 nm)/AlO$_x$ (M=Ni, Cu, and Zn) films. Results show distinct loops of the first cycle and nearly saturated exchange bias after the second cycle, similar to the magnetometry results.

4.5. Theoretical Calculations

To clarify the hybrid interfacial interactions between Co and MOEP layers, first-principles density functional theory (DFT) calculations were performed. As illustrated in Figure 4.9, the calculation considered three Co/MOEP systems in which AA'-stacked bilayer MOEP molecules were adsorbed on three unit cells of a Co layer oriented as (111). Here, regardless of the metal ion in the MOEP molecule, the optimal on-surface configuration of the first MOEP molecule was a slightly tilted (by about 2.5°) AA' stacking with respect to the top Co layer to maximize binding to the Co substrate (Figure 4.9(a)). The second MOEP molecule also energetically favored the AA' configuration with a 45° rotation angle with respect to the first MOEP molecule (Figure 4.9(b)). Here, the AA' stacking develops a complete closed loop of C and N atoms (Figure 4.10 and 4.11) and thus promotes strong binding to the Co substrate through effective hybridization between the *d*-orbitals of Co and the *p*-orbitals of the MOEP molecules. The estimated distances between successive layers and the calculated moments in each successive MOEP molecular layer are displayed in Figure 4.12 and Table 4.1.

Figure 4.9(c-e) shows the calculated spin-resolved DOS for specific orbitals of individual atoms in our Co/MOEP systems, which reflects the type of magnetic interaction and ordering. The partial DOS for Co 3*d* orbitals seems to be unaffected, regardless of adsorbed MOEP molecules, whereas the *p* orbital of N is substantially different for the series of MOEP molecules absorbed on a Co surface. The projected DOS of the Co/NiOEP system indicates partial overlap between the *p* orbital of N and the 3*d* orbital of Ni. However, overlap between 3*d* of Co and Ni is not discernable. Thus, this can be speculated that the 3*d* orbitals from NiOEP and the 3*d* orbitals from a Co surface layer interact indirectly through N atoms rather than directly[44]. A significantly large distance between a Co substrate and the first NiOEP layer, 3.48 Å, supports the dominance of superexchange coupling between them.

The spin-resolved-atom projected DOS also reflects the type of magnetic ordering presented in our hybrid molecular films. The projected DOS of the N1 (N atom in the first MOEP molecule) *p* orbital is quite similar to that of the N2 (N atom in the second MOEP molecule) *p* orbital, but their spin-up and spin-down states are nearly reversed, suggesting that the first and second NiOEP molecules are antiferromagnetically ordered each other. A cross-sectional contour plot of the spin density in the Co/NiOEP shown in Figure 4.9(f) also displays antiferromagnetic coupling between successive molecules. On the other hand, it shows ferromagnetic coupling between the first NiOEP molecule and Co substrate. Based on Figure 4.9(d,g), overall magnetic ordering and orbital hybridization in the CuOEP is similar to those in the NiOEP. In particular, the cross-sectional contour plot of the spin density in the Co/CuOEP reveals superexchange interaction between the first CuOEP layer and Co substrate though the N atom of the CuOEP layer. It displays a 90° indirect ferromagnetic coupling though Co-N-Cu atoms, similar to other hybrid systems[44,147]. Here, the calculated ferromagnetic coupling between the first CuOEP layer and Co substrate was 18 meV (Figure 4.13(a)), whereas the antiferromagnetic coupling between successive molecular layers was 11 meV (Figure 4.13(b)). For the ZnOEP molecule, the integrated spin moment of the first ZnOEP molecule was very week. Therefore, the magnetic coupling with the Co substrate was very weak (Figure 4.12). Worse yet, absence of antiferromagnetic ordering between the first and the second ZnOEP molecules was predicted (Table 4.2). The projected DOS reveals that the ZnOEP molecules were almost paramagnetic. Here, the absence of magnetic moments in the second ZnOEP as well as antiferromagnetic coupling between molecules contradicts our experimental observations. One possible explanation for this discrepancy is the presence of surface effects. Two different configurations for the magnetic moment of the first MOEP molecule were computed to explore the surface effects; the first configuration was exposed to a vacuum, and the second was protected by the second MOEP molecule (Figure 4.16). The estimated magnetic moment of the first CuOEP was increased by about 2% from 0.95 μ_B to 0.97 μ_B owing to the presence of the second CuOEP. In particular, the on-surface first ZnOEP molecule started to exhibit small magnetic moment once it was covered with the second ZnOEP (Table 4.5). The surface effect together with the variation of moments between successive molecule layers will lead to incommensurate AFM layers in our studied systems.

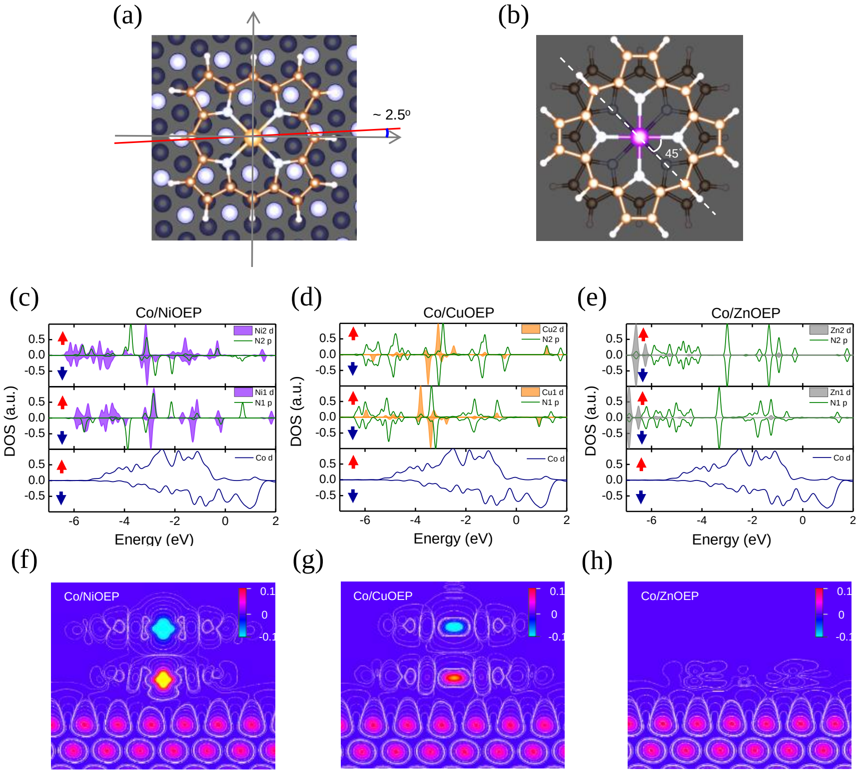

Figure 4.9. Theoretical simulations of optimal stacking configuration, spin-resolved atom projected density of states (DOS), and the corresponding spin density contour plots of the Co/MOEP systems. (a) Top view of AA' stacking structure of the first MOEP molecule on a Co (111) surface. The OEP molecule is slightly (about 2.5˚) rotated with respect to the Co top layer. (b) Top view of the optimized MOEP molecules with AA' stacking configurations. (c-e) Each top and middle plot show the atom projected density of states for the second and first MOEP molecule, respectively. The bottom panels show the density of states projected onto the Co substrate. A positive (negative) projected DOS corresponds to the spin-up (-down) indicated by red (blue) arrows. The Fermi level was set to zero. (f-h) Cross-sectional contour plots of the spin density in the Co/MOEP systems. Solid lines represent density contours. The red region indicates that the density of spin-up electrons dominates the density of spin-down electrons, whereas the bright blue region indicates the density of spin-down electrons prevails. The first MOEP molecules are ferromagnetically ordered with respect to the Co substrate, and they are antiferromagnetically aligned to the second MOEP molecules.

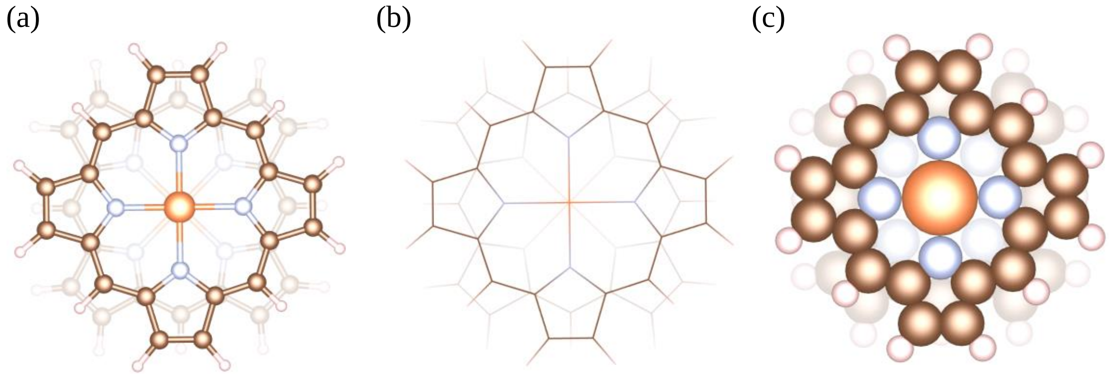

Figure 4.10. Optimal configuration of the first (transparent color) and the second MOEP (bright color) molecule. (a-c) AA' stacked MOEP molecules are represented by three different styles of ball-and-stick, wireframe, and space-filling respectively, which represents that the first MOEP molecule is rotated by almost 45° with respect to the second MOEP molecule.

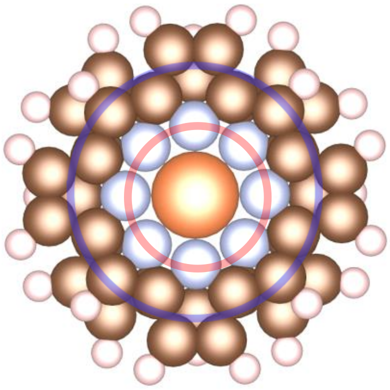

Figure 4.11. The formation of closed loop consisting of C and N atoms. Because of the relative 45° rotation between the first and the second MOEP molecule, from the top view, it can be identified that the bilayer MOEP molecules form the complete closed loops consisting of C atoms (indicated in blue line) and N atoms (in red line).

The high-vacuum deposited MOEP films may have planar stacking across a few layers, as observed in other planar molecular films[31]. In order to confirm overall magnetic behavior in the studied hybrid films, extended calculations were performed by including the third molecular layer for Co/CuOEP and Co/ZnOEP (Figure 4.14 - 4.17 and Table 4.3 - 4.5). The additional third molecular layer also energetically favors AA' stacking configuration with respect to the second molecule. Slight variation in optimal distances, magnetic moments, and magnetic coupling energies can be observed for both Co/CuOEP and Co/ZnOEP systems. However, overall magnetic configuration of FM/AFM interlayer orderings was consistent as the interaction between the second molecule and third molecule also favors AFM ordering.

As a concluding remark, the magnetic ordering of MOEP molecules is mediated by N *p* orbitals and the magnetic moment in OEP molecule other than the central atom mainly originates from N *p* orbital as shown in spin density contour plots of Figure 4.9. This indicates that the N atoms of MOEP played a critical role in developing the magnetic exchange coupling at the hybrid interfaces formed between the Co film and MOEP molecules. In the other words, exchange coupling appears to be controllable at the molecular level through the design of the metal-organic hybrid interface. This interfacial magnetic interaction should highly rely on the molecular structure and orbital symmetry, which will determine orbital hybridization. Molecular design of interfacial magnetic coupling will allow to achieve higher magnitude of exchange bias and extend it above room temperature. AFM molecular spin ordering at room temperature is also necessary to realize room temperature exchange bias and is more challenging to achieve. The calculation showed that the AFM exchange interactions between successive molecular layers are around ~ 10 meV. Recent theoretical simulation showed that AFM molecular coupling in a specific configuration of molecular stacking can be much higher than room temperature[63]. Another important aspect for the molecular spin ordering is the development of well-ordered molecular layers. In general, high-vacuum deposition used for the growth of the molecular film leads to partially irregular layered structure as it solely relies on the self-assembly of molecules during the deposition. A new methodology is needed to develop for the well-defined molecular stacking with enhanced layer by layer interaction, which will eventually bring up strong interlayer magnetic coupling.

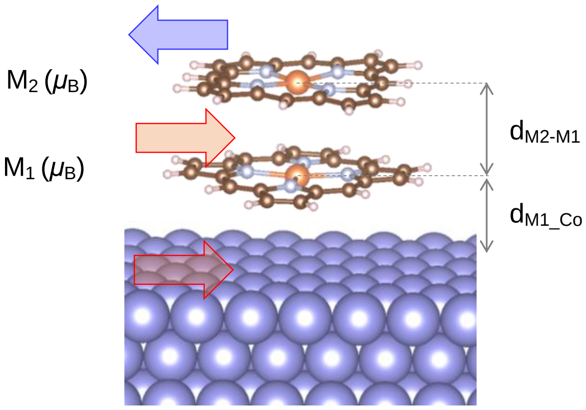

Figure 4.12. Magnetic properties of Co/MOEP systems and optimal distances between metal atoms (Co to Ni, Cu, and Zn). Using DFT calculations, magnetic moments of individual MOEP layers and optimal distances were calculated for the lowest energy configuration of Co/MOEP systems. The distance between the Co on the substrate and the metal on the MOEP is always shorter than the metal-metal distance between subsequent MOEPs because the first MOEP molecule is more strongly bound to the Co substrate than the second MOEP molecule. The estimated magnetic moments of MOEP molecules varies for successive layers. See the calculated values in the below Table 4.1.

	Co/NiOEP	Co/CuOEP	Co/ZnOEP
M_2 (μ_B)	-1.896	-0.950	-0.001
M_1 (μ_B)	1.850	0.971	0.016
$d_{M2\text{-}M1}$ (Å)	4.06	3.89	3.94
$d_{M1\text{-}Co}$ (Å)	3.48	3.59	3.51

Table 4.1. Calculated magnetic moments of individual MOEP layers and optimal distances between metal atoms (Co to Ni, Cu, and Zn) in Co/MOEP systems

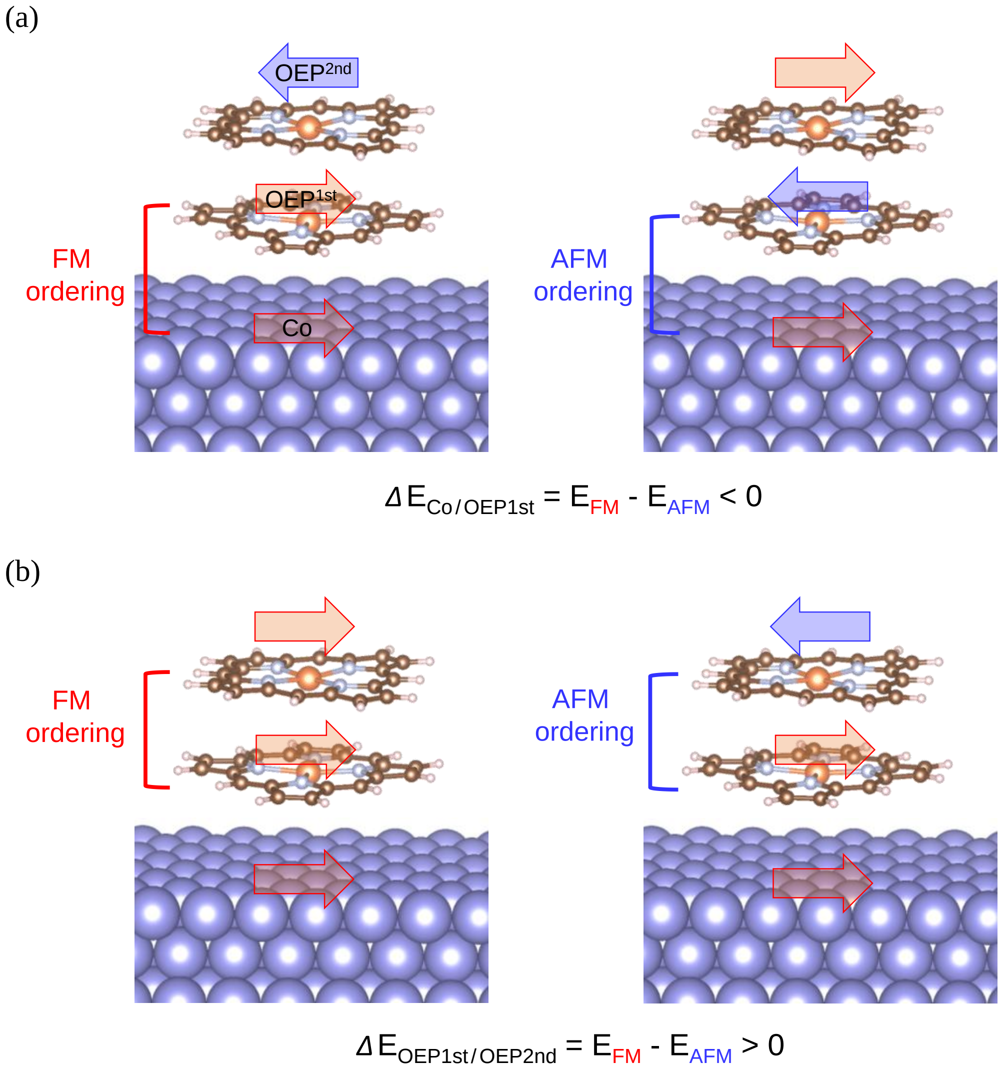

Figure 4.13. Energy configuration of a Co/MOEP$_{1st}$/MOEP$_{2nd}$ structure. (a) Energy difference of the Co/MOEP$_{1st}$ layers (in the consecutive antiferromagnetic coupling of MOEP$_{1st}$/MOEP$_{2nd}$) between FM and AFM interfacial ordering. (b) Energy difference between the MOEP$_{1st}$ and MOEP$_{2nd}$ layer (in the ferromagnetic Co/MOEP$_{1st}$ coupling) between FM and AFM interfacial ordering (See the values in Table 4.2).

E_{FM} - E_{AFM}	Co/CuOEP	Co/ZnOEP
MOEP$_{1st}$ / MOEP$_{2nd}$	11 meV	0 meV
Co / MOEP$_{1st}$	-18 meV	-2 meV

Table 4.2. Calculated exchange coupling energy (E_{FM}-E_{AFM}) in between the Co and MOEP$_{1st}$ layer and in between the MOEP$_{1st}$ and MOEP$_{2nd}$ layer for a Co/CuOEP and Co/ZnOEP system.

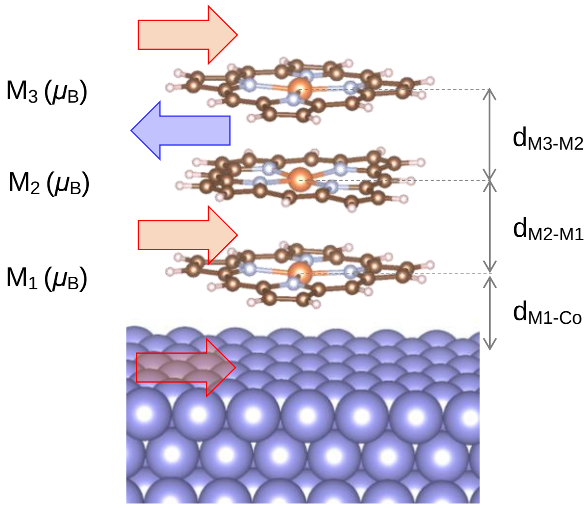

Figure 4.14. Recalculated magnetic properties and optimal distances between metal atoms of Co/MOEP systems for three stacked MOEP layers. Using DFT calculations, the lowest energy configuration of Co/MOEP systems was obtained. The estimated magnetic moments of MOEP molecules vary for successive layers (See the calculated values in Table 4.3).

	Co/CuOEP	Co/ZnOEP
M_3 (μ_B)	0.951	0.000
M_2 (μ_B)	-0.945	-0.001
M_1 (μ_B)	0.971	0.020
$d_{M3\text{-}M2}$ (Å)	3.89	3.94
$d_{M2\text{-}M1}$ (Å)	3.89	3.94
$d_{M1\text{-}Co}$ (Å)	3.59	3.51

Table 4.3. Calculated magnetic moments of individual MOEP layers and optimal distances between metal atoms in Co/MOEP systems (See the schematic illustration in Figure 4.14).

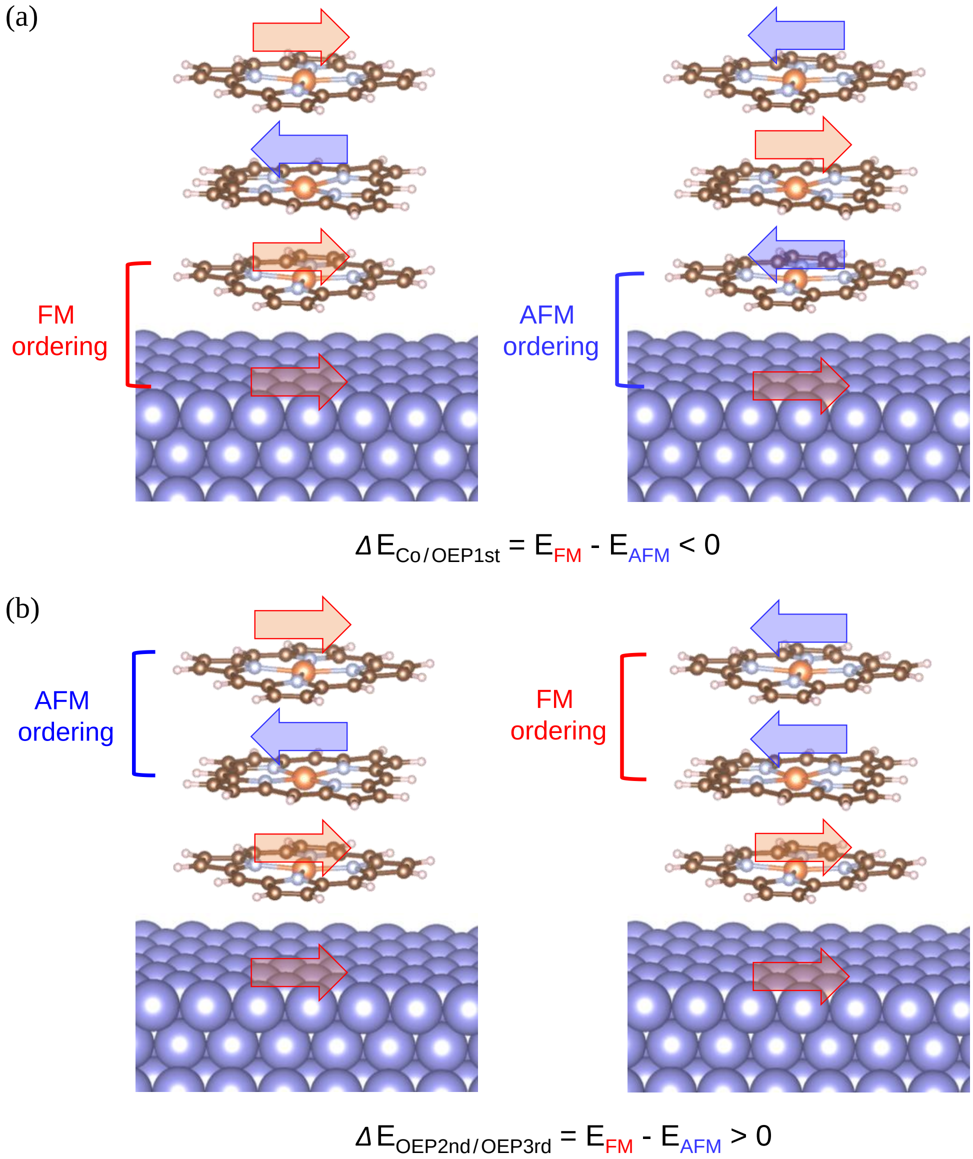

Figure 4.15. Energy difference between FM and AFM interfacial ordering in Co/CuOEP$_{1st}$/CuOEP$_{2nd}$/CuOEP$_{3rd}$ systems. (a) Stable FM interfacial coupling than the AFM configuration at the interface between the Co and CuOEP$_{1st}$. (b) Stable AFM coupling than FM ordering (See the values in Table 4.4).

E_{FM} - E_{AFM}	Co/CuOEP
MOEP$_{2nd}$ / MOEP$_{3rd}$	14 meV
Co / MOEP$_{1st}$	-10 meV

Table 4.4. Calculated exchange coupling energy (E_{FM}-E_{AFM}) in between a Co and CuOEP$_{1st}$ layer and in between the CuOEP$_{2nd}$ and CuOEP$_{3rd}$ layer for a Co/CuOEP system.

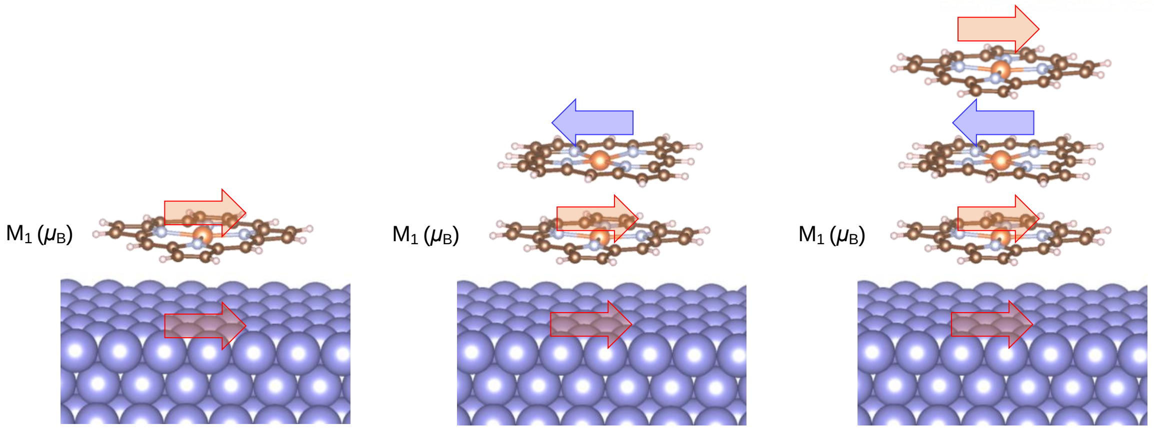

M_1 exposed to vaccum

M_1 with the MOEP$_{2nd}$ layer

M_1 with the MOEP$_{2nd}$ and MOEP$_{3rd}$ layer

Figure 4.16. Surface effect on the magnetic moment of the first MOEP molecule layer. In order to figure out the surface effect on the MOEP magnetic moment, the magnetic moments of the first MOEP molecule exposed to vacuum (left) and protected by the second MOEP molecule (center) and protected by the second and third MOEP molecules (right) were computed. For a Co/CuOEP system, the MOEP magnetic moment was increased by about 2% (from 0.95 μ_B to 0.97 μ_B) by covering with additional molecules. In the case of a ZnOEP molecule, the moment was increased from 0.001 μ_B, 0.016 μ_B to 0.020 μ_B successively (See the values in Table 4.5).

	M_1 (μ_B)		
	exposed to vacuum	with the MOEP$_{2nd}$	with the MOEP$_{2nd}$ and MOEP$_{3rd}$
Co/CuOEP	0.952	0.971	0.971
Co/ZnOEP	0.001	0.016	0.020

Table 4.5. Surface effect on the magnetic moment (M_1) of the MOEP$_{1st}$ molecule in a Co/CuOEP and Co/ZnOEP system.

4.6. Summary

The emergence of spin moments at metal-organic hybrid interfaces provides versatile manipulation of electron spins flowing across the interface[28,30,111-114]. The magnetic moment and coupling at the hybrid interface could even allow further active control over the spins in a neighboring film. Here, this study demonstrated that the magnetic exchange bias in a Co/MOEP hybrid film can be extended up to 170 mT, the largest value reported. Magnetic characteristics of the studied hybrid films exhibit the features of the exchange bias including training effect, its temperature dependence, and dependence on the ferromagnet thickness. Magnetotransport studies offered a direct assessment of the exchange bias by measuring AMR or PHR with angular dependence, which can be immediately applicable to the electrical signal processing. Our theoretical simulations elucidated the types of magnetic coupling and ordering between a Co substrate and MOEP molecules and between the subsequent molecule layers. In particular, the interfacial magnetic coupling strongly relies on the neighboring N atoms in the molecule, leading to the superexchange interaction. Also, simulated strong surface effects indicate MOEP films form incommensurate antiferromagnetic layers. These fundamental studies of the hybrid interfacial coupling and its impact on the magnetic and magnetotransport characteristics open a new channel for controlling hybrid magnetic layers. The demonstrated tuning of magnetic pinning via the molecular approach will certainly extend versatile functionalities of organic spinterfaces.

* **Chapter IV** is reproduced in part with permission of “J. Jo *et al*. Molecular Tunability of Magnetic Exchange Bias and Asymmetrical Magnetotransport in Metalloporphyrin/Co Hybrid Bilayers. ACS Nano, DOI: 10.1021/acsnano.8b08689”. Copyright © 2018 American Chemical Society.

V. Exchange Bias in a Fe/CoOEP System with Interfacial Antiferromagnetic Coupling

5.1. Motivation

Molecular spins as fundamental magnetic building-blocks have received enormous attentions for its functionality and potential that can cover the overall spectrum of nanotechnology. Through the period of initial molecular magnetism in bulk systems[148,149], emergence of molecular magnetism at interface, called molecular spinterface, begun to spotlight for the sake of intrinsic interfacial features and its applicative advantage for architectural low dimension devices. Stacking structures of paramagnetic planar molecules on proper underlying films can have aligned spins as FM[30,43,44] or AFM[59,60,62] configuration. Emergence of these interesting interfacial features led to extend its realm to development of new functional structures and related device application. The interfaces allowed to realize a molecular spin valve with one FM film[30] and exchange bias resulting from AFM ordered molecular interlayers[31]. Highly thermal stable molecular interface with FM or AFM coupling[60,62] and highly spin-polarized spin-states near the Fermi level[150] were demonstrated at room temperature. In this way, the aim to molecular spinterface field have extended from the understanding of fundamental mechanism to functionality and practical use for futural device applications.

Exchange bias is one of the representative phenomena in spintronics[74], which have widely utilized in commercial magnetic devices. When a FM film meets an AFM film, formed through a FC procedure, the AFM film is strongly intertwined with the FM film to resist or assist spin-flipping during a magnetic field sweep. This results in an asymmetric magnetic hysteresis loop from the zero magnetic field, making the exchange bias an indispensable component for commercial memory devices[124], where AFM layers help to reduce switching magnetic fields in a FM/NM/FM/AFM structure. Conventional exchange bias occurs under FM coupling between the films, which means the interfacial spin configurations of the FM and AFM layer are parallel. In this case, the hysteresis loop shifts to the opposite direction to the applied magnetic field in a field cooling procedure (H_{FC}), called negative exchange bias (NEB), which widely represented not only in conventional metal and oxide systems but also in molecular systems[31,92,151]. On the contrary, exchange bias having AFM coupling at the interface can exhibit distinctive features. As the low H_{FC} applies to the AFM coupling system, it is a stable state having an AFM interfacial configuration right after the FC, showing NEB behaviors. However, as the H_{FC} increases as enough to make the AFM layers follow the H_{FC} direction, which means Zeeman energy is dominant than the interfacial exchange coupling, the interface is in an unstable state. This makes the loop shift with the same direction to the H_{FC}, called positive exchange bias (PEB)[86]. The controllable exchange bias through the tuning of interfacial coupling has been systemically analyzed in the fluoride[86], spin glass[72], and oxide systems[90], but not in molecular systems.

This study demonstrated the functional molecular spinterface having a newly developed FM-like molecular layer and the consecutive AFM layers at the interface between paramagnetic cobalt-porphyrin (CoOEP) molecules and the underlying ferromagnetic iron (Fe) layers. The two different FM layers of the Fe and interfacial CoOEP showed distinguishable magnetic hysteresis loops and further generated exchange bias phenomena by the AFM molecular CoOEP layers. Although the exchange bias for the underlying Fe layers was controlled by the upper AFM molecular layers, the FM-like molecular layer was affected by two layers acting as a pinning layer that one was the underlying Fe layers and the other was the upper AFM molecular layers. Also, it is found out that the exchange interaction associated with the exchange bias in this system was ruled by AFM interfacial coupling leading to tunable exchange bias via controlling H_{FC}. Comparison with a FM coupled molecular system and theoretical calculation strongly underpinned the result of the molecular exchange bias system under AFM coupling. Thus, our results demonstrated the transformation of paramagnetic CoOEP layers (on the Fe layers) to the interfacial independent FM layer and the consecutive AFM layers, leading to the emergence of controllable exchange bias via AFM interfacial coupling. This transformable molecular spinterface with peculiar functionality and easy fabrication will extend its use to the applicative magnetic devices.

5.2. Experimental Methods

The heterostructure of a Fe/CoOEP system was fabricated on a *p*-Si/SiO$_2$ (300 nm) substrate. A buffer layer of Ta (6 nm) was first deposited on the substrate, and then Fe (2 nm) layers were deposited by using an electron beam evaporation. The rate of depositions was 0.1 Å/s. A CoOEP (Sigma Aldrich) was sublimed by 0.15 Å/s to fabricate uniform hybrid interfaces. The top layer was an AlO$_x$ (20 nm) film to prevent oxidation of the whole structure. All process was performed in a high-vacuum chamber under a base pressure of 10^{-7} Torr without breaking the vacuum. The thickness of each layer was controlled by using a quartz crystal monitor.

Magnetometry of the sample was performed by using a SQUID-VSM (Quantum Design). The sample was cut to the size of 4 mm × 7 mm and placed in a gelatin capsule within a plastic straw to minimize unnecessary background signals. In measurement, a static field mode was used with 2 mT for large field ranges and 0.2 mT in a low field scan. All measurements were proceeded immediately after the sample fabrication to minimize unexpected changes. Additionally, the magnetic features after storage a sample under a vacuum for a few months were almost same with the fresh sample.

The electrical measurement was carried out in a PPMS (Quantum Design) with a horizontal rotator. A Keithley 2636/Keithley 2182A system for a source meter and voltage measurement, respectively. The sample for the the electrical measurement was fabricated by using a Hall bar type shadow mask. The Ta/Fe/OEP/AlO$_x$ channel had 500 μm width and 2 mm length and each contact consisted of Ti/Au pads. The current applied at the Hall bar channel was 200 μA which displayed a negligible heating effect. The same procedure was used with the rate of magnetic field sweeps, stable time, sequence, etc. for the measurement.

5.3. Control of Two Different Exchange Bias

A metal-organic hybrid interface between a ferromagnetic Fe and paramagnetic metallo-octaethyl-porphyrin (MOEP, M = Co^{2+}) was prepared through a stacking structure of Ta(6 nm)/Fe(2 nm)/CoOEP(8 nm)/AlO_x(20 nm) on a Si/SiO_2 substrate, named Fe/CoOEP in this study. Figure 5.1(a) displays a schematic structure of the molecules CoOEP film on the Fe film. The planar structure of the CoOEP molecule is indispensable for layer-by-layer molecular stacks to form interacting molecular spin texture and to induce new magnetic properties at the interfaces[151]. Figure 5.1(b) shows a magnetic hysteresis loops of the Fe/CoOEP system measured at 10 K, after a FC procedure with 20 kOe from 300 K. The result displayed a large asymmetric hysteresis loop (black, named the main loop) from the center (H = 0 kOe). The main loop was shifted to the negative-field side as H_{EB} = -154 Oe, where $H_{\mathrm{EB}} = (H_{\mathrm{c}}^{+} + H_{\mathrm{c}}^{-})/2$. There was a sharp step near H = 0 kOe in the hysteresis loop. To unravel this unusual change of magnetization, additional measurements for magnetic hysteresis loops were performed within the range of H = 0.3 kOe, which did not exceed the coercivity of the Fe film. The results are shown in the insets of Figure 5.1(b), displaying distinct hysteresis loops with small coercivities (red, named the minor loop). This minor hysteresis loop indicates the emergence of the newly developed FM domains at the Fe/CoOEP interface. In particular, the observed minor loop showed PEB behavior. This clear feature assures that the newly developed interfacial layer acts as an individual FM layer distinguished from the underlying Fe film. This is called a rotatable spin layer that could be generated at the interface between an AFM film and FM film and its spin configuration could easily align to applied magnetic field even though it is the component of the AFM film[90,152,153]. Similarly, anisotropic magnetoresistance (AMR) on a fabricated device also exhibited the interfacial effect of the Fe/CoOEP in Figure 5.1(c). It strongly supported these interfacial phenomena because a current on the device flows through the conducting Fe film. Then, the current dropped by the rotatable OEP layer which may be connected to the Fe layers through charge transfer. The data showed not only the conventional behaviors of exchange bias which were almost same with the magnetometry results but also two notable peaks for coercivity near H = 0 kOe that is same feature with the minor hysteresis loop. Thus, this limited path for the current flow in the Fe film and further its adjoining interface assures that the existence of the newly developed rotatable OEP layer occurred at the hybrid interface.

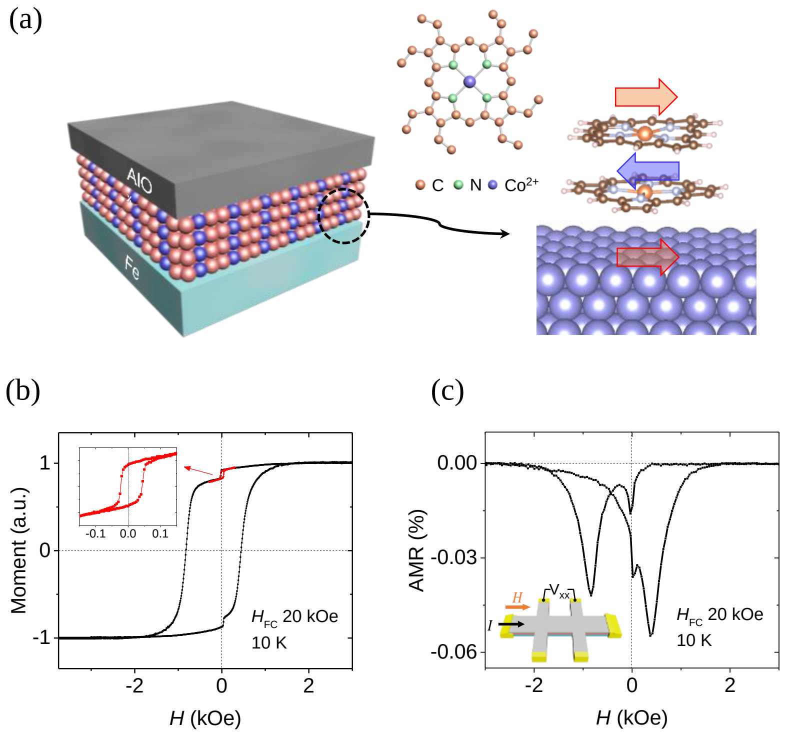

Figure 5.1. Exchange bias of a Fe/CoOEP system. (a) Schematic illustration of the exchange-biased Fe/CuOEP bilayer. The antiferromagnetic CoOEP molecular spin texture is on top of the ferromagnetic Fe film with antiferromagnetic exchange coupling. (b) Magnetic hysteresis loops measured at 10 K for a FC sample under H_{FC} = 20 kOe. The main hysteresis loop (black) displayed asymmetric behavior with the negative shift. In contrast, the minor loop (red) shifted to the positive direction to the H_{FC}. (c) AMR data for the same set of the Fe/CoOEP sample. Inset indicates the geometry of a Hall bar patterned device.

There are two different exchange bias features in the hysteresis loop of the Fe/CoOEP structure, showing different directions of anisotropy. To unveil the essence of distinctive molecular exchange bias here, separated investigations are needed for two different layers of the main loop and minor loop. First, the measurement of H_{FC} dependent exchange bias for the main loop showed the change of exchange bias as H_{FC} was enhanced NEB values decreased exponentially from -243 Oe (H_{FC} = 2 kOe) to -112 Oe (H_{FC} = 60 kOe) at 10 K (Figure 5.2(a)). This H_{FC} dependence is well related to antiferromagnetic interfacial coupling which could induce positive exchange bias. To elucidate this phenomenon systemically, schematic spin configurations of the FC sample under a low H_{FC} and high H_{FC} case are proposed shown in Figure 5.2(c) and Figure 5.2(d), respectively. There are two conceptually parts of the molecule CoOEP. One is “the rotatable OEP layer (red)” in charge of the minor hysteresis loop. The other is “the pinned OEP layers (green)” which acts as a conventional AFM film. Note that each arrow in Figure 5.2(c,d) represents not a single spin as individual but a domain-like assembly in layers. Here, uncompensated and pinned AFM layers (green) play a role of exchange biasing layers to the adjacent FM film. The other, uncompensated and rotatable (unpinned) interfacial layer (red arrow) acts as a FM layer reactive to an applied magnetic field. In the initial state of low H_{FC} (☆) in Figure 5.2(c) for the main loop, the Fe and pinned OEP layers are in the state of antiferromagnetic interfacial exchange coupling which induces NEB. Here, note that the intermediate layer (the rotatable OEP layer in this study) in between FM and AFM layers could reduce or enhance the exchange bias[154,155], but it does not significantly affect the existence of exchange bias. In contrast, when H_{FC} is high enough (★) in Figure 5.2(d), the Zeemann energy of pinned AFM layers overcomes the interfacial (antiferromagnetic) exchange coupling and leads to align the pinned AFM layers to the H_{FC} direction, resulting in PEB[86,90]. In this viewpoint, results in Figure 5.2(a) indicates the Zeemann energy (up to H_{FC} = 60 kOe) is insufficient to fully overcome the exchange coupling at the interface but displays its effect on the spin-flip of the pinned OEP layers. In the previous report, Nogues *et al*. experimentally showed complete reversal of the sign of exchange bias in a Fe/MnF$_2$ system when H_{FC} is high enough[86,156,157]. Kiwi *et al*. also theoretically showed the inversion of exchange bias by increasing H_{FC} in the Fe/MnF$_2$ system, but the inversion did not occur in the Fe/FeF$_2$ system[158]. The difference in the two systems came from a high value of $J_{F/AF}$ in the Fe/FeF$_2$ of -1.2 meV, compared to -0.35 meV for the Fe/MnF$_2$ (with both similar values of J_{AF} as -1.2 meV), making it hard to overcome the exchange coupling. Our Fe/CoOEP system is also expected a relatively high value of $J_{F/AF}$, which would be too large to induce the complete spin-flip and the inversion to PEB.

The newly developed rotatable OEP layer (the minor loop) at the Fe/CoOEP interface also exhibited exchange bias in response to the magnetic coupling with adjacent spin textures. Figure 5.2(c,d) shows that there are two pinned layers which can induce exchange bias to the rotatable OEP layer; the underlying Fe layers and the upper pinned OEP layers. First, in the low H_{FC} condition (☆) after a FC procedure in Figure 5.2(c), the Fe layers have a parallel spin configuration to the rotatable OEP layer, but the pinned OEP layers are antiparallel at the interface. Because the interface coupling favors antiferromagnetic, the Fe layers will give rise to PEB to the rotatable OEP layer, but the pinned OEP layers will promote NEB. Thus, the PEB in the minor loop at 10 K in Figure 5.2(b) can be interpreted that the Fe layers affected to the rotatable OEP layer more strongly than the pinned OEP layers. When H_{FC} is high enough, the pinned OEP layers also induces the PEB to the minor loop by rearranging their spin configurations as parallel to the applied H_{FC} (★ in Figure 5.2(d)), resulting in further enhanced PEB for the rotatable OEP layer. In short, the type of the exchange bias and its H_{FC} dependence for the PEB strongly underpins the existence of the three distinctive spin textures and the ground state of interfacial antiferromagnetic coupling.

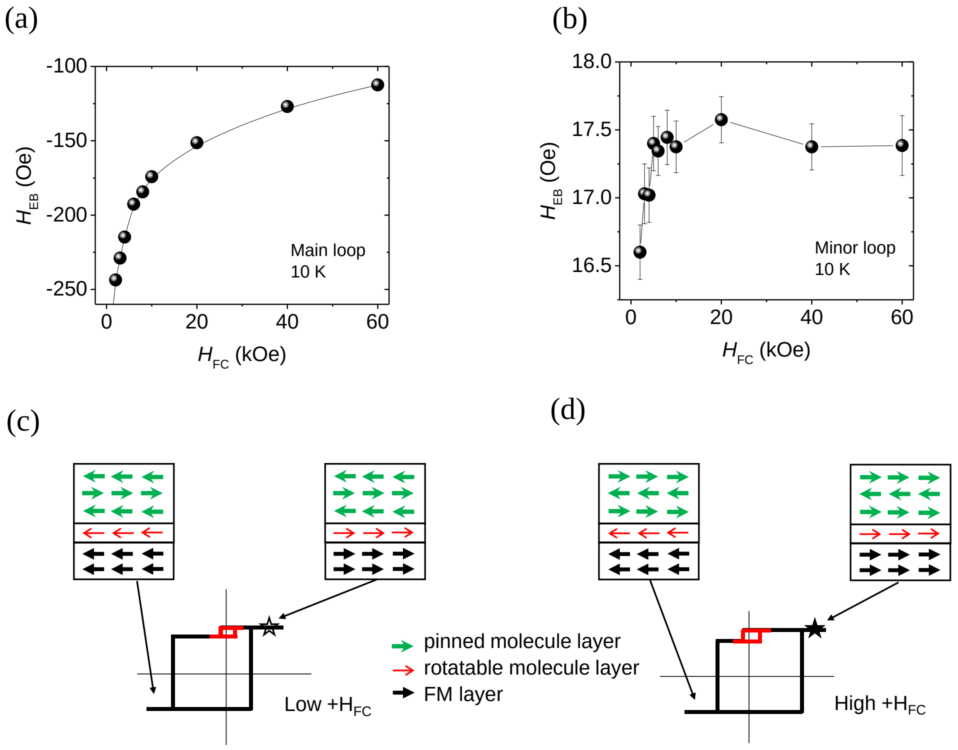

Figure 5.2. H_{FC} dependent exchange bias of a Fe/CoOEP system. (a) Evolution of the exchange bias for the main loop measured at 10 K with increasing H_{FC}. The exchange bias was significantly reduced with increasing H_{FC}, but it maintained the negative sign. (b) The exchange bias for the minor loop as a function of H_{FC} measured at 10 K. As the H_{FC} increased, the PEB was slightly increased and then saturated after H_{FC} = 0.8 kOe. (c,d) Schematic illustrations of spin textures under low H_{FC} and high H_{FC}, respectively. The star marks (☆ and ★) indicate a starting point of hysteresis loops after a positive H_{FC} procedure.

5.3 Positive sign of exchange bias via frustration

Figure 5.3(a) displays the temperature dependence of exchange bias for the main loop measured after the sample was FC with H_{FC} = 20 kOe. There is the inversion of the sign of exchange bias between the negative and positive around 40 K. The positive value exhibited the maximum value at around 55 K and then decreased with increasing temperature, and finally disappeared near 150 K which is associated with the blocking temperature (T_B) of the Fe/CoOEP system. If the positive sign of this exchange bias was really associated with positive exchange bias which people consider resulting from the interfacial antiferromagnetic coupling, there should be variation of exchange bias depending on H_{FC} condition. However, there cannot be found distinct change of exchange bias from H_{FC} = 2 kOe to 60 kOe for the both main loop and minor loop at 55 K (Figure 5.3(b,c)). Therefore, this inversion of the exchange bias type in this study should be associated with the distribution of AFM CoOEP domains. Figure 5.4(a) shows the temperature dependent coercivity (H_C), the half of the loop width, under H_{FC} = 20 kOe for the Fe/CoOEP system. The measured H_C (black dot) increased with decreasing temperature, but it seemed not to have a single shape but to possess two features by the inflection point around 40 K. Although the H_C before 40 K seemed to be saturated by decreasing temperature, the H_C after 40 K was well followed the exponential curve (red line) fitted. It should be noticed that the left H_C (in the negative field region, H_{C-}) had the exponential behavior (Figure 5.4(c)), but the right H_C (in the positive field region, H_{C+}) showed an upturn point at around 25 K (Figure 5.4(e)). This peculiar H_C dependence for the PEB system could be interpreted as a metastable AFM model, which simply assumes the existence of distribution of AFM domains with different blocking temperatures, inducing stable or unstable states to an adjacent ferromagnet by the direction of sweeping magnetic field[159,160]. At the intermediate temperature (the temperature in between blocking temperatures of AFM domains) some parts of domains are blocked, and others are unblocked. When the sample was FC to intermediate temperature, sweeping of magnetic field to the opposite direction from H_{FC} induces rotation of AFM domains with relatively low blocking temperature. This induces part of domains are parallel to the applied magnetic field and others are antiparallel leading to frustration. Thus, distribution of AFM domains induces higher anisotropy to an underlying Co layer at the negative field state than the initial positive field state because of domain wall pinning. In this way, there are certain temperature regions to generate upturn H_{C+} and PEB features, which usually get the maximum point at a similar temperature that is around 40 K in our system. If the H_{FC} is low, the growth of AFM domains with higher blocking temperature won’t be effective, leading to absence of PEB at the intermediate temperature (Figure 5.5(a)).

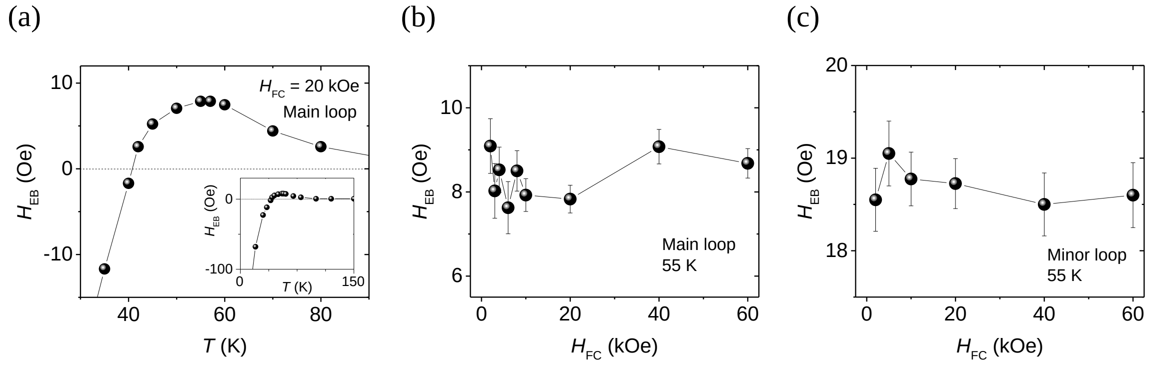

Figure 5.3. Positive sign of exchange bias in a Fe/CoOEP system. (a) Temperature dependent exchange bias of the main loop with H_{FC} = 20 kOe. Positive sign of exchange bias was observed from 40 K. Exchange bias of (b) the main loop and (c) the minor loop as a function of H_{FC} measured at 55 K. The magnitudes of PEB were nearly constant upon varying H_{FC} at 55 K.

Reminding the conventional exchange bias resulting in NEB behaviors based on interfacial ferromagnetic coupling, a Co/NiOEP system was introduced to compare the opposite feature of the Fe/CoOEP system. Although the Co/NiOEP has very similar structural properties with the Fe/CoOEP, it only represented NEB behaviors and did not depend on H_{FC} at low temperatures (Figure 5.6) because of the ferromagnetic coupling[151]. Figure 5.5 shows temperature dependent magnetic properties for the Co/NiOEP, with the same measurements for the Fe/CoOEP. Obviously, it displayed the exponential dependence of H_C in all temperature ranges (Figure 5.4(a)) and in the case of H_{C-} (Figure 5.4(e)). As was expected, the H_{C+}, the key component to occur PEB in certain temperatures, displayed smooth increasing tendency without any distinctive features like an upturn shape (Figure 5.4(c)). Thus, it is inferred that the key element for these different coercivities and exchange bias behaviors between the two systems is related to their fundamental interfacial couplings. The incommensurate net moment of molecular stacking on a FM film would likely to have the direction of moment of the first layer. Thus, antiferromagnetic interfacial coupling in the Fe/CoOEP could induce higher anisotropy at intermediate temperature under high H_{FC} leading to inversion of NEB to PEB. On the contrary, the absence of PEB at intermediate temperature in the Co/NiOEP can be attributed to the combination of interfacial ferromagnetic coupling which do not significantly enhance anisotropy in a high H_{FC} state at the intermediate temperature.

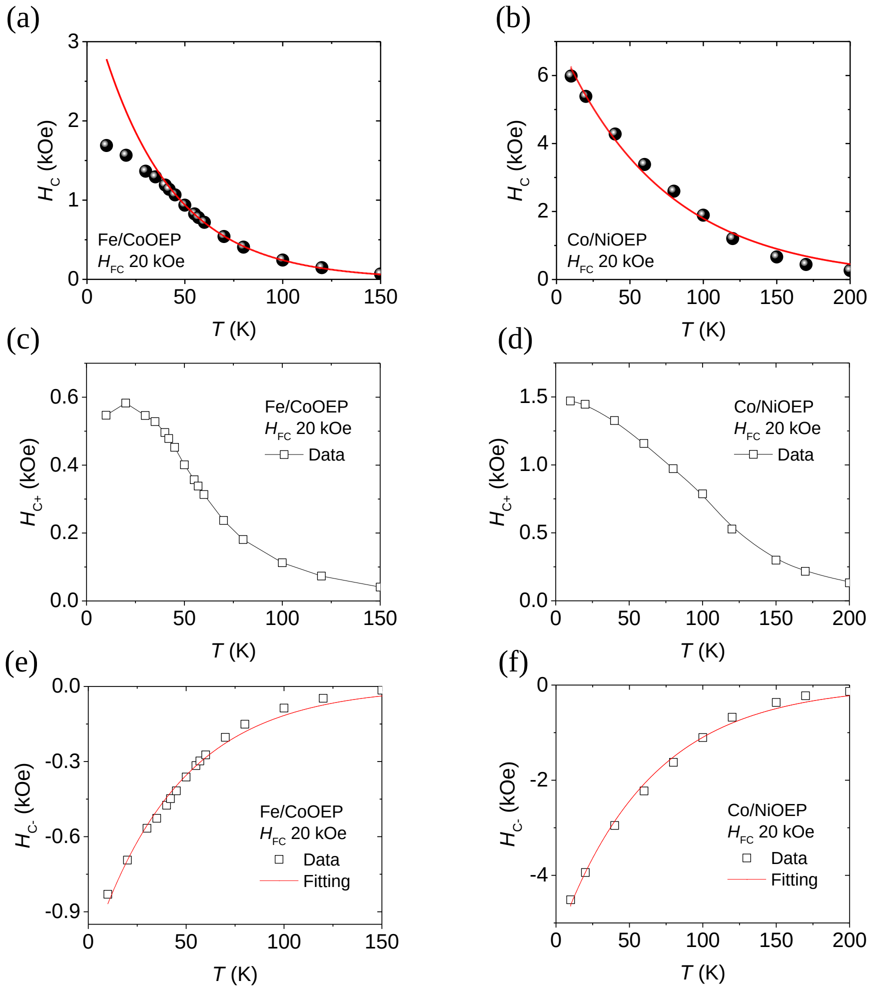

Figure 5.4. Temperature dependent coercivity in a Fe/CoOEP and Co/NiOEP system via a FC procedure with +20 kOe. (a) Coercivity H_C (the half of loop width), (c) H_{C+} for the positive field region, and (e) H_{C-} for the negative field region on varying temperature in the Fe/CoOEP system. (b) Coercivity H_C (the half of loop width), (d) H_{C+} for the positive field region, and (f) H_{C-} for the negative field region on varying temperature in the Co/NiOEP system. The difference between the two H_C in the systems came from the variation of H_{C+} in antiferromagnetic coupling of the Fe/CoOEP system.

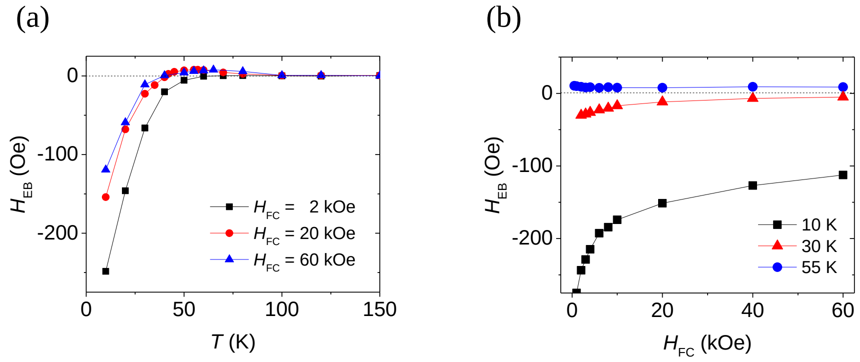

Figure 5.5. Variation of exchange bias depending on H_{FC} and temperature in a Fe/CoOEP system. (a) Temperature dependent exchange bias on H_{FC} = 2, 20, and 60 kOe. There was inversion of exchange bias in the condition of H_{FC} = 20 (red circle) and 60 kOe (blue triangle) around 50 K, but it was not shown in the low H_{FC} = 2 kOe (black square). (b) H_{FC} dependent exchange bias on T = 10, 30, and 50 K.

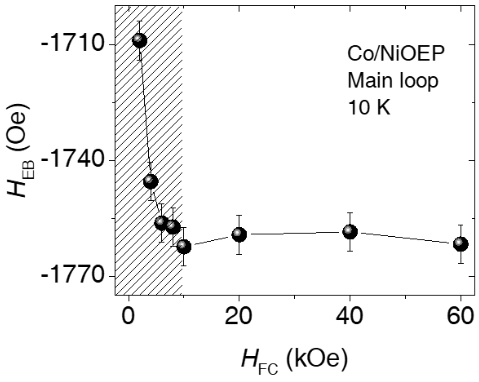

Figure 5.6. H_{FC} dependent exchange bias at 10 K in a Co/NiOEP system having ferromagnetic interfacial coupling. There was no distinct change of exchange bias according to the H_{FC} up to 60 kOe. The low H_{FC} region less than 20 kOe (gray diagonal) showed increasing exchange bias, but it was due to the unsaturated magnetic state of the underlying Co film (saturated magnetic field was around 15 kOe).

VI. Conclusion

Organic molecules composed of various atoms are attractive Lego-blocks which can be used in constructing nanostructures. Variety of molecules and a wide range of properties make the molecules indispensable elements in electronics for practical application, and it further extends its leverage to spintronics. Among them, molecules on a metal layer develop fascinating interfaces having notable change or emergence of charge and spin properties. These peculiar hybrid interfaces will play a key role in applicative spintronics owing to its functionality, low-dimensionality, and easy fabrication.

This thesis demonstrated that paramagnetic MOEP molecules on a ferromagnetic film can develop an interfacial ferromagnetic molecular layer and subsequent antiferromagnetic molecular interlayers from their interface. This established ferromagnet/antiferromagnet structure clearly showed the features of exchange bias such as unidirectional anisotropy, blocking temperature, thickness dependence, and training effect. Different kinds of MOEP molecules having various exchange bias underpinned the existence of the exchange bias resulting from molecular spinterface. Controlling the underlying ferromagnetic film allowed tuning the interfacial coupling between the ferromagnetic film and molecules as ferromagnetic and antiferromagnetic coupling, which resulted in tunable exchange bias depending a magnetic field in a field-cooled procedure. Magnetotransport with anisotropic and angle-dependence displayed an alternative assessment of exchange bias, especially revealing the existence of the induced molecular layers at the interface. Furthermore, the transport measurement on a fabricated device showed feasibility to device application. Theoretical calculations elucidated the experimental data by analyzing spin moment, distance, and interfacial exchange coupling for each layer. In particular, the interfacial magnetic coupling relies on the neighboring N atoms in the molecule, leading to the indirect superexchange interaction.

Fundamental studies of ferromagnet/molecule structures via experiment and theoretical calculation showcased the emergence of molecular spinterface and its application to exchange bias. These molecules at hybrid interfaces will open a new channel for organic spintronics in the low dimension, and versatile functionalities of the molecules will enrich the research area and give abundant opportunities.

References

1 W. Thomson; F. R. S. On the electro-dynamic qualities of metals:--Effects of magnetization on the electric conductivity of nickel and of iron. *Proc. R. Soc. Lond.* **1857**, *8*, 546-550.

2 M. N. Baibich; J. M. Broto; A. Fert; F. N. Vandau; F. Petroff; P. Eitenne; G. Creuzet; A. FriederichJ. Chazelas. Giant Magnetoresistance of (001)Fe/(001) Cr Magnetic Superlattices. *Phys. Rev. Lett.* **1988**, *61*, 2472-2475.

3 P. Grunberg; R. Schreiber; Y. Pang; M. B. BrodskyH. Sowers. Layered Magnetic-Structures-Evidence for Antiferromagnetic Coupling of Fe Layers across Cr Interlayers. *Phys. Rev. Lett.* **1986**, *57*, 2442-2445.

4 M. Julliere. Tunneling between Ferromagnetic-Films. *Phys. Lett. A* **1975**, *54*, 225-226.

5 T. MiyazakiN. Tezuka. Giant Magnetic Tunneling Effect in Fe/Al2o3/Fe Junction. *J. Magn. Magn. Mater.* **1995**, *139*, L231-L234.

6 J. S. Moodera; L. R. Kinder; T. M. WongR. Meservey. Large Magnetoresistance at Room-Temperature in Ferromagnetic Thin-Film Tunnel-Junctions. *Phys. Rev. Lett.* **1995**, *74*, 3273-3276.

7 S. Yuasa; T. Nagahama; A. Fukushima; Y. SuzukiK. Ando. Giant room-temperature magnetoresistance in single-crystal Fe/MgO/Fe magnetic tunnel junctions. *Nat. Mater.* **2004**, *3*, 868-871.

8 L. Q. Liu; C. F. Pai; Y. Li; H. W. Tseng; D. C. Ralph; R. A. Buhrman. Spin-Torque Switchingwith the Giant Spin Hall Effect of Tantalum. *Science* **2012**, *336*, 555-558.

9 Y. K. Kato; R. C. Myers; A. C. Gossard; D. D. Awschalom. Observation of the spin hall effect in semiconductors. *Science* **2004**, *306*, 1910-1913.

10 K. Uchida; S. Takahashi; K. Harii; J. Ieda; W. Koshibae; K. Ando; S. Maekawa; E. Saitoh. Observation of the spin Seebeck effect. *Nature* **2008**, *455*, 778-781.

11 H. C. Koo; J. H. Kwon; J. Eom; J. Chang; S. H. Han; M. Johnson. Control of Spin Precession in a Spin-Injected Field Effect Transistor. *Science* **2009**, *325*, 1515-1518.

12 R. Fiederling; M. Keim; G. Reuscher; W. Ossau; G. Schmidt; A. Waag; L. W. Molenkamp. Injection and detection of a spin-polarized current in a light-emitting diode. *Nature* **1999**, *402*, 787-790.

13 S. Ikeda; J. Hayakawa; Y. Ashizawa; Y. M. Lee; K. Miura; H. Hasegawa; M. Tsunoda; F. Matsukura; H. Ohno. Tunnel magnetoresistance of 604% at 300 K by suppression of Ta diffusion in CoFeB/MgO/CoFeB pseudo-spin-valves annealed at high temperature. *Appl. Phys. Lett.* **2008**, *93*, 082508.

14 V. Dediu; M. Murgia; F. C. Matacotta; C. Taliani; S. Barbanera. Room temperature spin polarized injection in organic semiconductor. *Solid State Commun.* **2002**, *122*, 181-184.

15 Z. H. Xiong; D. Wu; Z. V. Vardeny; J. Shi. Giant magnetoresistance in organic spin-valves. *Nature* **2004**, *427*, 821-824.

16 L. E. Hueso; J. M. Pruneda; V. Ferrari; G. Burnell; J. P. Valdes-Herrera; B. D. Simons; P. B. Littlewood; E. Artacho; A. Fert; N. D. Mathur. Transformation of spin information into large electrical signals using carbon nanotubes. *Nature* **2007**, *445*, 410-413.

17 X. M. Zhang; S. Mizukami; T. Kubota; Q. L. Ma; M. Oogane; H. Naganuma; Y. Ando; T. Miyazaki. Observation of a large spin-dependent transport length in organic spin valves at room temperature. *Nat. Commun.* **2013**, *4*, 1392.

18 M. Gobbi; F. Golmar; R. Llopis; F. Casanova; L. E. Hueso. Room-Temperature Spin Transport in C60-Based Spin Valves. *Adv. Mater.* **2011**, *23*, 1609-1613.

19 S. Pramanik; C. G. Stefanita; S. Patibandla; S. Bandyopadhyay; K. Garre; N. Harth; M. Cahay. Observation of extremely long spin relaxation times in an organic nanowire spin valve. *Nat. Nanotechnol.* **2007**, *2*, 216-219.

20 J. H. Shim; K. V. Raman; Y. J. Park; T. S. Santos; G. X. Miao; B. Satpati; J. S. Moodera. Large spin diffusion length in an amorphous organic semiconductor. *Phys. Rev. Lett.* **2008**, *100*, 226603.

21 S. Majumdar; H. Huhtinen; H. S. Majumdar; R. Laiho; R. Osterbacka. Effect of La(0.67)Sr(0.33)MnO(3) electrodes on organic spin valves. *J. Appl. Phys.* **2008**, *104*, 033910.

22 T. D. Nguyen; G. Hukic-Markosian; F. J. Wang; L. Wojcik; X. G. Li; E. Ehrenfreund; Z. V. Vardeny. The hyperfine interaction role in the spin response of pi-conjugated polymer films and spin valve devices. *Synth. Met.* **2011**, *161*, 598-603.

23 F. J. Wang; C. G. Yang; Z. V. Vardeny; X. G. Li. Spin response in organic spin valves based on La2/3Sr1/3MnO3 electrodes. *Phys. Rev. B* **2007**, *75*, 245324.

24 Y. H. Zheng; F. Wudl. Organic spin transporting materials: present and future. *J. Mater. Chem. A* **2014**, *2*, 48-57.

25 H. Vinzelberg; J. Schumann; D. Elefant; R. B. Gangineni; J. Thomas; B. Buchner. Low temperature tunneling magnetoresistance on (La,Sr)MnO(3)/Co junctions with organic spacer layers. *J. Appl. Phys.* **2008**, *103*, 093720.

26 F. J. Wang; Z. H. Xiong; D. Wu; J. Shi; Z. V. Vardeny. Organic spintronics: The case of Fe/Alq(3)/Co spin-valve devices. *Synth. Met.* **2005**, *155*, 172-175.

27 J. M. De Teresa; A. Barthelemy; A. Fert; J. P. Contour; R. Lyonnet; F. Montaigne; P. Seneor; A. Vaures. Inverse tunnel magnetoresistance in Co/SrTiO3/La0.7Sr0.3MnO3: New ideas on spin-polarized tunneling. *Phys. Rev. Lett.* **1999**, *82*, 4288-4291.

28 C. Barraud; P. Seneor; R. Mattana; S. Fusil; K. Bouzehouane; C. Deranlot; P. Graziosi; L. Hueso; I. Bergenti; V. Dediu; F. Petroff; A. Fert. Unravelling the role of the interface for spin injection into organic semiconductors. *Nat. Phys.* **2010**, *6*, 615-620.

29 S. Sanvito. Molecular Spintronics The rise of spinterface science. *Nat. Phys.* **2010**, *6*, 562-564.

30 K. V. Raman; A. M. Kamerbeek; A. Mukherjee; N. Atodiresei; T. K. Sen; P. Lazic; V. Caciuc; R. Michel; D. Stalke; S. K. Mandal; S. Blugel; M. Munzenberg; J. S. Moodera. Interface-engineered templates for molecular spin memory devices. *Nature* **2013**, *493*, 509-513.

31 M. Gruber; F. Ibrahim; S. Boukari; H. Isshiki; L. Joly; M. Peter; M. Studniarek; V. Da Costa; H. Jabbar; V. Davesne; U. Halisdemir; J. J. Chen; J. Arabski; E. Otero; F. Choueikani; K. Chen; P. Ohresser; W. Wulfhekel; F. Scheurer; W. Weber; M. Alouani; E. Beaurepaire; M. Bowen. Exchange bias and room-temperature magnetic order in molecular layers. *Nat. Mater.* **2015**, *14*, 981-984.

32 S. Jakobs; A. Narayan; B. Stadtmuller; A. Droghetti; I. Rungger; Y. S. Hor; S. Klyatskaya; D. Jungkenn; J. Stockl; M. Laux; O. L. A. Monti; M. Aeschlimann; R. J. Cava; M. Ruben; S. Mathias; S. Sanvito; M. Cinchetti. Controlling the Spin Texture of Topological Insulators by Rational Design of Organic Molecules. *Nano Lett.* **2015**, *15*, 6022-6029.

33 M. Studniarek; S. Cherifi-Hertel; E. Urbain; U. Halisdemir; R. Arras; B. Taudul; F. Schleicher; M. Herve; C. H. Lambert; A. Hamadeh; L. Joly; F. Scheurer; G. Schmerber; V. Da Costa; B. Warot-Fonrose; C. Marcelot; O. Mauguin; L. Largeau; F. Leduc; F. Choueikani; E. Otero; W. Wulfhekel; J. Arabski; P. Ohresser; W. Weber; E. Beaurepaire; S. Boukari; M. Bowen. Modulating the Ferromagnet/Molecule Spin Hybridization Using an Artificial Magnetoelectric. *Adv. Funct. Mater.* **2017**, *27*, 1700259.

34 K. M. Kadish; K. M. Smith; R. Guilard. *The Porphyrin Handbook. vol.17 Phthalocyanines: Properties and Materials.* Academic Press: San Diego, CA, **2003**

35 L. Edwards; M. Gouterman. Porphyrins: XV. Vapor Absorption Spectra and Stability: Phthalocyanines. *J. Mol. Spectrosc.* **1970**, *33*, 292-310.

36 G. H. Heilmeier; G. Warfield; S. E. Harrison. Applicability of Band Model to Metal-Free Phthalocyanine Single Crystas. *J. Appl. Phys.* **1963**, *34*, 2278-2281.

37 H. Ishii; K. Sugiyama; E. Ito; K. Seki. Energy level alignment and interfacial electronic structures at organic/metal and organic/organic interfaces. *Adv. Mater.* **1999**, *11*, 972-972.

38 S. Braun; W. R. SalaneckM. Fahlman. Energy-Level Alignment at Organic/Metal and Organic/Organic Interfaces. *Adv. Mater.* **2009**, *21*, 1450-1472.

39 T. Suzuki; M. Kurahashi; Y. Yamauchi. Spin polarization in molecular orbitals of copper-phthalocyanine deposited on a magnetized Fe(100) substrate. *J. Phys. Chem. B* **2002**, *106*, 7643-7646.

40 T. Suzuki; M. Kurahashi; X. Ju; Y. Yamauchi. Adsorption structure and spin polarization of pentacene on a magnetized Fe(100) substrate: SPMDS and ERDA study. *Surf. Sci.* **2004**, *549*,

97-102.

41 X. Sun; Y. Yamauchi; M. Kurahashi; T. Suzuki; Z. P. Wang; S. Entani. Spin polarization study of benzene molecule adsorbed on Fe(100) surface with metastable-atom deexcitation spectroscopy and density functional calculations. *J. Phys. Chem. C* **2007**, *111*, 15289-15298.

42 G. Schutz; W. Wagner; W. Wilhelm; P. Kienle; R. Zeller; R. Frahm; G. Materlik. Absorption of Circularly Polarized X-Rays in Iron. *Phys. Rev. Lett.* **1987**, *58*, 737-740.

43 A. Scheybal; T. Ramsvik; R. Bertschinger; M. Putero; F. Nolting; T. A. Jung. Induced magnetic ordering in a molecular monolayer. *Chem. Phys. Lett.* **2005**, *411*, 214-220.

44 H. Wende; M. Bernien; J. Luo; C. Sorg; N. Ponpandian; J. Kurde; J. Miguel; M. Piantek; X. Xu; P. Eckhold; W. Kuch; K. Baberschke; P. M. Panchmatia; B. Sanyal; P. M. Oppeneer; O. Eriksson. Substrate-induced magnetic ordering and switching of iron porphyrin molecules. *Nat. Mater.* **2007**, *6*, 516-520.

45 M. Bernien; J. Miguel; C. Weis; M. E. Ali; J. Kurde; B. Krumme; P. M. Panchmatia; B. Sanyal; M. Piantek; P. Srivastava; K. Baberschke; P. M. Oppeneer; O. Eriksson; W. Kuch; H. Wende. Tailoring the Nature of Magnetic Coupling of Fe-Porphyrin Molecules to Ferromagnetic Substrates. *Phys. Rev. Lett.* **2009**, *102*, 047202.

46 C. Wackerlin; D. Chylarecka; A. Kleibert; K. Muller; C. Iacovita; F. Nolting; T. A. Jung; N. Ballav. Controlling spins in adsorbed molecules by a chemical switch. *Nat. Commun.* **2010**, *1*, 61.

47 S. Javaid; M. Bowen; S. Boukari; L. Joly; J. B. Beaufrand; X. Chen; Y. J. Dappe; F. Scheurer; J. P. Kappler; J. Arabski; W. Wulfhekel; M. Alouani; E. Beaurepaire. Impact on Interface Spin Polarization of Molecular Bonding to Metallic Surfaces. *Phys. Rev. Lett.* **2010**, *105*, 077201.

48 A. L. Rizzini; C. Krull; T. Balashov; J. J. Kavich; A. Mugarza; P. S. Miedema; P. K. Thakur; V. Sessi; S. Klyatskaya; M. Ruben; S. Stepanow; P. Gambardella. Coupling Single Molecule Magnets to Ferromagnetic Substrates. *Phys. Rev. Lett.* **2011**, *107*, 177205.

49 J. Miguel; C. F. Hermanns; M. Bernien; A. Kruger; W. Kuch. Reversible Manipulation of the Magnetic Coupling of Single Molecular Spins in Fe-Porphyrins to a Ferromagnetic Substrate. *J. Phys. Chem. Lett.* **2011**, *2*, 1455-1459.

50 A. L. Rizzini; C. Krull; T. Balashov; A. Mugarza; C. Nistor; F. Yakhou; V. Sessi; S. Klyatskaya; M. Ruben; S. Stepanow; P. Gambardella. Exchange Biasing Single Molecule Magnets: Coupling of TbPc2 to Antiferromagnetic Layers. *Nano Lett.* **2012**, *12*, 5703-5707.

51 C. Wackerlin; K. Tarafder; D. Siewert; J. Girovsky; T. Hahlen; C. Iacovita; A. Kleibert; F. Nolting; T. A. Jung; P. M. Oppeneer; N. Ballav. On-surface coordination chemistry of planar molecular spin systems: novel magnetochemical effects induced by axial ligands. *Chem. Sci.* **2012**, *3*, 3154-3160.

52 E. Annese; F. Casolari; J. Fujii; G. Rossi. Interface magnetic coupling of Fe-phthalocyanine layers on a ferromagnetic surface. *Phys. Rev. B* **2013**, *87*, 054420.

53 L. Malavolti; L. Poggini; L. Margheriti; D. Chiappe; P. Graziosi; B. Cortigiani; V. Lanzilotto; F. B. de Mongeot; P. Ohresser; E. Otero; F. Choueikani; P. Sainctavit; I. Bergenti; V. A. Dediu; M. Mannini; R. Sessoli. Magnetism of TbPc2 SMMs on ferromagnetic electrodes used in organic spintronics. *Chem. Commun.* **2013**, *49*, 11506-11508.

54 D. Klar; B. Brena; H. C. Herper; S. Bhandary; C. Weis; B. Krumme; C. Schmitz-Antoniak; B. Sanyal; O. Eriksson; H. Wende. Oxygen-tuned magnetic coupling of Fe-phthalocyanine molecules to ferromagnetic Co films. *Phys. Rev. B* **2013**, *88*, 224424.

55 C. F. Hermanns; K. Tarafder; M. Bernien; A. Kruger; Y. M. Chang; P. M. Oppeneer; W. Kuch. Magnetic Coupling of Porphyrin Molecules Through Graphene. *Adv. Mater.* **2013**, *25*, 3473-3477.

56 A. Candini; V. Bellini; D. Klar; V. Corradini; R. Biagi; V. De Renzi; K. Kummer; N. B. Brookes; U. del Pennino; H. Wende; M. Affronte. Ferromagnetic Exchange Coupling between Fe Phthalocyanine and Ni(111) Surface Mediated by the Extended States of Graphene. *J. Phys. Chem. C* **2014**, *118*, 17670-17676.

57 K. Eguchi; Y. Takagi; T. Nakagawa; T. Yokoyama. Magnetic Interactions of Vanadyl Phthalocyanine with Ferromagnetic Iron, Cobalt, and Nickel Surfaces. *J. Phys. Chem. C* **2014**, *118*, 17633-17637.

58 J. Girovsky; K. Tarafder; C. Waeckerlin; J. Nowakowski; D. Siewert; T. Haehlen; A. Waeckerlin; A. Kleibert; N. Ballav; T. A. Jung; P. M. Oppeneer. Antiferromagnetic coupling of Cr-porphyrin to a bare Co substrate. *Phys. Rev. B* **2014**, *90*, 220404.

59 C. Nistor; C. Krull; A. Mugarza; S. Stepanow; C. Stamm; M. Soares; S. Klyatskaya; M. Ruben; P. Gambardella. Exchange bias of TbPc2 molecular magnets on antiferromagnetic FeMn and ferromagnetic Fe films. *Phys. Rev. B* **2015**, *92*, 184402.

60 M. Gruber; F. Ibrahim; S. Boukari; L. Joly; V. Da Costa; M. Studniarek; M. Peter; H. Isshiki; H. Jabbar; V. Davesne; J. Arabski; E. Otero; F. Choueikani; K. Chen; P. Ohressee; W. Wulfhekel; F. Scheurer; E. Beaurepaire; M. Alouani; W. Weber; M. Bowen. Spin-Dependent Hybridization between Molecule and Metal at Room Temperature through Inter layer Exchange Coupling. *Nano Lett.* **2015**, *15*, 7921-7926.

61 S. Marocchi; A. Candini; D. Klar; W. Van den Heuvel; H. Huane; F. Troiani; V. Corradini; R. Biagi; V. De Renzi; S. Klyatskaya; K. Kummer; N. B. Brookes; M. Ruben; H. Wende; U. Del Pennino; A. Soncini; M. Affronte; V. Bellini. Relay-Like Exchange Mechanism through a Spin Radical between TbPc2 Molecules and Graphene/Ni(111) Substrates. *ACS Nano* **2016**, *10*, 9353-9360.

62 G. Avvisati; C. Cardoso; D. Varsano; A. Ferretti; P. Gargian; M. G. Betti. Ferromagnetic and Antiferromagnetic Coupling of Spin Molecular Interfaces with High Thermal Stability. *Nano Lett.* **2018**, *18*, 2268-2273.

63 M. Serri; W. Wu; L. R. Fleet; N. M. Harrison; C. F. Hirjibehedin; C. W. M. Kay; A. J. Fisher; G. Aeppli; S. Heutz. High-temperature antiferromagnetism in molecular semiconductor thin films and nanostructures. *Nat. Commun.* **2014**, *5*, 3079.

64 S. Lach; A. Altenhof; K. Tarafder; F. Schmitt; M. E. Ali; M. Vogel; J. Sauther; P. M. Oppeneer; C. Ziegler. Metal-Organic Hybrid Interface States of A Ferromagnet/Organic Semiconductor Hybrid Junction as Basis For Engineering Spin Injection in Organic Spintronics. *Adv. Funct. Mater.* **2012**, *22*, 989-997.

65 F. Djeghloul; F. Ibrahim; M. Cantoni; M. Bowen; L. Joly; S. Boukari; P. Ohresser; F. Bertran; P. Le Fevre; P. Thakur; F. Scheurer; T. Miyamachi; R. Mattana; P. Seneor; A. Jaafar; C. Rinaldi; S. Javaid; J. Arabski; J. P. Kappler; W. Wulfhekel; N. B. Brookes; R. Bertacco; A. Taleb-Ibrahimi; M. Alouani; E. Beaurepaire; W. Weber. Direct observation of a highly spin-polarized organic spinterface at room temperature. *Sci. Rep.* **2013**, *3*, 1272.

66 E. Urbain; F. Ibrahim; M. Studniarek; F. N. Nyakam; L. Joly; J. Arabski; F. Scheurer; F. Bertran; P. Le Fevre; G. Garreau; E. Denys; P. Wetzel; M. Alouani; E. Beaurepaire; S. Boukari; M. Bowen; W. Weber. Cu Metal/Mn Phthalocyanine Organic Spinterfaces atop Co with High Spin Polarization at Room Temperature. *Adv. Funct. Mater.* **2018**, *28*, 1707123.

67 J. Brede; N. Atodiresei; S. Kuck; P. Lazic; V. Caciuc; Y. Morikawa; G. Hoffmann; S. Blugel; R. Wiesendanger. Spin- and Energy-Dependent Tunneling through a Single Molecule with Intramolecular Spatial Resolution. *Phys. Rev. Lett.* **2010**, *105*, 047204.

68 J. Schwobel; Y. S. Fu; J. Brede; A. Dilullo; G. Hoffmann; S. Klyatskaya; M. Ruben; R. Wiesendanger. Real-space observation of spin-split molecular orbitals of adsorbed single-molecule magnets. *Nat. Commun.* **2012**, *3*, 953.

69 W. H. Meiklejohn; C. P. Bean. New Magnetic Anisotropy. *Phys. Rev.* **1956**, *102*, 1413-1414.

70 W. C. Cain; M. H. Kryder. Investigation of the Exchange Mechanism in Nife-Tbco Bilayers. *J. Appl. Phys.* **1990**, *67*, 5722-5724.

71 P. J. Vanderzaag; R. M. Wolf; A. R. Ball; C. Bordel; L. F. Feiner; R. Jungblut. A Study of the Magnitude of Exchange Biasing in [111] Fe3o4/Coo Bilayers. *J. Magn. Magn. Mater.* **1995**, *148*, 346-348.

72 M. Ali; P. Adie; C. H. Marrows; D. Greig; B. J. Hickey; R. L. Stamps. Exchange bias using a spin glass. *Nat. Mater.* **2007**, *6*, 70-75.

73 W. H. Meiklejohn. Exchange Anisotropy - a Review. *J. Appl. Phys.* **1962**, *33*, 1328-1335.

74 J. Nogues; I. K. Schuller. Exchange bias. *J. Magn. Magn. Mater.* **1999**, *192*, 203-232.

75 A. P. Malozemoff. Random-Field Model of Exchange-Anisotropy at Rough Ferromagnetic-Antiferromagnetic Interfaces. *Phys. Rev. B* **1987**, *35*, 3679-3682.

76 D. Mauri; H. C. Siegmann; P. S. Bagus; E. Kay. Simple-Model for Thin Ferromagnetic-Films

Exchange Coupled to an Antiferromagnetic Substrate. *J. Appl. Phys.* **1987**, *62*, 3047-3049.

77 E. Fulcomer; S. H. Charap. Thermal Fluctuation Aftereffect Model for Some Systems with Ferromagnetic-Antiferromagnetic Coupling. *J. Appl. Phys.* **1972**, *43*, 4190-4199.

78 Y. Imry; S. Ma. Random-Field Instability of Ordered State of Continuous Symmetry. *Phys. Rev. Lett.* **1975**, *35*, 1399-1401.

79 P. Miltenyi; M. Gierlings; J. Keller; B. Beschoten; G. Guntherodt; U. Nowak; K. D. Usadel. Diluted antiferromagnets in exchange bias: Proof of the domain state model. *Phys. Rev. Lett.* **2000**, *84*, 4224-4227.

80 J. V. Kim; R. L. Stamps. Hysteresis from antiferromagnet domain-wall processes in exchange-biased systems: Magnetic defects and thermal effects. *Phys. Rev. B* **2005**, *71*, 094405.

81 K. Takano; R. H. Kodama; A. E. Berkowitz; W. Cao; G. Thomas. Role of interfacial uncompensated antiferromagnetic spins in unidirectional anisotropy in Ni81Fe19/CoO bilayers. *J. Appl. Phys.* **1998**, *83*, 6888-6892.

82 M. D. Stiles; R. D. McMichael. Model for exchange bias in polycrystalline ferromagnet-antiferromagnet bilayers. *Phys. Rev. B* **1999**, *59*, 3722-3733.

83 H. Zabel; S. D. Bader. *Magnetic heterostructures : advances and perspectives in spinstructures and spintransport*. Springer: Berlin, **2008,** 152-158.

84 U. Welp; S. G. E. te Velthuis; G. P. Felcher; T. Gredig; E. D. Dahlberg. Domain formation in exchange biased Co/CoO bilayers. *J. Appl. Phys.* **2003**, *93*, 7726-7728.

85 S. Brems; D. Buntinx; K. Temst; C. Van Haesendonck; F. Radu; H. Zabel. Reversing the training effect in exchange biased CoO/Co bilayers. *Phys. Rev. Lett.* **2005**, *95*, 157202.

86 J. Nogues; D. Lederman; T. J. Moran; I. K. Schuller. Positive exchange bias in FeF2-Fe bilayers. *Phys. Rev. Lett.* **1996**, *76*, 4624-4627.

87 M. Kiwi; J. Mejia-Lopez; R. D. Portugal; R. Ramirez. Positive exchange bias model: Fe/FeF2 and Fe/MnF2 bilayers. *Solid State Commun.* **2000**, *116*, 315-319.

88 M. Kiwi; J. Mejia-Lopez; R. D. Portugal; R. Ramirez. Exchange-bias systems with compensated interfaces. *Appl. Phys. Lett.* **1999**, *75*, 3995-3997.

89 J. Nogues; C. Leighton; I. K. Schuller. Correlation between antiferromagnetic interface coupling and positive exchange bias. *Phys. Rev. B* **2000**, *61*, 1315-1317.

90 D. A. Gilbert; J. Olamit; R. K. Dumas; B. J. Kirby; A. J. Grutter; B. B. Maranville; E. Arenholz; J. A. Borchers; K. Liu. Controllable positive exchange bias via redox-driven oxygen migration. *Nat. Commun.* **2016**, *7*, 11050.

91 A. L. Rizzini; C. Krull; T. Balashov; A. Mugarza; C. Nistor; F. Yakhou; V. Sessi; S. Klyatskaya; M. Ruben; S. Stepanow; P. Gambardella. Exchange Biasing Single Molecule Magnets: Coupling of TbPc2 to Antiferromagnetic Layers. *Nano Lett.* **2012**, *12*, 5703-5707.

92 S. Boukari; H. Jabbar; F. Schleicher; M. Gruber; G. Avedissian; J. Arabski; Victor Da Costa; G. Schmerber; P. Rengasamy; B. Vileno; W. Weber; M. Bowen; E. Beaurepaire. Disentangling Magnetic Hardening and Molecular Spin Chain Contributions to Exchange Bias in Ferromagnet/Molecule Bilayers. *Nano Lett.* **2018**, *18*, 4659−4663.

93 E. Grochowski. Future Technology Challenges for NAND Flash and HDD Products. *Flash Memory Summit* **2012**.

94 B. Dieny; V. S. Speriosu; S. S. P. Parkin; B. A. Gurney; D. R. Wilhoit; D. Mauri. Giant Magnetoresistance in Soft Ferromagnetic Multilayers. *Phys. Rev. B* **1991**, *43*, 1297-1300.

95 S. Fukami; C. L. Zhang; S. DuttaGupta; A. Kurenkov; H. Ohno. Magnetization switching by spin-orbit torque in an antiferromagnet-ferromagnet bilayer system. *Nat. Mater.* **2016**, *15*, 535-541.

96 Y. C. Lau; D. Betto; K. Rode; J. M. D. Coey; P. Stamenov. Spin-orbit torque switching without an external field using interlayer exchange coupling. *Nat. Nanotechnol.* **2016**, *11*, 758-762.

97 Y. W. Oh; S. H. C. Baek; Y. M. Kim; H. Y. Lee; K. D. Lee; C. G. Yang; E. S. Park; K. S. Lee; K. W. Kim; G. Go; J. R. Jeong; B. C. Min; H. W. Lee; K. J. Lee; B. G. Park. Field-free switching of perpendicular magnetization through spin-orbit torque in antiferromagnet/ferromagnet/oxide structures. *Nat. Nanotechnol.* **2016**, *11*, 878-884.

98 M. N. Leuenberger; D. Loss. Quantum computing in molecular magnets. *Nature* **2001**, *410*, 789-793.

99 J. Lehmann; A. Gaita-Arino; E. CoronadoD. Loss. Spin qubits with electrically gated polyoxometalate molecules. *Nat. Nanotechnol.* **2007**, *2*, 312-317.
100 M. Shiddiq; D. Komijani; Y. Duan; A. Gaita-Arino; E. Coronado; S. Hill. Enhancing coherence in molecular spin qubits via atomic clock transitions. *Nature* **2016**, *531*, 348-351.
101 P. Gutlich; Y. Garcia; H. A. Goodwin. Spin crossover phenomena in Fe(II) complexes. *Chem. Soc. Rev.* **2000**, *29*, 419-427.
102 O. Sato; T. Iyoda; A. Fujishima; K. Hashimoto. Photoinduced magnetization of a cobalt-iron cyanide. *Science* **1996**, *272*, 704-705.
103 J. F. Letard. Photomagnetism of iron(II) spin crossover complexes - the T(LIESST) approach. *J. Mater. Chem.* **2006**, *16*, 2550-2559.
104 J. R. Friedman; M. P. Sarachik; J. Tejada; R. Ziolo. Macroscopic measurement of resonant magnetization tunneling in high-spin molecules. *Phys. Rev. Lett.* **1996**, *76*, 3830-3833.
105 L. Thomas; F. Lionti; R. Ballou; D. Gatteschi; R. Sessoli; B. Barbara. Macroscopic quantum tunnelling of magnetization in a single crystal of nanomagnets. *Nature* **1996**, *383*, 145-147.
106 V. A. Dediu; L. E. Hueso; I. Bergenti; C. Taliani. Spin routes in organic semiconductors. *Nat. Mater.* **2009**, *8*, 707-716.
107 A. J. Drew; J. Hoppler; L. Schulz; F. L. Pratt; P. Desai; P. Shakya; T. Kreouzis; W. P. Gillin; A. Suter; N. A. Morley; V. K. Malik; A. Dubroka; K. W. Kim; H. Bouyanfif; F. Bourqui; C. Bernhard; R. Scheuermann; G. J. Nieuwenhuys; T. Prokscha; E. Morenzoni. Direct measurement of the electronic spin diffusion length in a fully functional organic spin valve by low-energy muon spin rotation. *Nat. Mater.* **2009**, *8*, 109-114.
108 M. Cinchetti; K. Heimer; J. P. Wustenberg; O. Andreyev; M. Bauer; S. Lach; C. Ziegler; Y. L. Gao; M. Aeschlimann. Determination of spin injection and transport in a ferromagnet/organic semiconductor heterojunction by two-photon photoemission. *Nat. Mater.* **2009**, *8*, 115-119.
109 J. W. Yoo; C. Y. Chen; H. W. Jang; C. W. Bark; V. N. Prigodin; C. B. Eom; A. J. Epstein. Spin injection/detection using an organic-based magnetic semiconductor. *Nat. Mater.* **2010**, *9*, 638-642.
110 L. Fang; K. D. Bozdag; C. Y. Chen; P. A. Truitt; A. J. Epstein; E. Johnston-Halperin. Electrical Spin Injection from an Organic-Based Ferrimagnet in a Hybrid Organic-Inorganic Heterostructure. *Phys. Rev. Lett.* **2011**, *106*, 156602.
111 T. Gang; M. D. Yilmaz; D. Atac; S. K. Bose; E. Strambini; A. H. Velders; M. P. de Jong; J. Huskens; W. G. van der Wiel. Tunable doping of a metal with molecular spins. *Nat. Nanotechnol.* **2012**, *7*, 232-236.
112 A. Droghetti; P. Thielen; I. Rungger; N. Haag; N. Grossmann; J. Stockl; B. Stadtmuller; M. Aeschlimann; S. Sanvito; M. Cinchetti. Dynamic spin filtering at the Co/Alq(3) interface mediated by weakly coupled second layer molecules. *Nat. Commun.* **2016**, *7*, 12668.
113 A. Atxabal; M. Ribeiro; S. Parui; L. Urreta; E. Sagasta; X. Sun; R. Llopis; F. CasanovaL. E. Hueso. Spin doping using transition metal phthalocyanine molecules. *Nat. Commun.* **2016**, *7*.
114 M. Cinchetti; V. A. Dediu; L. E. Hueso. Activating the molecular spinterface. *Nat. Mater.* **2017**, *16*, 507-515.
115 F. Al Ma'Mari; T. Moorsom; G. Teobaldi; W. Deacon; T. Prokscha; H. Luetkens; S. Lee; G. E. Sterbinsky; D. A. Arena; D. A. MacLaren; M. Flokstra; M. Ali; M. C. Wheeler; G. Burnell; B. J. Hickey; O. Cespedes. Beating the Stoner criterion using molecular interfaces. *Nature* **2015**, *524*, 69-73.
116 C. Wackerlin; D. Chylarecka; A. Kleibert; K. Muller; C. Iacovita; F. Nolting; T. A. Jung; N. Ballav. Controlling spins in adsorbed molecules by a chemical switch. *Nat. Commun.* **2010**, *1*, 61.
117 S. Schmaus; A. Bagrets; Y. Nahas; T. K. Yamada; A. Bork; M. Bowen; E. Beaurepaire; F. Evers; W. Wulfhekel. Giant magnetoresistance through a single molecule. *Nat. Nanotechnol.* **2011**, *6*, 185-189.
118 T. Miyamachi; M. Gruber; V. Davesne; M. Bowen; S. Boukari; L. Joly; F. Scheurer; G. Rogez; T. K. Yamada; P. Ohresser; E. Beaurepaire; W. Wulfhekel. Robust spin crossover and memristance across a single molecule. *Nat. Commun.* **2012**, *3*, 938.
119 F. Djeghloul; F. Ibrahim; M. Cantoni; M. Bowen; L. Joly; S. Boukari; P. Ohresser; F. Bertran; P.

Le Fevre; P. Thakur; F. Scheurer; T. Miyamachi; R. Mattana; P. Seneor; A. Jaafar; C. Rinaldi; S. Javaid; J. Arabski; J. P. Kappler; W. Wulfhekel; N. B. Brookes; R. Bertacco; A. Taleb-Ibrahimi; M. Alouani; E. Beaurepaire; W. Weber. Direct observation of a highly spin-polarized organic spinterface at room temperature. *Sci. Rep.* **2013**, *3*, 1272.

120 M. Serri; W. Wu; L. R. Fleet; N. M. Harrison; C. F. Hirjibehedin; C. W. M. Kay; A. J. Fisher; G. Aeppli; S. Heutz. High-temperature antiferromagnetism in molecular semiconductor thin films and nanostructures. *Nat. Commun.* **2014**, *5*, 3079.

121 W. H. MeiklejohnC. P. Bean. New Magnetic Anisotropy. *Phys. Rev.* **1957**, *105*, 904-913.

122 J. Nogues; J. Sort; V. Langlais; V. Skumryev; S. Surinach; J. S. Munoz; M. D. Baro. Exchange bias in nanostructures. *Phys Rep* **2005**, *422*, 65-117.

123 M. Gibert; P. Zubko; R. Scherwitzl; J. Iniguez; J. M. Triscone. Exchange bias in LaNiO3-LaMnO3 superlattices. *Nat. Mater.* **2012**, *11*, 195-198.

124 S. S. P. Parkin; K. P. Roche; M. G. Samant; P. M. Rice; R. B. Beyers; R. E. Scheuerlein; E. J. O'Sullivan; S. L. Brown; J. Bucchigano; D. W. Abraham; Y. Lu; M. Rooks; P. L. Trouilloud; R. A. Wanner; W. J. Gallagher. Exchange-biased magnetic tunnel junctions and application to nonvolatile magnetic random access memory (invited). *J. Appl. Phys.* **1999**, *85*, 5828-5833.

125 A. Moser; K. Takano; D. T. Margulies; M. Albrecht; Y. Sonobe; Y. Ikeda; S. H. SunE. E. Fullerton. Magnetic recording: advancing into the future. *J. Phys. D Appl. Phys.* **2002**, *35*, R157-R167.

126 S. Parkin; X. Jiang; C. Kaiser; A. Panchula; K. Roche; M. Samant. Magnetically engineered spintronic sensors and memory. *Proc. IEEE* **2003**, *91*, 661-680.

127 S. Fukami; C. L. Zhang; S. DuttaGupta; A. Kurenkov; H. Ohno. Magnetization switching by spin-orbit torque in an antiferromagnet-ferromagnet bilayer system. *Nat. Mater.* **2016**, *15*, 535-541.

128 K. Vahaplar; S. Tari; H. Tokuc; S. Okur. Effect of Ta buffer layer and thickness on the structural and magnetic properties of Co thin films. *J. Vac. Sci. Technol. B* **2009**, *27*, 2112-2116.

129 G. Kresse; J. Furthmuller. Efficient iterative schemes for ab initio total-energy calculations using a plane-wave basis set. *Phys. Rev. B* **1996**, *54*, 11169-11186.

130 P. E. Blochl. Projector Augmented-Wave Method. *Phys. Rev. B* **1994**, *50*, 17953-17979.

131 G. KresseD. Joubert. From ultrasoft pseudopotentials to the projector augmented-wave method. *Phys. Rev. B* **1999**, *59*, 1758-1775.

132 F. Radu; H. Zabel. *Magnetic heterostructures : Advances and Perspectives in Spinstructures and Spintransport*. Springer: Berlin, **2008,** 97-138.

133 N. Moutis; C. Christides; I. Panagiotopoulos; D. Niarchos. Exchange-coupling properties of La1-xCaMnO3 ferromagnetic/antiferromagnetic multilayers. *Phys. Rev. B* **2001**, *64*, 094429.

134 J. F. Ding; O. I. Lebedev; S. Turner; Y. F. Tian; W. J. Hu; J. W. Seo; C. Panagopoulos; W. Prellier; G. Van Tendeloo; T. Wu. Interfacial spin glass state and exchange bias in manganite bilayers with competing magnetic orders. *Phys. Rev. B* **2013**, *87*, 054428.

135 A. Migliorini; B. Kuerbanjiang; T. Huminiuc; D. Kepaptsoglou; M. Munoz; J. L. F. Cunado; J. Camarero; C. Aroca; G. Vallejo-Fernandez; V. K. Lazarov; J. L. Prieto. Spontaneous exchange bias formation driven by a structural phase transition in the antiferromagnetic material. *Nat. Mater.* **2018**, *17*, 28-35.

136 U. Welp; S. G. E. te Velthuis; G. P. Felcher; T. Gredig; E. D. Dahlberg. Domain formation in exchange biased Co/CoO bilayers. *J. Appl. Phys.* **2003**, *93*, 7726-7728.

137 F. Radu; M. Etzkorn; R. Siebrecht; T. Schmitte; K. Westerholt; H. Zabel. Interfacial domain formation during magnetization reversal in exchange-biased CoO/Co bilayers. *Phys. Rev. B* **2003**, *67*, 134409.

138 J. Keller; P. Miltenyi; B. Beschoten; G. Guntherodt; U. Nowak; K. D. Usadel. Domain state model for exchange bias. II. Experiments. *Phys. Rev. B* **2002**, *66*, 014431.

139 U. Nowak; K. D. Usadel; J. Keller; P. Miltenyi; B. Beschoten; G. Guntherodt. Domain state model for exchange bias. I. Theory. *Phys. Rev. B* **2002**, *66*, 014430.

140 A. Hoffmann. Symmetry driven irreversibilities at ferromagnetic-antiferromagnetic interfaces. *Phys. Rev. Lett.* **2004**, *93*, 097203.

141 R. Morales; A. C. Basaran; J. E. Villegas; D. Navas; N. Soriano; B. Mora; C. Redondo; X. Batlle;

I. K. Schuller. Exchange-Bias Phenomenon: The Role of the Ferromagnetic Spin Structure. *Phys. Rev. Lett.* **2015**, *114*, 097202.

142 J. Barzola-Quiquia; A. Lessig; A. Ballestar; C. Zandalazini; G. Bridoux; F. Bern; P. Esquinazi. Revealing the origin of the vertical hysteresis loop shifts in an exchange biased Co/YMnO3 bilayer. *J. Phys. Condens. Matter* **2012**, *24*, 366006.

143 X. Zhou; L. Ma; Z. Shi; W. J. Fan; R. F. L. Evans; J. G. Zheng; R. W. Chantrell; S. Mangin; H. W. Zhang; S. M. Zhou. Mapping motion of antiferromagnetic interfacial uncompensated magnetic moment in exchange-biased bilayers. *Sci. Rep.* **2015**, *5*, 9183.

144 S. Brems; D. Buntinx; K. Temst; C. Van Haesendonck; F. Radu; H. Zabel. Reversing the training effect in exchange biased CoO/Co bilayers. *Phys. Rev. Lett.* **2005**, *95*, 157202.

145 C. Barraud; K. Bouzehouane; C. Deranlot; S. Fusil; H. Jabbar; J. Arabski; R. Rakshit; D. J. Kim; C. Kieber; S. Boukari; M. Bowen; E. Beaurepaire; P. Seneor; R. Mattana; F. Petroff. Unidirectional Spin-Dependent Molecule-Ferromagnet Hybridized States Anisotropy in Cobalt Phthalocyanine Based Magnetic Tunnel Junctions. *Phys. Rev. Lett.* **2015**, *114*, 206603.

146 T. Gredig; I. N. Krivorotov; E. D. Dahlberg. Magnetization reversal in exchange biased Co/CoO probed with anisotropic magnetoresistance. *J. Appl. Phys.* **2002**, *91*, 7760-7762.

147 S. Bhandary; B. Brena; P. M. Panchmatia; I. Brumboiu; M. Bernien; C. Weis; B. Krumme; C. Etz; W. Kuch; H. Wende; O. Eriksson; B. Sanyal. Manipulation of spin state of iron porphyrin by chemisorption on magnetic substrates. *Phys. Rev. B* **2013**, *88*, 024401.

148 J. M. Manriquez; G. T. Yee; R. S. Mclean; A. J. Epstein; J. S. Miller. A Room-Temperature Molecular Organic Based Magnet. *Science* **1991**, *252*, 1415-1417.

149 J. W. Yoo; C. Y. Chen; H. W. Jang; C. W. Bark; V. N. Prigodin; C. B. Eom; A. J. Epstein. Spin injection/detection using an organic-based magnetic semiconductor. *Nat. Mater.* **2010**, *9*, 638-642.

150 F. Djeghloul; M. Gruber; E. Urbain; D. Xenioti; L. Joly; S. Boukari; J. Arabski; H. Bulou; F. Scheurer; F. Bertran; P. Le Fevre; A. Taleb-Ibrahimi; W. Wulfhekel; G. Garreau; S. Hajjar-Garreau; P. Wetzel; M. Alouani; E. Beaurepaire; M. Bowen; W. Weber. High Spin Polarization at Ferromagnetic Metal-Organic Interfaces: A Generic Property. *J. Phys. Chem. Lett.* **2016**, *7*, 2310-2315.

151 J. Jo; J. Byun; I. Oh; J. Park; M. J. Jin; B. C. Min; J. Lee; J. W. Yoo. Molecular Tunability of Magnetic Exchange Bias and Asymmetrical Magnetotransport in Metalloporphyrin/Co Hybrid Bilayers. *ACS Nano*, DOI: 10.1021/acsnano.8b08689.

152 H. Ohldag; A. Scholl; F. Nolting; E. Arenholz; S. Maat; A. T. Young; M. Carey; J. Stohr. Correlation between exchange bias and pinned interfacial spins. *Phys. Rev. Lett.* **2003**, *91*, 017203.

153 H. Ohldag; H. Shi; E. Arenholz; J. Stohr; D. Lederman. Parallel versus antiparallel interfacial coupling in exchange biased Co/FeF2. *Phys. Rev. Lett.* **2006**, *96*, 027203.

154 J. Ni; J. W. Cai; W. Y. Lai; Y. K. An; Z. H. Mai. Enhancement of exchange bias in Ir-Mn/Co0.9Fe0.1 bilayers by inserting an ultra-thin Co0.6Fe0.4 layer. *J. Phys. D Appl. Phys.* **2006**, *39*, 730-733.

155 M. Tsunoda; S. Yoshitaki; Y. Ashizawa; D. Y. Kim; C. Mitsumata; M. Takahashi. Enhancement of exchange bias by ultra-thin Mn layer insertion at the interface of Mn-Ir/Co-Fe bilayers. *Phys. Stat. Sol. B* **2007**, *244*, 4470-4473.

156 C. Leighton; J. Nogues; B. J. Jonsson-Akerman; I. K. Schuller. Coercivity enhancement in exchange biased systems driven by interfacial magnetic frustration. *Phys. Rev. Lett.* **2000**, *84*, 3466-3469.

157 J. Nogues; C. Leighton; I. K. Schuller. Correlation between antiferromagnetic interface coupling and positive exchange bias. *Phys. Rev. B* **2000**, *61*, 1315-1317.

158 M. Kiwi; J. Mejia-Lopez; R. D. Portugal; R. Ramirez. Positive exchange bias model: Fe/FeF2 and Fe/MnF2 bilayers. *Solid State Commun.* **2000**, *116*, 315-319.

159 T. Gredig; I. N. Krivorotov; P. Eames; E. D. Dahlberg. Unidirectional coercivity enhancement in exchange-biased Co/CoO. *Appl. Phys. Lett.* **2002**, *81*, 1270-1272.

160 J. T. Kohlhepp; H. Wieldraaijer; W. J. M. de Jonge. Onset of magnetic interface exchange interactions in epitaxially grown Mn/Co(001). *J. Mater. Res.* **2007**, *22*, 569-572.

Curriculum Vitae

Junhyeon Jo
The School of Materials Science and Engineering
Ulsan National Institute of Science and Technology (UNIST)
Republic of Korea
E-mail : jhjo@unist.ac.kr
Phone : +82-10-2698-4309

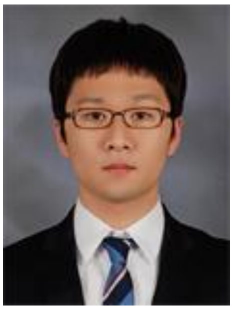

Education

M.S. & Ph.D. Ulsan National Institute of Science and Technology (Mar. 2013 - Feb. 2019)
The School of Materials Science and Engineering
Research Advisor : Prof. Jung-Woo Yoo
Thesis Title : Molecular Exchange Bias at Ferromagnet/Organic Interfaces

B.S. Pusan National University (Mar. 2006 - Feb. 2013)
Department of Materials Science & Engineering
Military Service (2007-2009)

Research Theme

Major Research

- Organic Spintronics
- Organic/Inorganic Hybrid Interface

Minor Research

- Organic thermoelectric generator (OTEG) and Organic photovoltaics (OPV)
- Field effect transistor (FET) with 2D, organic, and oxide materials

Experimental Skill

Device Fabrication

Thin Film Deposition : Thermal-, Electron beam-, Sputtering-, Atomic layer deposition
Device Pattern : Photolithography, Electron beam lithography, Wet & Dry etching

Measurement

Electrical transport : DC & AC (Keithley 2400, 2636A, 2182A, 6221) instruments
PPMS (Quantum Design), Labview
Magnetometry : SQUID-VSM (MPMS3, Quantum Design)
Thermoelectric transport : Thermal Transport System (PPMS), Home-made equipment

Analysis

SEM, AFM, Raman, UV-Vis-NIR, FT-IR, XPS/UPS, XMCD

Publication

(1) **J. Jo**, J. Byun, I. Oh, J. Park, M.-J. Jin, B.-C. Min, J. Lee, and J.-W. Yoo. *Molecular tunability of magnetic exchange bias and asymmetrical magnetotransport in metalloporphyrin/Co hybrid bilayers*. accepted in ACS Nano (2019)

(2) Mi-Jin Jin, D. Choe, S.Y. Lee, J. Park, **J. Jo**, I. Oh, S.-I. Kim, S.-H. Baek, C. Jeon, and J.-W. Yoo. *Probing surface electronic properties of a patterned conductive STO by reactive ion etching*. Appl. Surf. Sci. 466, 730 (2019)

(3) M.-J. Jin, S.-I. Kim, S.Y. M, D. Choe, J. Park, V. Modepalli, **J. Jo**, I. Oh, S.-H. Baek, J.-W. Yoo. *Study of Rashba spin orbit field at LAO/STO heterointerfaces*. accepted in J. Electron. Mater. (2018)

(4) I. Oh, J. Park, **J. Jo**, M.-J. Jin, M.-S. Jang, K.-S. Lee, and J.-W. Yoo. *Solution-processed ferrimagnetic insulator thin film for the microelectronic spin Seebeck energy conversion*. ACS Appl. Mater. Interfaces 10, 28608 (2018)

(5) **J. Jo**, I. Oh, M.-J. Jin, J. Park, J.S. Son, K.-S. An, J.-W. Yoo. *Highly stretchable organic thermoelectrics with an enhanced power factor due to extended localization length*. Org. Electron. 50, 367 (2017)

(6) J. Park, H. Yun, M.-J. Jin, **J. Jo**, I. Oh, V. Modepalli, S.-Y. Kwon, and J.-W. Yoo. *Gate-dependent*

spin Hall induced nonlocal resistance and the symmetry of spin-orbit scattering in Au-clustered graphene. Phys. Rev. B 95, 245414 (2017)

(7) H.-K. Hong¶, **J. Jo**¶, D. Hwang, J. Lee, N.Y. Kim, S. Son, M.-J. Jin, Y.C. Jun, R. Erni, S.K. Kwak, J.-W. Yoo and Z. Lee. *Atomic scale study on growth and heteroepitaxy of ZnO monolayer on graphene.* Nano Lett. 17, 120 (2017) (¶ : contributed equally)

(8) M.-J. Jin, S.Y. Moon, J. Park, V. Modepalli, **J. Jo**, S.-I. Kim, H.C. Koo, B.-C. Min, H.-W. Lee, S.-H. Baek, J.-W. Yoo. *Nonlocal spin diffusion driven by giant spin Hall effect at oxide heterointerfaces.* Nano Lett. 17, 36 (2017)

(9) I. Oh, **J. Jo**, J. Park, J. Lee, H. Shin, J.-W. Yoo. *Local crystallization and enhanced thermoelectric performance of glassy carbon induced by the electron beam irradiation*. Curr. Appl. Phys. 16, 1511 (2016)

(10) J.H. Chu, D. H. Lee, **J. Jo**, S.Y. Kim, J.-W. Yoo* & S.-Y. Kwon. *Highly conductive and environmentally stable organic transparent electrodes laminated with graphene.* Adv. Funct. Mat. 26, 7234 (2016)

(11) V. Modepalli, M.-J. Jin, J. Park, **J. Jo**, J.-H. Kim, J. M. Baik, C. Seo, J. Kim, and J.-W. Yoo. *Gate-tunable spin exchange interactions and inversion of magnetoresistance in single ferromagnetic ZnO nanowires.* ACS Nano 10, 4618 (2016)

(12) M.-J. Jin, **J. Jo**, J.-W. Yoo. *Impedance spectroscopy analysis on the effects of TiO2 interfacial atomic layers in ZnO nanorod polymer solar cells : Effects of interfacial charge extraction on diffusion and recombination.* Org. Electron. 19, 83 (2015)

(13) **J. Jo**, M.-J. Jin, J. Park, V. Modepalli, C.-Y. Kao, A. J. Epstein, M. Choi, N. Park, S.-Y. Lee, C. Jeon, and J.-W. Yoo. *Organic-based magnetic semiconductor thin film of Fe(TCNQ)x~2 developed by physical vapor deposition and local spin density induced core-level shifts.* Synth. Met. 196, 56 (2014)

(14) M.-J. Jin, **J. Jo**, J. H. Kim, K.-S. An, M. S. Jeong, J. Kim, and J.-W. Yoo. *Effects of TiO2 interfacial atomic layers on device performances and exciton dynamics in ZnO nanorod polymer solar cells.* ACS Appl. Mater. Interfaces 6, 11649 (2014)

(15) M.-J. Jin, **J. Jo**, G. P. Neupane, J. Kim, K.-S. An, and J.-W. Yoo. *Tuning of undoped ZnO thin film via plasma enhanced atomic layer deposition and its application for an inverted polymer solar cell.* AIP Advances 3, 102114 (2013)

Presentation at Conference

(1) Emerging exchange bias and magnetic coupled layer at molecular interface
American Physical Society March meeting (2018)

(2) Correlation between morphological crossover and thermoelectric performance in conducting polymer
The Korean Physical Society Spring Meeting (2016)

(3) Correlation between dimensional crossover and thermoelectric performance in conducting polymer
American Physical Society March meeting (2016)

(4) Bonding And Anti-bonding Nature of Magnetic Semiconductor Thin Film of Fe(TCNQ:tetracyanoquinodimethane)
The 46th The Korean Vacuum Society Conference (2014)

(5) Deposition of Metal-Organic Hybrid Magnetic Film : Fe-TCNQ
The Korean Physical Society Fall Meeting (2013)

(6) Bonding and anti-bonding nature of magnetic semiconductor thin film of Fe(TCNQ:tetracyanoquinodimethane)
The 25th Synchrotron Radiation Users' Workshop & KOSUA Meeting (2013)

Acknowledgements

First, I greatly appreciate my supervisor Prof. Jung-Woo Yoo for his guidance, assistance, and advices during my Ph.D. course. I am very lucky to get opportunity to study in his group. I could never have done this Ph.D. course without his help and advices.

I am grateful to founding members in Yoo group; Dr. Mi-Jin Jin, Dr. Vijayakumar Modepalli, and Dr. Jungmin Park who had hard time together to set up all systems and equipment. Especially, I deeply thank Dr. Mi-Jin Jin who taught me the base of experiments. Also, following members; Daeseong Choe, Inseon Oh, Jaebyeong Lee, and Jonghyeon Choi are very excellent members and co-workers for me, having great time and studying together. Also, I thank Prof. Jaekwang Lee and Mr. Jinho Byun to work with us for publishing excellent papers. Finally, I cannot forget to thank my friends and co-workers in UNIST who helped me and had great time together during my Ph.D. course, but I am sorry I could not list all of you guys.

I would like to appreciate to thesis committee members; Prof. Hyung-Joon Shin, Prof. Ki-Suk Lee, Prof. Hosub Jin, and Prof. Jaekwang Lee. Thanks to their valuable comments and advices, I noticed what I overlooked and the necessity of new insights from various viewpoints.

Most of all, I am grateful to my most favorite people. I could never thank my family and my friends enough for their devotion and support. They always believe in me and allow me to focus on my research. Also, they respect my work and plan for future, sincerely. Without their supports for me, I would never be here. Thanks again to my family, my friends, and my people!